

Wave Structures and Nonlinear Balances in a Family of Evolutionary PDEs

Darryl D. Holm^{1,2} and Martin F. Staley¹

¹Theoretical Division and Center for Nonlinear Studies

Los Alamos National Laboratory, MS B284

Los Alamos, NM 87545

email: dholm@lanl.gov, mstaley@lanl.gov

²Mathematics Department

Imperial College of Science, Technology and Medicine

London SW7 2AZ, UK

SIADS MS#41094, Submitted July 10, 2002
Resubmitted in revised form January 18, 2003
Accepted January 16, 2003

Abstract

We investigate the following family of evolutionary 1+1 PDEs that describe the balance between convection and stretching for small viscosity in the dynamics of 1D nonlinear waves in fluids:

$$m_t + \underbrace{um_x}_{\text{convection}} + \underbrace{bu_xm}_{\text{stretching}} = \underbrace{\nu m_{xx}}_{\text{viscosity}}, \quad \text{with } u = g * m.$$

Here $u = g * m$ denotes $u(x) = \int_{-\infty}^{\infty} g(x-y)m(y) dy$. This convolution (or filtering) relates velocity u to momentum density m by integration against the kernel $g(x)$. We shall choose $g(x)$ to be an even function, so that u and m have the same parity under spatial reflection. When $\nu = 0$, this equation is both reversible in time and parity invariant. We shall study the effects of the balance parameter b and the kernel

$g(x)$ on the solitary wave structures, and investigate their interactions analytically for $\nu = 0$ and numerically for small or zero viscosity.

This family of equations admits the classic Burgers “ramps and cliffs” solutions, which are stable for $-1 < b < 1$ with small viscosity.

For $b < -1$, the Burgers ramps and cliffs are unstable. The stable solution for $b < -1$ moves leftward instead of rightward and tends to a stationary profile. When $m = u - \alpha^2 u_{xx}$ and $\nu = 0$, this profile is given by $u(x) \simeq \text{sech}^2(x/(2\alpha))$ for $b = -2$, and by $u(x) \simeq \text{sech}(x/\alpha)$ for $b = -3$.

For $b > 1$, the Burgers ramps and cliffs are again unstable. The stable solitary traveling wave for $b > 1$ and $\nu = 0$ is the “pulson” $u(x, t) = cg(x - ct)$, which restricts to the “peakon” in the special case $g(x) = e^{-|x|/\alpha}$ when $m = u - \alpha^2 u_{xx}$. Nonlinear interactions among these pulsons or peakons are governed by the superposition of solutions for $b > 1$ and $\nu = 0$,

$$m(x, t) = \sum_{i=1}^N p_i(t) \delta(x - q_i(t)), \quad u(x, t) = \sum_{i=1}^N p_i(t) g(x - q_i(t)).$$

These pulson solutions obey a finite dimensional dynamical system for the time-dependent speeds $p_i(t)$ and positions $q_i(t)$. We study the pulson and peakon interactions analytically, and we determine their fate numerically under adding viscosity.

Finally, as outlook, we propose an n -dimensional vector version of this evolutionary equation with convection and stretching, namely,

$$\frac{\partial}{\partial t} \mathbf{m} + \underbrace{\mathbf{u} \cdot \nabla \mathbf{m}}_{\text{convection}} + \underbrace{\nabla \mathbf{u}^T \cdot \mathbf{m} + (b-1) \mathbf{m}(\text{div } \mathbf{u})}_{\text{stretching}} = 0,$$

for a defining relation, $\mathbf{u} = G * \mathbf{m}$. These solutions show quasi-one-dimensional behavior for $n, k = 2, 1$ that we find numerically to be stable for $b = 2$. The corresponding superposed solutions of the vector b -equation in n -dimensions exist, with coordinates $\mathbf{x} \in R^n$, $s \in R^k$, $n - k > 0$, and $2N$ parameters $\mathbf{P}_i(s, t), \mathbf{Q}_i(s, t) \in R^n$,

$$\begin{aligned} \mathbf{m}(\mathbf{x}, t) &= \sum_{i=1}^N \int \mathbf{P}_i(s, t) \delta(\mathbf{x} - \mathbf{Q}_i(s, t)) ds, \quad \mathbf{m} \in R^n, \\ \mathbf{u}(\mathbf{x}, t) &= \sum_{i=1}^N \int \mathbf{P}_i(s, t) G(\mathbf{x} - \mathbf{Q}_i(s, t)) ds, \quad \mathbf{u} \in R^n. \end{aligned}$$

These are momentum surfaces (or filaments, for $k = 1$), defined on surfaces (or curves), $\mathbf{x} = \mathbf{Q}_i(s, t)$, $i = 1, 2, \dots, N$. For $b = 2$, the $\mathbf{P}_i(s, t), \mathbf{Q}_i(s, t) \in R^n$ satisfy canonical Hamiltonian equations for geodesic motion on the space of n -vector valued k -surfaces with co-metric G .

Contents

1	Introduction	5
1.1	The b-family of fluid transport equations	5
1.2	Outline of the paper	6
2	History and general properties of the b-equation	7
3	Deriving b-equation (1) for shallow water	8
3.1	Linear and nonlinear balances in shallow water waves	8
3.2	Other work related to equation (8) with $b = 2$	9
3.3	Higher-order nonlinear/nonlocal integrable balance	10
3.3.1	CH peakon solutions	12
3.3.2	FH pulson solutions	13
3.4	Discrete symmetries: reversibility, parity and signature	13
3.5	Lagrangian representation	14
3.6	Preservation of the norm $\ m\ _{L^{1/b}}$ for $0 \leq b \leq 1$	15
3.7	Lagrangian representation for integer b	15
3.8	Reversibility and Galilean covariance	17
3.9	Integral momentum conservation	17
4	Traveling waves and generalized functions	18
4.1	Case $b = 0$	18
4.1.1	Pulsons for $b = 0$	18
4.1.2	Peakons, ramps, and cliffs for $b = 0$	18
4.2	Case $b \neq 0$	21
4.2.1	Special cases of traveling waves for $b \neq 0$	21
4.3	Case $b > 0$	22
4.3.1	Pulsons for $b > 0$	22
4.3.2	Peakons for $b > 1$	22
4.4	Case $b < 0$	25
4.4.1	Case $b = -1/2$	25

4.4.2	Case $b = -1$	25
4.4.3	Case $b = -2$ stationary solutions	29
4.4.4	Case $b = -3$ stationary solutions	30
4.4.5	Case $b = -4$ stationary solutions	30
4.4.6	Numerical Results for $b = -2$ and $b = -3$	32
5	Pulson interactions for $b > 0$	32
5.1	Pulson interactions for $b = 2$	34
5.2	Peakon interactions for $b = 2$ and $b = 3$: numerical results . .	37
5.3	Pulson-Pulson interactions for $b > 0$ and symmetric g	38
5.4	Pulson-antiPulson interactions for $b > 1$ and symmetric g . . .	41
5.5	Specializing Pulsons to Peakons for $b = 2$ and $b = 3$	44
6	Peakons of width α for arbitrary b	44
6.1	Slope dynamics for Peakons: inflection points and the steep- ening lemma when $1 < b \leq 3$	45
6.2	Cases $0 \leq b \leq 1$	47
7	Adding viscosity to peakon dynamics	48
7.1	Burgers- $\alpha\beta$ equation: analytical estimates	50
7.2	Burgers- $\alpha\beta$ traveling waves for $\beta(3 - b) = 1$ & $\nu = 0$	52
8	The fate of peakons under (1) adding viscosity and (2) Burgers-$\alpha\beta$ evolution	53
8.1	The fate of peakons under adding viscosity	53
8.2	The fate of peakons under Burgers- $\alpha\beta$ evolution	58
9	Numerical results for peakon scattering and initial value prob- lems	67
9.1	Peakon initial value problems	67
9.1.1	Inviscid b-family of equations	67
9.1.2	Viscous b-family of equations	70
9.1.3	Burgers- $\alpha\beta$ equation	71
9.2	Description of our numerical methods	71
10	Conclusions	73

11 Outlook: the vector b-equation for compressible motion of momentum filaments and surfaces in n-dimensions	76
11.1 n -dimensional vector b -equation	76
11.2 n -dimensional analogs of pulsons for the vector b -equation .	79
11.2.1 Momentum filaments in R^n	80
11.2.2 Canonical Hamiltonian dynamics of momentum filaments in R^n for $b = 2$	81
11.2.3 Zero-dispersion shallow water waves in 2D: Two interesting choices for the operator Q_{op} when $b = 2$	82

1 Introduction

1.1 The b -family of fluid transport equations

We shall investigate a one-dimensional version of fluid convection and stretching that is described by the following family of 1+1 evolutionary equations,

$$m_t + \underbrace{um_x}_{\text{convection}} + \underbrace{bu_xm}_{\text{stretching}} = 0, \quad \text{with} \quad u = g * m, \quad (1)$$

in independent variables time t and one spatial coordinate x .

We shall seek solutions for the fluid velocity $u(x, t)$ that are defined either on the real line and vanishing at spatial infinity, or on a periodic one-dimensional domain. Here $u = g * m$ denotes the convolution (or filtering),

$$u(x) = \int_{-\infty}^{\infty} g(x - y)m(y) dy, \quad (2)$$

which relates velocity u to momentum density m by integration against kernel $g(x)$ over the real line. We shall choose $g(x)$ in the defining relation (2) to be an even function, so that u and m have the same parity.

The family of equations (1) is characterized by the kernel g and the real dimensionless constant b , which is the ratio of stretching to convection. The function $g(x)$ will determine the traveling wave shape and length scale for equation (1), while the constant b will provide a balance or bifurcation parameter for the nonlinear solution behavior. Special values of b will include the first few positive and negative integers.

The quadratic terms in equation (1) represent the competition, or balance, in fluid convection between nonlinear steepening and amplification due

to b -dimensional stretching. Equation (1) with $b \neq -1$ arises in the nonlinear dynamics of shallow water waves, as shown in [7, 17, 18]. Equation (1) with $b = 2$ and $b = 3$ appears in the theory of integrable partial differential equations [7, 17, 15]. The three-dimensional analog of equation (1) with $b = 2$ was introduced in a larger variational context in [26, 27]. Applying the proper viscosity to this three-dimensional analog with $b = 2$ and enforcing incompressibility produces the Navier-Stokes-alpha model of turbulence [9]. The 1D version of this turbulence model is

$$m_t + \underbrace{um_x}_{\text{convection}} + \underbrace{bu_xm}_{\text{stretching}} = \underbrace{\nu m_{xx}}_{\text{viscosity}}, \quad \text{with} \quad u = g * m. \quad (3)$$

We shall compare our analysis of equation (1) with numerical simulations of (3), for small viscosity.

1.2 Outline of the paper

After summarizing previous investigations of particular cases in the b -family of convection equations (1), section 2 discusses its symmetries and other general properties such as parity and reversibility. Section 3 discusses the derivation of the b -equation (1) among a family of asymptotically equivalent equations for unidirectional shallow water waves. Section 4 discusses the traveling waves for equation (1) and derives their pulson solutions, which may be generalized functions for $b > 1$. Section 5 analyzes the interaction dynamics of the pulson solutions for any positive b and any g . Section 6 specializes the analysis of the pulson solutions to the peakons, for which $g(x) = e^{-|x|/\alpha}$ is a peaked pulse of width α , and b is taken to be arbitrary. In section 7 we add viscosity to the peakon equation, and describe our numerical methods for illustrating the different types of behavior that may arise in the initial value problems for peakon solutions with $b > 0$, $b = 0$ and $b < -1$. Section 8 uses these numerical methods to determine how viscosity affects the fate of the peakons. Section 9 provides a synopsis of the figures. Section 10 summarizes the paper's main conclusions and section 11 provides the outlook for generalizing the present work to higher dimensions.

Acknowledgements

We are grateful to A. Degasperis, A. N. W. Hone, J. M. Hyman, S. Kurien, C. D. Levermore, R. Lowrie and E. S. Titi for their thoughtful remarks,

careful reading and attentive discussions that provided enormous help and encouragement during the course of writing this paper. We are also grateful to the referees for their thoughtful comments. One referee pointed out a technical caveat that appeared in the original proofs of both the Peakon Steepening Lemmas in Propositions 6.1 and 7.2, and showed how to overcome the caveat without changing the validity of the results. The caveat and its solution are stated after the formal proofs of these propositions.

2 History and general properties of the b-equation

Camassa and Holm [7] derived the following equation for unidirectional motion of shallow water waves in a particular Galilean frame,

$$m_t + \underbrace{um_x}_{\text{convection}} + \underbrace{2u_xm}_{\text{stretching}} = \underbrace{-c_0u_x - \gamma u_{xxx}}_{\text{dispersion}}, \text{ with } m = u - \alpha^2 u_{xx}. \quad (4)$$

Here $m = u - \alpha^2 u_{xx}$ is a momentum variable, partial derivatives are denoted by subscripts, the constants α^2 and γ/c_0 are squares of length scales, and $c_0 = \sqrt{g'h}$ is the linear wave speed for undisturbed water of depth h at rest under gravity g' at spatial infinity, where u and m are taken to vanish. Any constant value $u = u_0$ is also a solution of (4).

Equation (4) was derived using Hamiltonian methods in [7] and was shown in [17] also to appear as a water wave equation at quadratic order in the asymptotic expansion for unidirectional shallow water waves in terms of their two small parameters (aspect ratio and wave height). The famous Korteweg-de Vries (KdV) equation appears at linear order in this asymptotic expansion and is recovered from equation (4) when $\alpha^2 \rightarrow 0$. Both KdV at linear order and its nonlocal, nonlinear generalization in equation (4) at quadratic order in this expansion have the remarkable property of being completely integrable by the isospectral transform (IST) method. The IST properties of KdV solitons are well known. The IST properties of equation (4) were discovered in [7] and were analyzed completely for the case that the initial distribution of momentum $m(x, 0)$ does not change sign in [6]. See also [10] for additional analysis of the scattering problem for the CH equation for this class of initial conditions. For an initial distribution of momentum that changes sign, the IST properties of the CH equation (4) remains an open problem.

3 Deriving b -equation (1) for shallow water

3.1 Linear and nonlinear balances in shallow water waves

The primary physical mechanism for the unidirectional propagation of solitary shallow water waves is the balance between nonlinear steepening and linear dispersion. This balance is *nearly* unique at linear order in an asymptotic expansion in the Korteweg-de Vries equation (KdV),

$$\underbrace{u_t + c_0 u_x}_{\text{Propagation}} + \underbrace{\frac{3\epsilon_1}{2} u u_x + \frac{3\epsilon_2}{20} u_{xxx}}_{\text{Balance}} = 0. \quad (5)$$

Here the expansion parameters satisfy $\epsilon_1 \geq \epsilon_2 > \epsilon_1^2$ and are defined by $\epsilon_1 = a/h$ and $\epsilon_2 = h^2/l^2$, in terms of wave amplitude a , mean water depth h , and typical horizontal length scale l (e.g., a wavelength). KdV possesses the famous sech^2 solitary wave solution $u(x, t) = u_0 \text{sech}^2((x - ct)\sqrt{u_0/\gamma}/2)$, for $u_0 = 2(c - c_0)/\epsilon_1$ and $\gamma = 3\epsilon_2/(5\epsilon_1)$; see [1].

The Benjamin-Bona-Mahoney equation (BBM)

$$\underbrace{u_t + c_0 u_x}_{\text{Propagation}} + \underbrace{\frac{3\epsilon_1}{2} u u_x - \frac{3\epsilon_2}{20} c_0^{-1} u_{xxt}}_{\text{Balance}} = 0, \quad (6)$$

has a solitary wave with the same sech^2 shape, but with γ replaced by $\gamma' = c\gamma/c_0$; see [1]. BBM is asymptotically equivalent to KdV at order $O(\epsilon_1, \epsilon_2)$. In comparison, the linear dispersion relation for BBM matches the exact relation for shallow water waves better than KdV. However, KdV is Galilean invariant, while BBM is not. And, of course, KdV is a completely integrable soliton equation, while BBM is not.

Beyond KdV and BBM at linear order, the asymptotic expansion at quadratic order in the small parameters ϵ_1 and ϵ_2 produces an infinite *family* of shallow water wave equations that are asymptotically equivalent to each other at quadratic order in the shallow water expansion parameters [18]. The equations in this family are related to each other by a continuous, three-parameter group of nonlinear, nonlocal transformations of variables introduced in [33],

$$u = v + \epsilon_1(a_1 v^2 + a_2 v_x \partial_x^{-1} v) + \epsilon_2 a_3 v_{xx}, \quad (7)$$

in which (a_1, a_2, a_3) are the three real parameters of the group. This transformation group was first introduced for determining normal forms of asymptotic shallow water wave equations by Kodama in [33].

Among the family of asymptotically equivalent shallow water wave equations at quadratic order accuracy in the small parameters $\epsilon_1 = a/h$ and $\epsilon_2 = h^2/l^2$ are several equations that are completely integrable. As for KdV at linear order, these integrable shallow water equations at quadratic order possess soliton solutions that interact via elastic collisions. In particular, the equation in the KdV hierarchy with fifth-order derivatives (KdV5) appears amongst these integrable equations, as shown in [35].

The family of asymptotically equivalent shallow water equations that emerges at quadratic order accuracy also contains the following sub-family derived in [18] in which the constant parameter b depends on the group parameters (a_1, a_2, a_3) appearing in the Kodama transformation (7),

$$m_t + c_0 u_x + \epsilon_1 (u m_x + b m u_x) + \frac{3\epsilon_2}{20} u_{xxx} = 0, \quad (8)$$

where $m = u - (19\epsilon_2/60)u_{xx}$. For any $b \neq -1$, an asymptotically equivalent shallow water equation may be achieved by a Kodama transformation. However, the case $b = -1$ violates the asymptotic ordering and the corresponding Kodama transformation is singular for $b = -1$, [18]. Notice that equation (8) is *not* Galilean invariant.

The cases $b = 2$ and $b = 3$ are special values for the b -equation (8). The case $b = 2$ restricts (8) to the integrable Camassa-Holm equation (CH) [7]. The case $b = 3$ in (8) recovers the Degasperis-Procesi equation (DP) [16], which was shown to be integrable in [15]. These two cases exhaust the integrable candidates for (8), as was shown using Painlevé analysis in [15]. The b -family of equations (8) was also shown in [36] to admit the symmetry conditions necessary for integrability only in the cases $b = 2$ for CH and $b = 3$ for DP.

3.2 Other work related to equation (8) with $b = 2$

Equation (8) with $b = 2$ was first derived by using asymptotic expansions directly in the Hamiltonian for Euler's equations in the shallow water regime and was thereby shown to be bi-Hamiltonian and IST-integrable in [7]. Additional details of its derivation and the analysis of its peakon solutions, as well as a numerical solution of the initial value problem for equation (8) with

$b = 2$ were provided in [8]. Its periodic solutions were treated in [2, 3, 4, 5] and references therein.

Equation (8) with $b = 2$ was recently re-derived as a shallow water equation by using asymptotic methods via three different approaches in [21, 17, 32]. These three derivations used different variants of the method of asymptotic expansions for shallow water waves. A recent paper [14] also obtains equation (8) with $b = 2$ as a model for waves in hyperelastic rods.

Hereditary symmetries The paper [19] rederives equation (8) with $b = 2$ from general asymptotic considerations and claims that the equation was already obtained in [24], [23] by the theory of hereditary symmetries. Indeed, before [7], families of integrable equations similar to equation (8) with $b = 2$ *could have been obtained* amidst a comprehensive list of other integrable equations provided by the theory of hereditary symmetries [20]. However, the integrable equation (8) with $b = 2$ was not written explicitly, nor was it derived physically as a water wave equation, and its solution properties were not studied before [7]. See [25] for an insightful discussion of how the integrable equation (8) with $b = 2$ relates to the theory of hereditary symmetries.

3.3 Higher-order nonlinear/nonlocal integrable balance

KdV in equation (5) and the cases $b = 2$ (CH) and $b = 3$ (DP) of equation (8) are three completely integrable Hamiltonian equations that possess solitons as traveling waves. In all of these equations, the leading order balance that confines the traveling wave soliton occurs between nonlinear steepening and linear dispersion. Physically, this is also the leading order asymptotic balance for shallow water waves. However, the parameter b in equation (8) introduces additional possibilities for higher-order balances, including the nonlinear/nonlocal balance occurring in the following dispersionless case of CH that was studied previously for $b = 2$ in [7],

$$m_t + \underbrace{um_x + bmu_x}_{\text{Nonlinear balance}} = 0, \text{ with } m = u - \alpha^2 u_{xx} \text{ and } \lim_{|x| \rightarrow \infty} u = 0. \quad (9)$$

To obtain equation (9) from (8), one absorbs the linear dispersion terms in (8) by a Galilean transformation and a velocity shift, followed by a rescaling.

Recall that equation (8) is not Galilean invariant; so Galilean transformations do not preserve the functional form of its solutions. Even in the absence of linear dispersion, the nonlinear and nonlocal terms that remain in equation (9) can still balance to produce a confined solitary traveling wave pulse $u(x, t) = ce^{-|x-ct|/\alpha}$, called the *peakon* [7].

The peakon solutions and other properties of dispersionless DP for the case $b = 3$ in equation (9) were studied in [15]. The properties of the class of dispersionless equations consisting of (9) for $b = 2$ with the more general defining relation $u = g * m$ in (2) for any even kernel $g(x) = g(-x)$ were studied in [22]. The CH peakon case is recovered for $g(x) = e^{-|x|/\alpha}$.

The peakon solution of equation (9) moves with speed equal to its amplitude and has a jump in derivative at its peak. Peakons for either $b = 2$ or $b = 3$ are true solitons that interact via elastic collisions under CH dynamics, or DP dynamics, respectively, [7], [15]. In addition, the CH and DP initial value problems are both completely integrable as Hamiltonian systems by using the inverse spectral transform (IST) method for an isospectral linear eigenvalue problem whose purely discrete spectrum gives the asymptotic speeds of the peakons [7], [15]. Figure 2 shows the evolution under dispersionless CH for the case $b = 2$ in equation (9) of a Gaussian initial velocity distribution of unit area and width 5α . In fact, peakon solutions exist for equation (9) with any value of b . However, we shall find numerically that the stability of these peakon solutions requires $b > 1$. For the case $b = 2$, stability of the single peakon was proved in [13].

Burgers equation The dispersionless limit of KdV in (5) upon rescaling velocity u is the Burgers equation,

$$u_t + uu_x - \nu u_{xx} = 0, \quad (10)$$

in which we have added constant viscosity ν . The Burgers solution is the classic ramp and cliff shown arising from a Gaussian initial condition in Figure 1. In the ramp/cliff solution, nonlinear steepening is balanced by linear viscosity to produce the “cliff” whose width is controlled by the magnitude of ν . The “ramp” is the self-similar $u \approx x/t$ part of the solution for which the viscous term vanishes.

Total momentum The equations KdV, BBM, CH, DP, the other b equations (9) with $u = g * m$ and Burgers all preserve the area $M = \int_{-\infty}^{\infty} u \, dx$ (total momentum) for a solution u that vanishes at spatial infinity.

3.3.1 CH peakon solutions

Linear dispersion was absorbed in (8) by a Galilean transformation and a velocity shift. For $b = 2$, this procedure reduces the CH equation (4) with linear dispersion to the following purely nonlinear evolution equation that contains competing quadratically nonlinear terms representing convection and stretching,

$$m_t + \underbrace{um_x}_{\text{convection}} + \underbrace{2u_xm}_{\text{stretching}} = 0, \quad \text{with} \quad m = u - \alpha^2 u_{xx}. \quad (11)$$

This is a special case of equation (1), or (9), for which $b = 2$ and $g(x) = e^{-|x|/\alpha}$ in the defining relation (2). The traveling wave solution of (11) is the “peakon,” $u(x, t) = ce^{-|x-ct|/\alpha}$ found in [7], where $e^{-|x|/\alpha}$ is the Green’s function for the Helmholtz operator that relates m and u . The interactions among N peakons are governed by the $2N$ dimensional dynamical system for the speeds $p_i(t)$ and positions $q_i(t)$, $i = 1, \dots, N$, appearing in the *superposed* solution,

$$u(x, t) = \sum_{i=1}^N p_i(t) e^{-|x-q_i(t)|}. \quad (12)$$

As shown in Camassa and Holm [7], a closed integrable Hamiltonian system of ordinary differential equations for the speeds $p_i(t)$ and positions $q_i(t)$ results upon substituting the superposition of peakons (12) into equation (11). This integrable system governs the dynamics of the peakon interactions.

A variant of equation (11) with coefficient $b = 2 \rightarrow b = 3$,

$$m_t + \underbrace{um_x}_{\text{convection}} + \underbrace{3u_xm}_{\text{stretching}} = 0, \quad \text{with} \quad m = u - \alpha^2 u_{xx}, \quad (13)$$

was first singled out for further analysis by Degasperis and Procesi [16]. Degasperis, Holm and Hone [15] discovered that this $b = 2 \rightarrow b = 3$ variant of equation (11) also possesses superposed peakon solutions (12) and is completely integrable by the isospectral transform method. Thus, the N –peakon solution (12) is a completely integrable dynamical system under the evolution of either (11) or (13), but these two integrable cases have *different* dynamics for the speeds $p_i(t)$ and positions $q_i(t)$ of the peakons. The proof that N –peakon solutions (12) exist for any b in equation (9) follows by direct substitution of the solution ansatz into the equation.

3.3.2 FH pulson solutions

Fringer and Holm [22] extended the zero-dispersion shallow water equation (11) for the peakons to the “pulson” equation, which is contained in the family of equations (1) for $b = 2$,

$$m_t + \underbrace{um_x}_{\text{convection}} + \underbrace{2u_xm}_{\text{stretching}} = 0, \quad \text{with} \quad u = g * m. \quad (14)$$

Here $u = g * m$ denotes the convolution (or filtering),

$$u(x) = \int_{-\infty}^{\infty} g(x-y)m(y)dy, \quad (15)$$

that relates velocity u to momentum density m by integration against the kernel $g(x)$. Fringer and Holm [22] chose $g(x)$ to be an even function, so that u and m have the same parity. They studied the effects of the shape of the traveling wave $u(x, t) = cg(x - ct)$ on its interactions with other traveling waves in the superposed solution,

$$u(x, t) = \sum_{i=1}^N p_i(t) g(x - q_i(t)), \quad (16)$$

This superposed solution of traveling wave forms with time dependent speeds $p_i(t)$ and positions $q_i(t)$, $i = 1, \dots, N$, revealed that the nonlinear interactions among these pulsons occur by elastic two-pulson scattering, even though the Fringer-Holm pulson equation (14) is not integrable for an arbitrary choice of the kernel g . When $g(x) = e^{-|x|/\alpha}$ is assumed, the pulson equation for $b = 2$ in (14) specializes to the peakon equation for $b = 2$ in (11). The proof that N -pulson solutions (16) exist for any b in equation (1), or (14), follows by direct substitution of the solution ansatz into the equation. The resulting reduced, or collective, dynamics for the speeds $p_i(t)$ and positions $q_i(t)$ of the pulsons depends upon the value of b in (14) and the choice of the function g in the defining relation (15).

3.4 Discrete symmetries: reversibility, parity and signature

Equation (1) for m is reversible, or invariant under $t \rightarrow -t$ and $u \rightarrow -u$. The latter implies $m \rightarrow -m$. Hence, the transformation $u(x, t) \rightarrow -u(x, -t)$

takes solutions into solutions, and in particular, it reverses the direction and amplitude of the traveling wave $u(x, t) = cg(x - ct)$.

We chose $g(x)$ to be an even function so that m and $u = g * m$ would both have odd parity under mirror reflections. Hence, equation (1) is invariant under the parity reflections $u(x, t) \rightarrow -u(-x, t)$, and the solutions of even and odd parity form invariant subspaces.

Equation (1) implies a similar reversible, parity invariant equation for the **absolute value** $|m|$,

$$\partial_t |m| + u|m|_x + b u_x |m| = 0, \quad \text{with} \quad u = g * m. \quad (17)$$

So, the positive and negative components $m_{\pm} = \frac{1}{2}(m \pm |m|)$ satisfy equation (1) separately. Also, if m is initially zero, it remains so. This is conservation of the signature of m .

3.5 Lagrangian representation

If $m^{1/b}$ is well-defined, equation (1) may be written as the conservation law

$$\partial_t m^{1/b} + \partial_x (m^{1/b} u) = 0, \quad (18)$$

and equation (17) for the absolute value implies

$$\partial_t |m|^{1/b} + \partial_x (|m|^{1/b} u) = 0. \quad (19)$$

Adding and subtracting equations (18) and (19) implies

$$\partial_t (m^{1/b})_{\pm} + \partial_x ((m^{1/b})_{\pm} u) = 0 \quad \text{with} \quad (m^{1/b})_{\pm} = \frac{1}{2}(m^{1/b} \pm |m|^{1/b}). \quad (20)$$

Consequently, regions of positive and negative m are both transported by the velocity $u = g * m$ and their boundaries propagate so as to separately preserve the two integrals,

$$\int_{-\infty}^{\infty} (m^{1/b})_{\pm} dx. \quad (21)$$

The shared velocity relation $u = g * m$ allows a transformation to Lagrangian coordinates X_{\pm} defined by

$$dX_{\pm} = (m^{1/b})_{\pm}(dx - udt) \quad \text{so that} \quad \partial_t X_{\pm} + u \partial_x X_{\pm} = 0. \quad (22)$$

This formal transformation is not strictly defined where $(m^{1/b})_{\pm}$ vanishes. However, by equation (20), regions where $(m^{1/b})_{\pm}$ vanishes do not propagate and do not contribute to the integrated value of $X_{\pm} = \int_{-\infty}^x (m^{1/b})_{\pm}(y, 0) dy$. Hence, these regions may be identified and excluded initially. The formal inverse relation holding in the remaining regions,

$$dx = (m^{1/b})_{\pm}^{-1} dX_{\pm} + u dt, \quad (23)$$

implies that

$$\left. \frac{dx}{dt} \right|_{X_{\pm}} = u(x, t), \quad (24)$$

so the Lagrangian trajectories $x = x(X_{\pm}, t)$ of positive and negative integrated initial values of $X_{\pm} = \int_{-\infty}^x (m^{1/b})_{\pm}(y, 0) dy$ are transported by the same velocity $u = g * m$.

3.6 Preservation of the norm $\|m\|_{L^{1/b}}$ for $0 \leq b \leq 1$

If $|m|^{1/b}$ is well-defined, the continuity equation form (19) of equation (1) implies conservation of

$$\int_{-\infty}^{\infty} |m|^{1/b} dx = \int_{-\infty}^{\infty} |m_0|^{1/b} dx, \quad \text{where } m_0(x) = m(x, 0). \quad (25)$$

This integral is conserved for all b , but only defines a norm (the $L^{1/b}$ norm $\|m\|_{L^{1/b}}$) in the closed interval $0 \leq b \leq 1$. In the limit $b \rightarrow 0$ this becomes the L_{∞} norm, $|m|_{\max}$. Hence, when $b = 0$, equation (1) has both a maximum principle and a minimum principle for m . Such a principle is meaningful only if $m^{1/b}$ is an ordinary function, e.g., if m is not a generalized function, such as the delta functions that occur for the peakons we shall discuss below.

Thus, the $L^{1/b}$ norm $\|m\|_{L^{1/b}}$ is conserved by equation (1), provided $|m|^{1/b}$ is well-defined for the closed interval $0 \leq b \leq 1$. One may also define the corresponding conserved norm for $1/m$ in the closed interval $-1 \leq b \leq 0$, provided $|1/m|^{1/b}$ is well-defined on this interval.

3.7 Lagrangian representation for integer b

Fluid convection means transport of a quantity by the fluid motion. Examples of transported fluid quantities are circulation (a one-form) in Kelvin's theorem for the Euler equations, and its exterior derivative the vorticity (a

two-form, by Stokes theorem) in the Helmholtz equation. For a Lagrangian trajectory $x(X, t)$ satisfying $x(X, 0) = X$ and

$$dx = (m^{1/b})^{-1} dX + u dt, \quad (26)$$

we have seen that the conservation law (18) implies

$$m^{1/b}(x, t) dx = m^{1/b}(X, 0) dX, \quad (27)$$

provided that $m^{1/b}$ is a well defined function. The last issue may be avoided when b is an integer, as follows. In 1D, higher order differential forms may be created by using the direct, or tensor, product, e.g., $dx \otimes dx = dx^{\otimes 2}$. Consequently, the tensor product of each side of equation (27) b times gives¹

$$m(x, t) dx^{\otimes b} = m(X, 0) dX^{\otimes b}. \quad (28)$$

Taking the partial time derivative of this equation at constant Lagrangian coordinate X and using $dx/dt|_X = u$ yields equation (1) in the form

$$\left. \frac{d}{dt} \right|_X \left(m(x, t) dx^{\otimes b} \right) = (m_t + u m_x + b u_x m) dx^{\otimes b} = 0. \quad (29)$$

Thus, when the parameter b in equation (1) is an integer, it may be regarded geometrically as the number of dimensions that are brought into play by coordinate transformations of the quantity $m dx^{\otimes b}$ associated with m . Cases of equation (1) with negative integer $b < 0$ may be interpreted as

$$\left. \frac{d}{dt} \right|_X \left(m(\partial_x)^{\otimes (-b)} \right) = 0. \quad (30)$$

For example, the case $b = -1$ may be written as²

$$\left. \frac{d}{dt} \right|_X (m \partial_x) = (m_t + u m_x - u_x m) \partial_x = 0, \quad (31)$$

in which the difference of terms $(u m_x - u_x m) \partial_x$ is the commutator of the vector fields $u \partial_x$ and $m \partial_x$ on the real line. The rest of the paper will remain in the Eulerian (spatial) representation.

¹Cases with positive integer values of b will allow m to be a generalized function. Cases with non-integer values of b will revert to equation (27) for which m is required to be a classical function.

²Remarkably, this nonlinear equation for $b = -1$ has stationary plane wave solutions, $u(x) = \cos(kx)$, and exponential solutions, $u(x) = e^{\pm \kappa x}$.

3.8 Reversibility and Galilean covariance

Equation (1) is reversible, i.e., it is invariant under the discrete transformation $u(x, t) \rightarrow -u(x, -t)$. Equation (1) is also Galilean-covariant for all b . In fact, equation (1) keeps its form under transformations to an *arbitrarily* moving reference frame for all b . This includes covariance under transforming to a *uniformly* moving Galilean frame. However, only in the case $b = 0$ is equation (1) Galilean *invariant*, assuming that m Galileo-transforms in the same way as u . If so, then equation (1) transforms under

$$t \rightarrow t + t_0, \quad x \rightarrow x + x_0 + ct, \quad u \rightarrow u + c + u_0, \quad m \rightarrow m + c + u_0, \quad (32)$$

to the form

$$m_t + um_x + bu_x m + u_0 m_x + bu_x(c + u_0) = 0, \quad \text{with} \quad u = g * m. \quad (33)$$

Thus, equation (1) is invariant under space and time translations (constants x_0 and t_0), covariant under Galilean transforms (constant c), and acquires linear dispersion terms under velocity shifts (constant u_0). Equation (1) regains Galilean invariance if m is Galilean invariant. However, the dispersive term $u_0 m_x$ introduced by the constant velocity shift $u_0 \neq 0$ breaks the reversibility of equation (1) even if m is invariant under this shift.

3.9 Integral momentum conservation

Equation (18) implies that $M = \int_{-\infty}^{\infty} m dx$ is conserved for any g when $b = 1$. However, when $g(x)$ is even, the family of equations (1) also conserves the total momentum integral M for any b . This is shown by directly calculating from (1) that

$$\frac{d}{dt} \int_{-\infty}^{\infty} m(x) dx = (1 - b) \int_{-\infty}^{\infty} \int_{-\infty}^{\infty} m(x) g'(x - y) m(y) dx dy = 0, \quad (34)$$

in which the double integral vanishes as the product of an even function and an odd function under interchange of x and y , when $g'(-x) = -g'(x)$. Hence, for even $g(x)$, $M = \int_{-\infty}^{\infty} m dx$ is conserved for either periodic or vanishing boundary conditions and for any b . We shall assume henceforth that $g(x)$ is even and, moreover, that the integral $\int m g * m dx$ is sign-definite, so that it defines a norm (the kinetic energy),

$$\|m\|_g^2 = \int_{-\infty}^{\infty} m g * m dx = \int_{-\infty}^{\infty} \int_{-\infty}^{\infty} m(x) g(x - y) m(y) dx dy \geq 0. \quad (35)$$

This kinetic energy norm is conserved by equation (1), provided $b = 2$.

4 Traveling waves and generalized functions

Its invariance under space and time translations ensures that equation (1) admits traveling wave solutions for any b . Let us write the traveling wave solutions as

$$u = u(z) \quad \text{and} \quad m = m(z), \quad \text{where} \quad z = x - ct, \quad (36)$$

and let prime $'$ denote d/dz .

4.1 Case $b = 0$

4.1.1 Pulsons for $b = 0$

For $b = 0$, equation (1) is Galilean invariant and its traveling wave solutions satisfy

$$(u(z) - c)m'(z) = 0, \quad z = x - ct, \quad (37)$$

where prime $'$ denotes d/dz . Equation (37) admits generalized functions $m'(z) \simeq \delta(z)$ matched by $u - c = 0$ at $z = 0$. The velocity u is given by the integral of the Green's function that relates m and $u = g * m$,

$$u - c \simeq c \left[\int g(y) dy \right]_0^z. \quad (38)$$

4.1.2 Peakons, ramps, and cliffs for $b = 0$

When $g(x) = e^{-|x|/\alpha}$ (the Green's function for the 1D Helmholtz operator), we have $m = u - \alpha^2 u_{xx}$. Consequently, the equation $m' = u' - \alpha^2 u''' = \pm 2\delta(z)$ with $u - c = 0$ at $z = 0$ is satisfied by

$$u - c = \pm c \left[\int e^{-|y|/\alpha} dy \right]_0^z = \pm c \operatorname{sgn}(z) \left(1 - e^{-|z|/\alpha} \right). \quad (39)$$

This represents a rightward moving traveling wave that connects the left states $u - c = \pm c$ to the same two right states.

Definition 4.1 (Peakons) *The symmetric solutions $u = \pm ce^{-|z|/\alpha}$, with a jump in derivative at $z = 0$, are the peakons, for which $m = u - \alpha^2 u_{xx}$ and $g(x) = e^{-|x|/\alpha}$.*

Definition 4.2 (Cliffs) *The antisymmetric solutions $u = \pm c \operatorname{sgn}(z)(1 - e^{-|z|/\alpha})$ (with $u - c = \pm c$ connecting to $u - c = \mp c$), with no jump in derivative at $z = 0$, are the regularized shocks (cliffs). These propagate rightward but may face either leftward or rightward, because equation (1) in the absence of viscosity has no entropy condition that would distinguish between leftward and rightward facing solutions. For more discussion of entropy conditions for the cliff solutions, see [28].*

Definition 4.3 (Ramps) *Equation (1) also has ramp-like similarity solutions $u \simeq x/t$ when $g(x) = e^{-|x|/\alpha}$ for any b . These may emerge in the initial value problem for the peakon case of equation (1) and interact with the peakons and cliffs.*

Remark 4.4 (First integral for $b = 0$ traveling waves) *For $b = 0$, the traveling wave equation (37) apparently has only the first integral for $m = u - \alpha^2 u_{xx}$,*

$$(u - c)(u - \alpha^2 u'') - \frac{u^2}{2} + \frac{\alpha^2}{2} u'^2 = K. \quad (40)$$

Thus, perhaps surprisingly, we have been unable to find a second integral for the traveling wave equation for peakons when $b = 0$.

Remark 4.5 (Reversibility) *Reversibility means that equation (1) is invariant under the transformation $u(x, t) \rightarrow -u(x, -t)$. Consequently, the rightward traveling waves have leftward moving counterparts under the symmetry $c \rightarrow -c$. The case of constant velocity $u = \pm c$ is also a solution.*

Figure 1 shows that the ramp and cliff pattern develops in the velocity profile under the peakon equation (1) with $g(x) = e^{-|x|/\alpha}$ for a set of Gaussian initial conditions $(5\sqrt{\pi})^{-1} \exp(-(x - 50)^2/w)$ of increasing widths $w = 2.5, 5, 10$, for $\alpha = 1$ and $b = 0$. Apparently, the ramp solution is numerically stable, but the coexisting peakon solution is not stable in this case. A complete stability analysis of these various solutions is outside the scope of the present paper. Instead we shall investigate the solutions of equation (1) by numerically integrating selected examples.

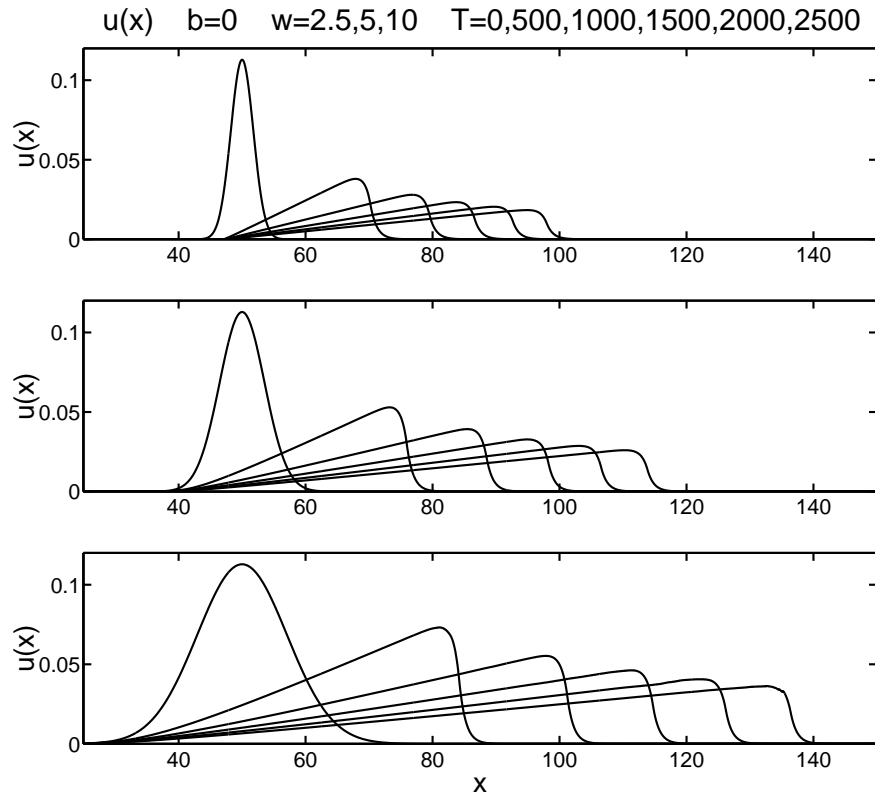


Figure 1: **Ramps and cliffs for $b = 0$.** Inviscid b -family, $b = 0$, $\alpha = 1$, initial width $w = 2.5, 5, 10$.

4.2 Case $b \neq 0$

For $b \neq 0$, the conservation law (18) for traveling waves becomes

$$\left((u - c)m^{1/b}\right)' = 0, \quad (41)$$

which yields after one integration

$$(u - c)^b m = K, \quad (42)$$

where K is the first integral. For $g(x) = e^{-|x|/\alpha}$, so that $m = u - \alpha^2 u_{xx}$, this becomes

$$(u - c)^b (u - \alpha^2 u'') = K. \quad (43)$$

For $u - c \neq 0$ we rewrite this as

$$\alpha^2 u'' = u - K(u - c)^{-b} \quad (44)$$

and integrate again to give the second integral in two separate cases,

$$\alpha^2 u'^2 = \begin{cases} u^2 - \frac{2K}{1-b}(u - c)^{1-b} + 2H & \text{for } b \neq 1, \\ u^2 - 2K \log(u - c) + 2H & \text{for } b = 1. \end{cases}$$

We shall rearrange this into quadratures:

$$\pm \frac{dz}{\alpha} = \frac{du}{\left[u^2 - \frac{2K}{1-b}(u - c)^{1-b} + 2H\right]^{1/2}} \quad \text{for } b \neq 1, \quad (45)$$

and

$$\pm \frac{dz}{\alpha} = \frac{du}{\left[u^2 - 2K \log(u - c) + 2H\right]^{1/2}} \quad \text{for } b = 1. \quad (46)$$

For $b = 1$ and $K \neq 0$, the integral in equation (46) is transcendental.

4.2.1 Special cases of traveling waves for $b \neq 0$

- For $K = 0$ the two quadratures (45) and (46) are equal, independent of b , and elementary, thereby yielding the traveling wave solutions

$$e^{-|z|/\alpha} = \frac{u + \sqrt{u^2 + 2H}}{c + \sqrt{c^2 + 2H}}, \quad (47)$$

with $u - c = 0$ at $z = 0$.

- For $H = 0$ equation (47) recovers the peakon traveling wave.
- For $H > 0$ equation (47) gives a rightward moving traveling wave that is a continuous deformation of the peakon.
- For $H > 0$ and $c = 0$ equation (47) gives stationary solutions of the form

$$u + \sqrt{u^2 + 2H} \simeq e^{-|z|/\alpha}. \quad (48)$$

4.3 Case $b > 0$

4.3.1 Pulsons for $b > 0$

Equation (1) for $b > 0$ has nontrivial solutions vanishing as $|z| \rightarrow \infty$ that allow $K = 0$ in equation (42), so that

$$(u - c)^b m = 0. \quad (49)$$

This admits the generalized function solutions

$$m = c\delta(z) \quad \text{and} \quad u = g * m = cg(z), \quad (50)$$

matched by $u - c = 0$ at $z = 0$. This is the **pulson traveling wave**, whose shape in u is given by the kernel g . The constant velocity case $u = c$ is a trivial traveling wave.

Remark 4.6 (Pulson and peakon traveling waves) *The pulson solution (50) requires $g(0) = 1$ and $g'(0) = 0$. We shall assume for definiteness that the even function $g(z)$ achieves its maximum at $g(0) = 1$, so that the symmetric pulson traveling wave $u(x, t) = cg(x - ct)$ moves at the speed of its maximum, which occurs at its center of symmetry. For example, the peakon $u(x, t) = ce^{-|x-ct|}$ moves at the speed of its peak.*

4.3.2 Peakons for $b > 1$

Equation (43), for which $g(x) = e^{-|x|/\alpha}$, yields the peakon traveling wave,

$$u(z) = ce^{-|z|/\alpha} \quad \text{and} \quad m(z) = u - \alpha^2 u'' = 2c\delta(z/\alpha) \quad (51)$$

when $K = 0$.

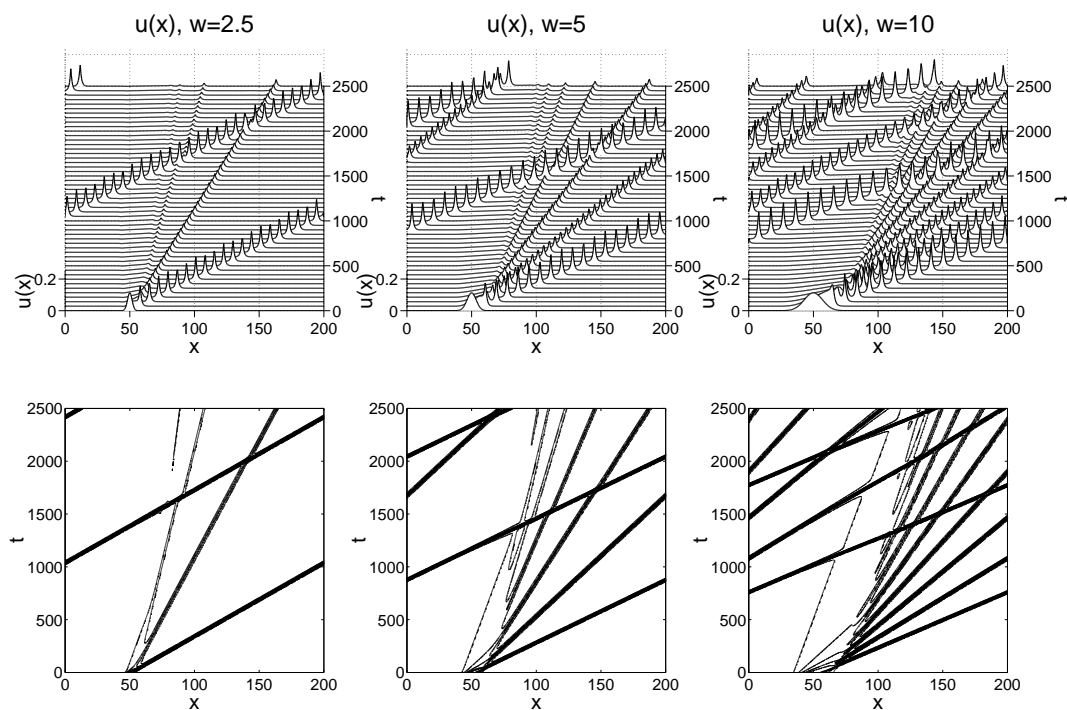


Figure 2: **Peakons** for $b = 2$. Inviscid b -family, $b = 2$, $\alpha = 1$, initial width $w = 2.5, 5, 10$.

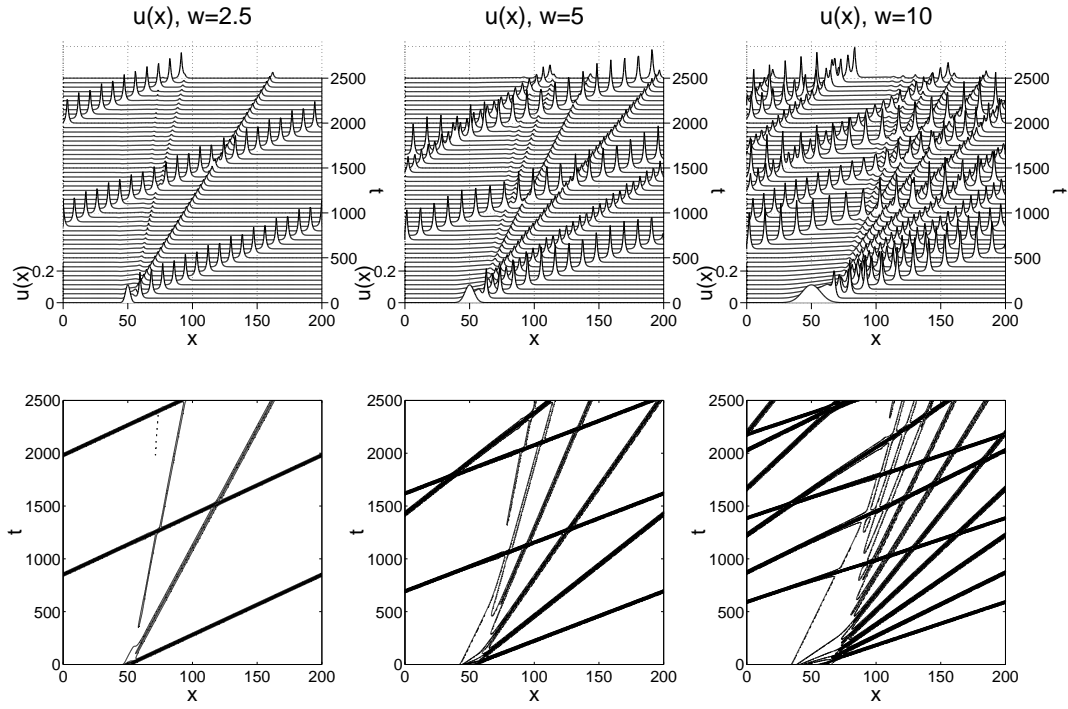


Figure 3: **Peakons for $b = 3$.** Inviscid b -family, $b = 3$, $\alpha = 1$, initial width $w = 2.5, 5, 10$.

Figures 2 and 3 show the effects of varying the width w of a Gaussian initial condition $(5\sqrt{\pi})^{-1} \exp(-(x - 50)^2/w)$ for the peakon equation in a periodic domain, when $\alpha = 1$ and $b = 2, 3$. As the width of the initial Gaussian increases, the figures show that more peakons of width $\alpha = 1$ are emitted. (This is consistent with conservation of momentum.) The peakons are observed to be stable for $b > 1$, they propagate as solitary traveling waves, and they interact elastically. We shall discuss the peakon interactions in more detail in sections 6 through 9.

4.4 Case $b < 0$

We shall examine the cases $b = -0.5, -1, -2, -3, -4$. Numerical results for $b = -2$ and $b = -3$ are described in section 4.4.6. For other values of $b < 0$ the analysis is similar, but it involves less elementary considerations such as transcendental or hyperelliptic functions. The numerics shown later will demonstrate that the elementary solutions discussed here, many of them stationary, do tend to emerge in numerical integrations of the initial value problem for equation (1) with $b \leq -1$.

4.4.1 Case $b = -1/2$

Figure 4 shows that a ramp and cliff pattern develops in the velocity profile under the peakon equation (1) with $g(x) = e^{-|x|/\alpha}$ for a set of Gaussian initial conditions $(5\sqrt{\pi})^{-1} \exp(-(x - 100)^2/w)$ of increasing width $w = 10, 15, 20$, for $\alpha = 1$ and $b = -1/2$. Apparently, the ramp solution is numerically stable for $b = -1/2$.

4.4.2 Case $b = -1$

For $b = -1$, equation (45) becomes

$$\pm \frac{dz}{\alpha} = \frac{du}{\left[u^2 - K(u - c)^2 + 2H \right]^{1/2}}, \quad (52)$$

which integrates to

$$e^{-|z|/\alpha} = \frac{u + \sqrt{u^2 - K(u - c)^2 + 2H} + Kc}{c + \sqrt{c^2 + 2H} + Kc}, \quad (53)$$

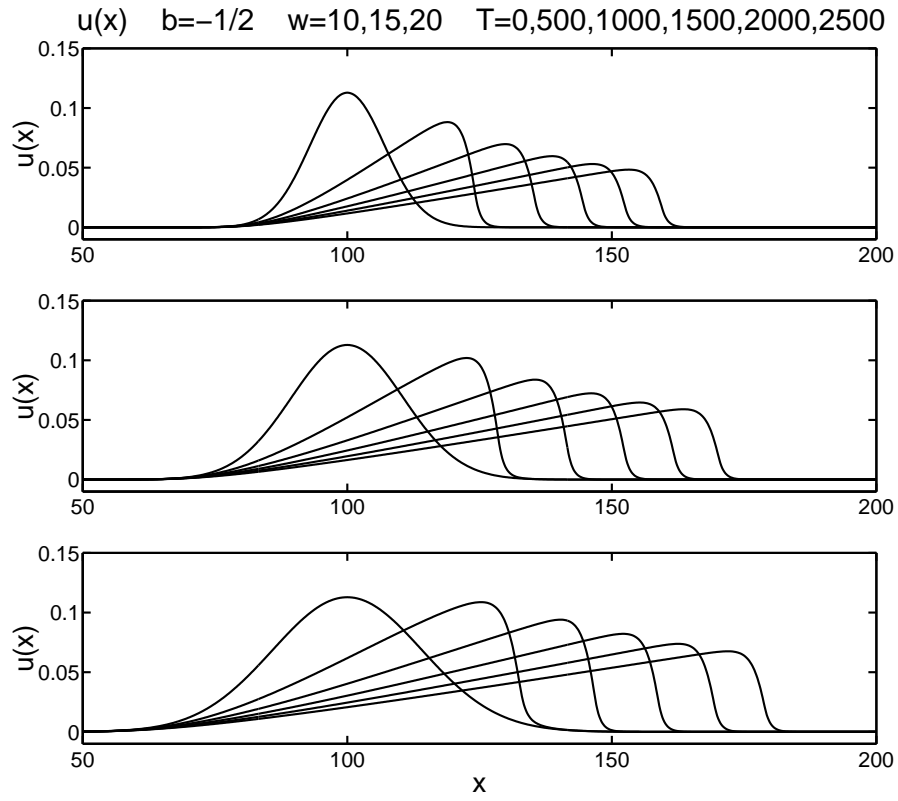


Figure 4: **Ramps and cliffs for $b = -1/2$.** Inviscid b -family, $b = -1/2$, $\alpha = 1$, initial width $w = 10, 15, 20$.

with $u - c = 0$ at $z = 0$. ($K = 0$ and $H = 0$ recovers the peakon traveling wave.)

Remark 4.7 (Stationary plane wave solutions for $b = -1$) Equation (1) for $b = -1$ is satisfied for any wavenumber k by

$$m = \cos(k(x - ct) + \phi_0) \quad \text{and} \quad u = \hat{g}(k) \cos(k(x - ct) + \phi_0), \quad (54)$$

where $\hat{g}(k)$ is the Fourier transform of the kernel $g(x)$ and ϕ_0 is a constant phase shift. In the absence of linear dispersion, these solutions are stationary, $c = 0$. When linear dispersion is added to equation (1), these solutions are the 1D analogs of Rossby waves in the 2D quasigeostrophic equations.

Figure 5 shows the velocity profiles under evolution by the peakon equation, (1) with $g(x) = e^{-|x|/\alpha}$, for a set of Gaussian initial conditions of increasing width $w = 10, 15, 20$ for $\alpha = 1$ and $b = -1$. Evidently, the coexisting peakon solution for $b = -1$ does not emerge because $K \neq 0$ and $H \neq 0$ for this initial condition. Instead, the stable solution is essentially stationary with a slight rightward drift and leaning slightly to the right. The reason for this lethargic propagation becomes clear upon writing the b-equation solely in terms of the velocity $u(x, t)$ as

$$\begin{aligned} u_t + (b + 1)uu_x &= \alpha^2(u_{xxt} + uu_{xxx} + bu_xu_{xx}) \\ &= \alpha^2\partial_x\left(u_{xt} + uu_{xx} + \frac{b-1}{2}u_x^2\right) \\ &= \alpha^2\partial_x^2\left(u_t + uu_x + \frac{b-3}{2}u_x^2\right). \end{aligned} \quad (55)$$

Remark 4.8 ($b = -1$ is a turning point) When $b = -1$ the nonlinear steepening term $(b + 1)uu_x$ vanishes in (55) and the residual propagation is due to its nonlinear “curvature terms” with higher order derivatives. In the parameter regime $b > -1$ (resp. $b < -1$) the solutions of equation (1) or (55) move rightward (resp. leftward), provided the curvature terms on the right hand side of equation (55) are either negative or sufficiently small.

Remark 4.9 (Short wave limit equation) The high wavenumber, or short wave, limit of equation (55) is

$$\partial_x^2\left(u_t + uu_x + \frac{b-3}{2}u_x^2\right) = 0. \quad (56)$$

For $b = 2$ and $\lim_{x \rightarrow -\infty} u_x = 0$, this integrates to become the Hunter-Saxton equation [31]. For $b = 3$, it is the second derivative of the Burgers equation.

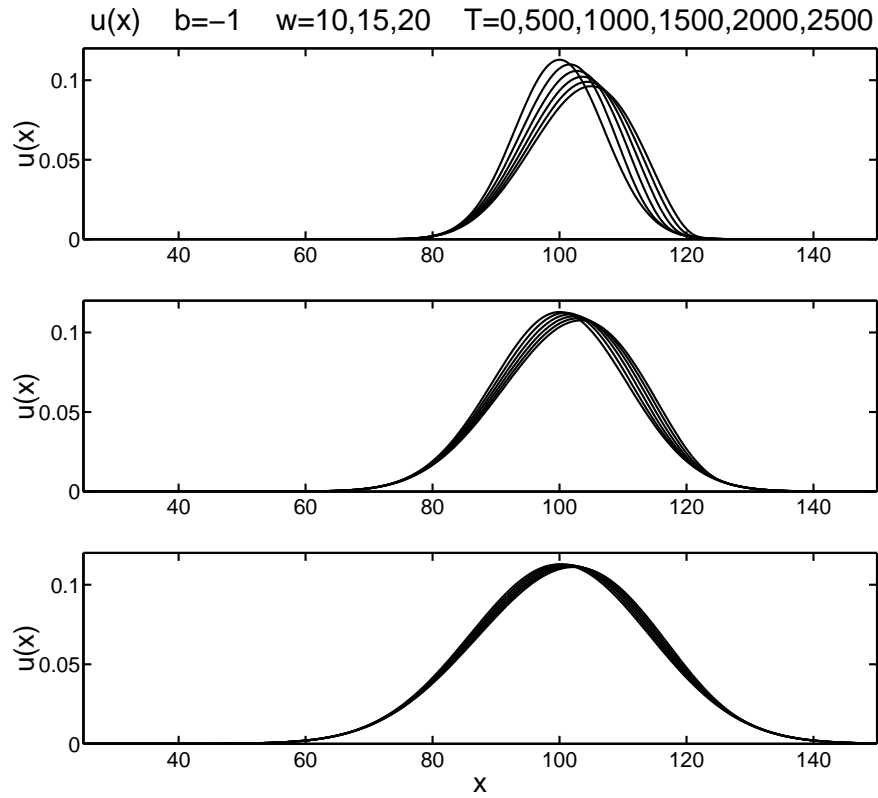


Figure 5: **Nearly-stationary solutions for $b = -1$.** Inviscid b -family, $b = -1$, $\alpha = 1$, initial width $w = 10, 15, 20$.

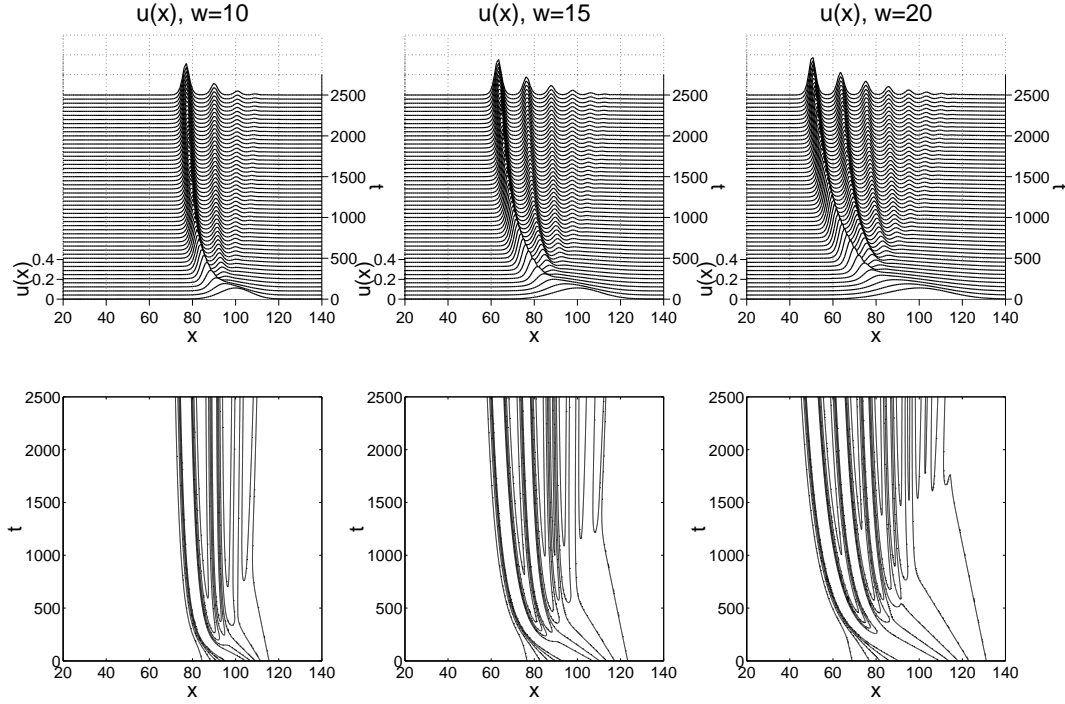


Figure 6: **Stationary solutions for $b = -2$.** Inviscid b -family, $b = -2$, $\alpha = 1$, initial width $w = 10, 15, 20$.

4.4.3 Case $b = -2$ stationary solutions

For $b = -2$, the traveling wave quadrature (45) becomes an elliptic integral,

$$\pm \frac{dz}{\alpha} = \frac{d(u - c)}{\left[u^2 - \frac{2K}{3}(u - c)^3 + 2H \right]^{1/2}}. \quad (57)$$

The hyperbolic limit of this equation for $H = 0$ vanishes at infinity for the stationary solution ($c = 0$) to give

$$u(z) = \frac{3}{2K} \operatorname{sech}^2 \frac{z}{2\alpha}. \quad (58)$$

4.4.4 Case $b = -3$ stationary solutions

For $b = -3$, the hyperbolic limit $H = 0$ of equation (45) is

$$\pm \frac{dz}{\alpha} = \frac{du}{\left[u^2 - \frac{K}{2}(u - c)^4\right]^{1/2}}, \quad (59)$$

which for $c = 0$ is

$$\pm \frac{dz}{\alpha} = \frac{du}{u \left[1 - \frac{K}{2}u^2\right]^{1/2}}, \quad (60)$$

and may be integrated in closed form to obtain a continuous deformation of the peakon,

$$\frac{e^{-|z|/\alpha}}{1 + \sqrt{1 - K/2}} = \frac{u}{1 + \sqrt{1 - Ku^2/2}}, \quad \text{for } b = -3, \ c = 0 \text{ and } H = 0. \quad (61)$$

Rearranging equation (61) and scaling u by u_0 gives,

$$u(z) = \frac{u_0}{\frac{A}{2}e^{|z|/\alpha} + (1 - \frac{A}{2})e^{-|z|/\alpha}}, \quad (62)$$

with $A = 1 + \sqrt{1 - K/2}$, so that $A \in [1, 2]$ for $K \in [0, 2]$. For $A = 1$, we have $u(z) = u_0 \operatorname{sech}(z/\alpha)$. And for $A = 2$, we recover the stationary peakon, $u(z) = u_0 e^{-|z|/\alpha}$.

4.4.5 Case $b = -4$ stationary solutions

For $b \leq -4$ the analytical expressions for the cnoidal waves become less elementary, because the integral in equation (45) is then hyperelliptic. However, our numerics show that the dynamical behavior for $b = -4$ is similar to that of the cases $b = -2$ and $b = -3$ shown in Figures 6-7. Namely, a series of transient leftward propagating pulses, or *leftons*, of width α emerge and tend to a nearly steady state. Consistent with momentum (area) conservation and the tendency toward pulses of width α , the number of emerging leftons increases with the width of the initial Gaussian. At a longer time scale, this train of pulses appears to tend toward stationary ($c \rightarrow 0$).

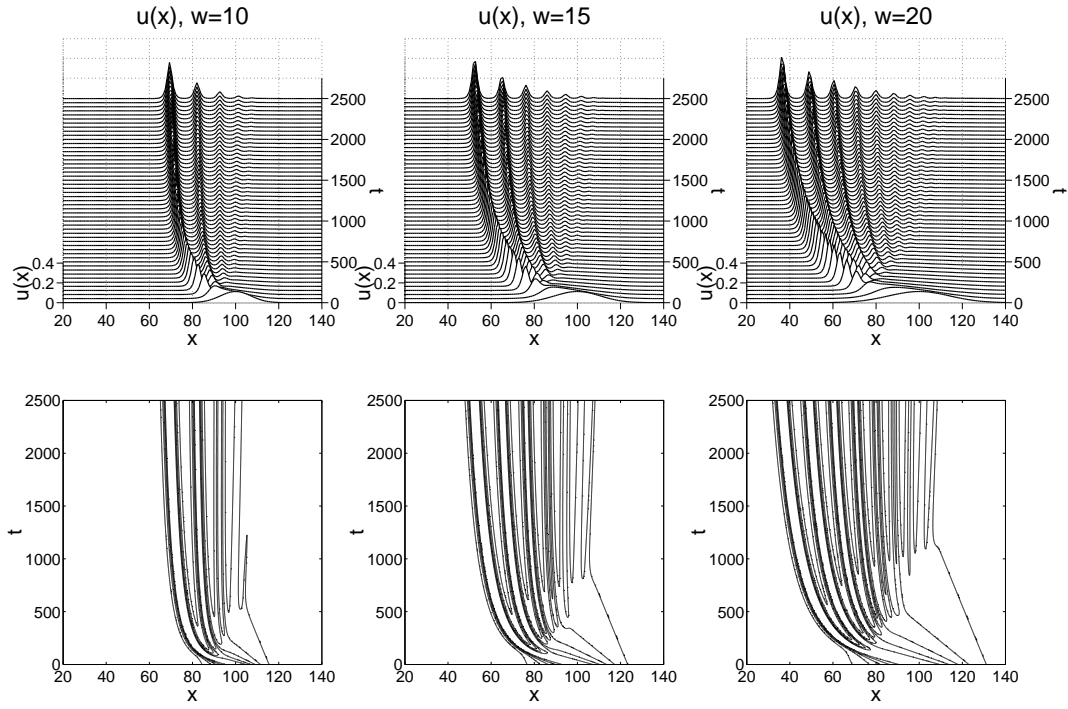


Figure 7: **Stationary solutions for $b = -3$.** Inviscid b -family, $b = -3$, $\alpha = 1$, initial width $w = 10, 15, 20$.

4.4.6 Numerical Results for $b = -2$ and $b = -3$

Figures 6 and 7 show that a series of leftons in the velocity profile emerges under the peakon equation for a set of Gaussian initial conditions of increasing width $w = 10, 15, 20$, for $\alpha = 1$ and $b = -2, -3$. Apparently these are not peakons, because the velocity at which they move is not equal to their height. The leftons emerge from the initial Gaussian in order of height and then tend toward a nearly stationary state. The number of emerging pulses increases with the width of the initial Gaussian, as expected from momentum (area) conservation and the tendency toward pulses of width α , and the leftward speed of the emerging pulses increases with the magnitude of b . The latter is consistent with the coefficient $(b + 1)$ of the nonlinearity in equation (55) as b becomes more negative.

Figure 8 shows the leftons at time $T = 2500$, versus $u(x) \simeq \text{sech}^2(x/(2\alpha))$ for $b = -2$, and versus $u(x) \simeq \text{sech}(x/\alpha)$ for $b = -3$. By this time, the leftons have become stationary solutions with $c = 0$ for both $b = -2$ and $b = -3$.

5 Pulson interactions for $b > 0$

As we have seen in section 4.3.1, the b -family of equations (1) admits the pulson traveling wave solution (50) for $b > 0$. The interaction dynamics among N of these pulsons is obtained by superposing the traveling wave solutions $u(x, t) = cg(x - ct)$ as

$$u(x, t) = \sum_{i=1}^N p_i(t)g(x - q_i(t)) \quad \text{and} \quad m(x, t) = \sum_{i=1}^N p_i(t)\delta(x - q_i(t)), \quad (63)$$

for any $b > 0$ and $u = g * m$, where the function g is even so that $g'(0) = 0$ and bounded and we may set $g(0) = 1$. For these superpositions of pulsons to be exact solutions, the time dependent parameters $p_i(t)$ and $q_i(t)$ must satisfy the following N -dimensional particle dynamics equations obtained by substituting (63) into equation (1),

$$\dot{p}_i = (1 - b) p_i \sum_{j=1}^N p_j g'(q_i - q_j) = (1 - b) \frac{\partial G_N}{\partial q_i}, \quad (64)$$

$$\dot{q}_i = \sum_{j=1}^N p_j g(q_i - q_j) = \frac{\partial G_N}{\partial p_i}. \quad (65)$$

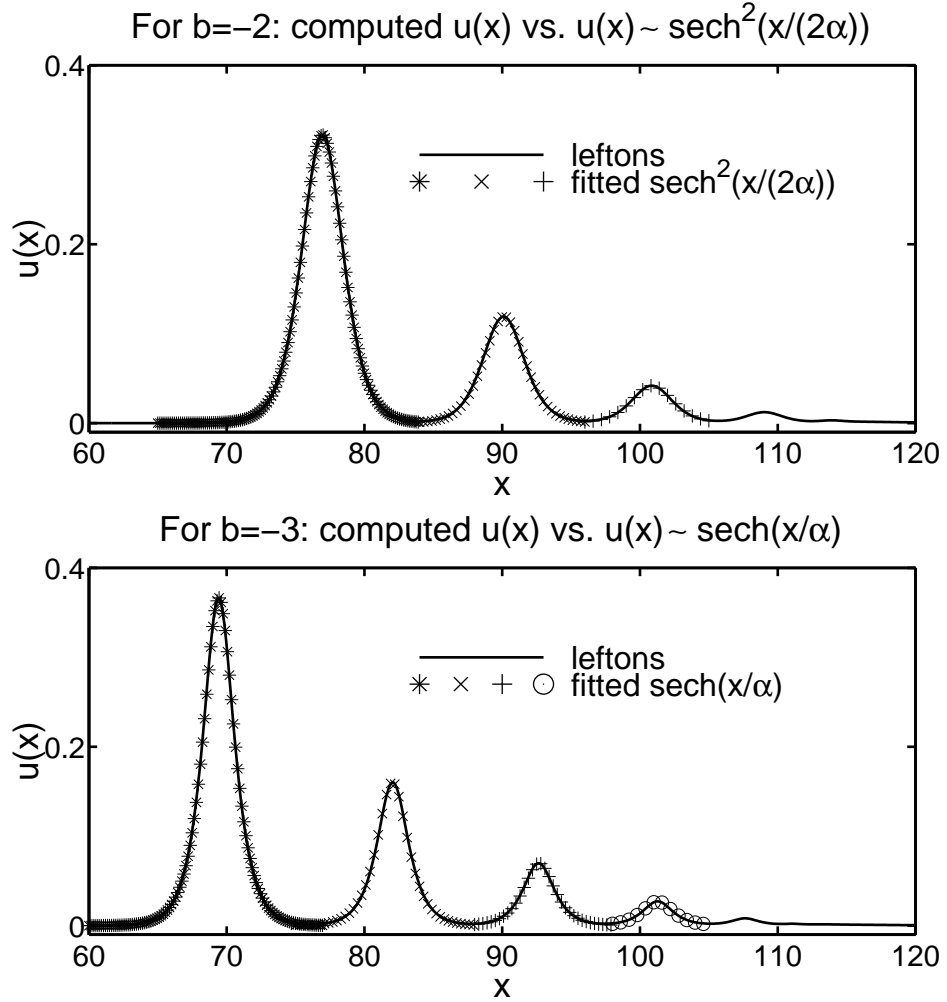


Figure 8: **Stationary solutions for $b = -2$ versus $u(x) \simeq \text{sech}^2(x/(2\alpha))$, and for $b = -3$ versus $u(x) \simeq \text{sech}(x/\alpha)$.** Inviscid b -family, $b = -2, -3$, $\alpha = 1$, initial width $w = 10$.

Here the generating function G_N is obtained by restricting the norm $\|m\|_g^2$ in (35) to the class of superposed traveling wave solutions (63), as

$$G_N = \frac{1}{2} \sum_{i,j=1}^N p_i p_j g(q_i - q_j). \quad (66)$$

Thus, the symmetric kernel $g(x)$ determines the shape of the traveling wave solutions (63), and these traveling waves interact nonlinearly via the pulson dynamics of $p_i(t)$ and $q_i(t)$ with $i = 1, \dots, N$ in equations (64) and (65) for $b > 0$. We shall see that the character of these interactions depends vitally on the value of b .

5.1 Pulson interactions for $b = 2$

When $b = 2$, equations (64) and (65) describe the canonical dynamics of a Hamiltonian system with N degrees of freedom. These are the geodesic pulson equations studied in Fringer and Holm [22], in which the following results are obtained:

- Equation (1) conserves the kinetic energy $\frac{1}{2}\|m\|_g^2 = \frac{1}{2} \int_{-\infty}^{\infty} m g * m dx$.
- Equations (64) and (65) describe canonical geodesic motion in an N -dimensional configuration space whose co-metric is $g^{ij}(q) = g(q_i - q_j)$.
- The generating function G_N is the kinetic energy Hamiltonian for the canonical geodesic motion.
- The solutions in (63) behave as particle-like pulses whose pairwise interactions as determined by equations (64) and (65) comprise nonlinear, but elastic, scattering events.
- The pairwise interactions for the pulsions can be solved analytically for any symmetric function $g(x)$.

Remark 5.1 *As we shall show, the last two statements also hold for any $b > 1$.*

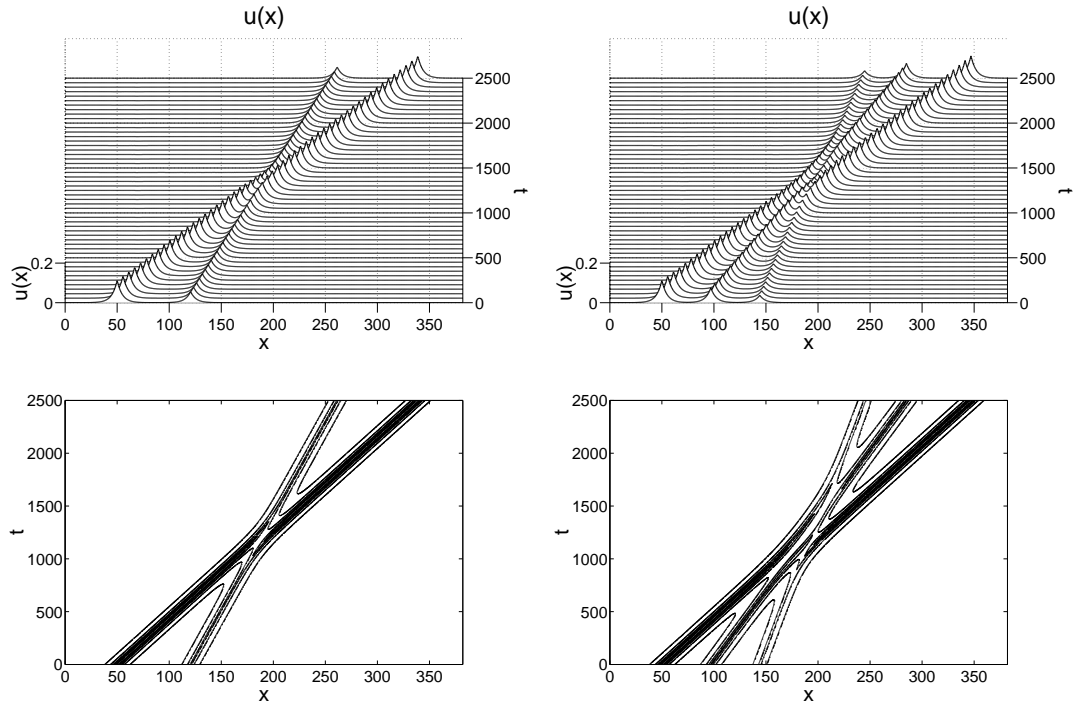


Figure 9: **Peakons of width α for $b = 2$: collisions.** Inviscid b -family, $b = 2$, $\alpha = 5$, initial width $w = 5$.

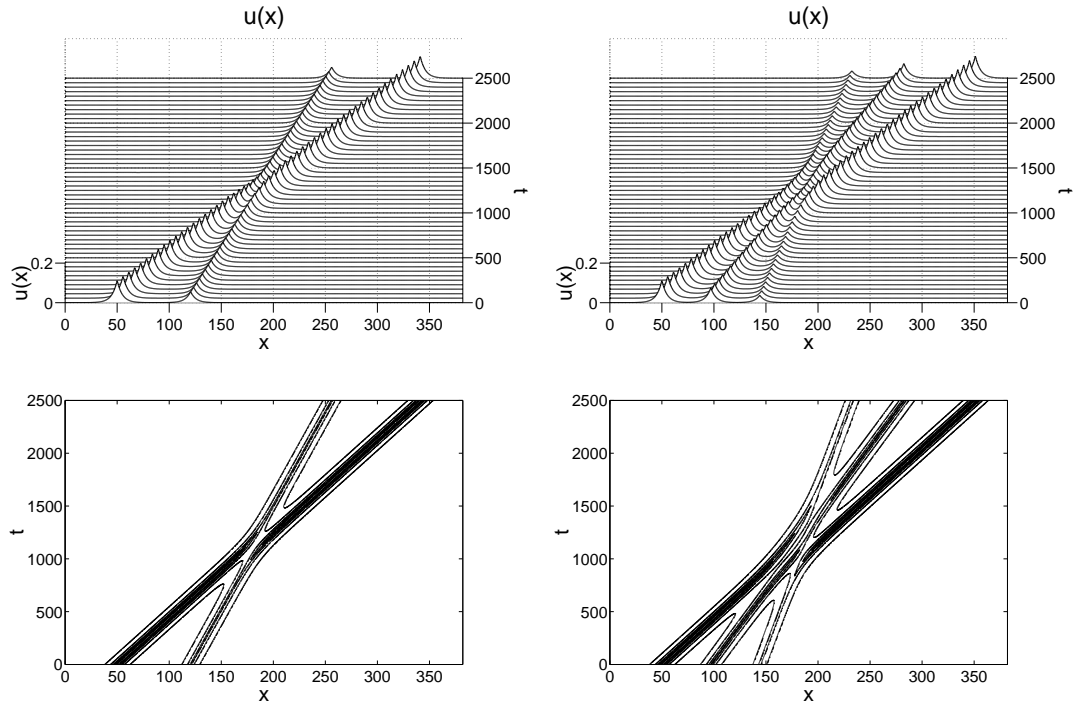


Figure 10: **Peakons of width α for $b = 3$: collisions.** Inviscid b -family, $b = 3$, $\alpha = 5$, initial width $w = 5$.

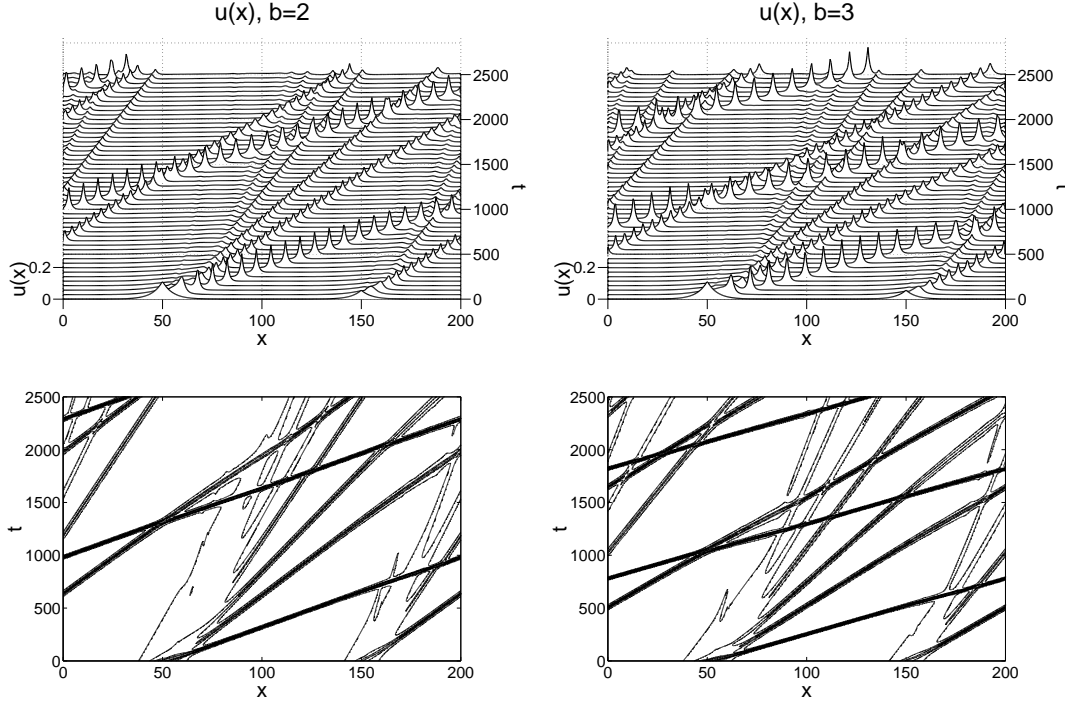


Figure 11: **Peakons of width $> \alpha$ for $b = 2, 3$: emergence of width- α peakons.** Inviscid b -family, $b = 2, 3$, $\alpha = 1$, initial width $w = 5$.

5.2 Peakon interactions for $b = 2$ and $b = 3$: numerical results

- Figure 9 shows the evolution of the velocity profiles in the 2-peakon and 3-peakon interactions for $b = 2$, with $g(x) = e^{-|x|/\alpha}$ and a periodic domain. The 3-peakon interaction decomposes into a series of 2-peakon interactions. These simulations verify the analytical results for the 2-peakon interaction to three significant figures over propagation distances of about sixty peakon widths.
- Figure 10 shows the evolution of the velocity profiles in the 2-peakon and 3-peakon interactions for $b = 3$, with $g(x) = e^{-|x|/\alpha}$ and a periodic domain.

- Figure 11 shows that peakons of initial width greater than α break up into peakons of width α under the evolution of the peakon equation in a periodic domain at fixed values of $\alpha = 1$ and $b = 2, 3$. The emitted peakons are stable, propagate as solitary traveling waves, and interact elastically. Conversely, a peakon or other initial condition that is narrower than α will decompose into two oppositely moving trains of peakons and antipeakons, each of width α .

5.3 Pulson-Pulson interactions for $b > 0$ and symmetric g

For $N = 2$, the pulson dynamics in equations (64) and (65) for $b > 0$ reduces to

$$\frac{dp_1}{dt} = (1 - b) \frac{\partial G}{\partial q_1}, \quad \frac{dp_2}{dt} = (1 - b) \frac{\partial G}{\partial q_2}, \quad (67)$$

$$\frac{dq_1}{dt} = \frac{\partial G}{\partial p_1}, \quad \frac{dq_2}{dt} = \frac{\partial G}{\partial p_2}, \quad (68)$$

and the generating function from (66) is given by

$$G = \frac{1}{2}(p_1^2 + p_2^2) + p_1 p_2 g(q_1 - q_2). \quad (69)$$

The equations are canonically Hamiltonian only for $b = 2$, which includes the Camassa-Holm case for which $g(q_1 - q_2) = e^{-|q_1 - q_2|}$ gives the peakon solutions.

Conservation laws and reduction to quadrature

Besides the total momentum

$$P = p_1 + p_2, \quad (70)$$

the two-pulson system for $b > 0$ and symmetric g also conserves a second quantity that is quadratic in p_1 and p_2 , namely

$$H = p_1 p_2 (1 - g(q_1 - q_2))^{b-1}. \quad (71)$$

For a Hamiltonian system with two degrees of freedom this second conservation law would be enough to ensure integrability, by Liouville's theorem.

Even in the present case of $b > 0$ without a Hamiltonian structure, this will be sufficient to reduce the 2-pulson system to quadratures.³

Following the analysis for the case $b = 2$ and arbitrary g in Fringer and Holm [22], we introduce sum and difference variables as

$$P = p_1 + p_2, \quad Q = q_1 + q_2, \quad p = p_1 - p_2, \quad q = q_1 - q_2. \quad (72)$$

In these variables, the generating function (69) becomes

$$G = \frac{1}{4}P^2(1 + g(q)) + \frac{1}{4}p^2(1 - g(q)), \quad (73)$$

and the second constant of motion (71) becomes

$$H = \frac{1}{4}(P^2 - p^2)(1 - g(q))^{b-1}. \quad (74)$$

Likewise, the 2-pulson equations of motion transform to sum and difference variables as

$$\begin{aligned} \frac{dP}{dt} &= 2(1 - b)\frac{\partial G}{\partial Q} = 0, \\ \frac{dQ}{dt} &= 2\frac{\partial G}{\partial P} = P(1 + g(q)), \\ \frac{dp}{dt} &= 2(1 - b)\frac{\partial G}{\partial q} = \frac{1}{2}(1 - b)(P^2 - p^2)g'(q), \\ \frac{dq}{dt} &= 2\frac{\partial G}{\partial p} = p(1 - g(q)). \end{aligned}$$

Eliminating p^2 between the formula for H and the equation of motion for q yields

$$\left(\frac{dq}{dt}\right)^2 = P^2(1 - g(q))^2 - 4H(1 - g(q))^{3-b}. \quad (75)$$

We rearrange this into the following quadrature,

$$dt = \frac{dg(q)}{g'(q)\sqrt{Z}}, \quad Z = P^2(1 - g(q))^2 - 4H(1 - g(q))^{3-b}. \quad (76)$$

This simplifies to the quadratic $Z = P^2(1 - g(q))^2 - 4H$ when $b = 3$. For the peakon case, we have $g(q) = e^q$ so that $g'(q) = g(q)$ and the quadrature (76) simplifies to an elementary integral for $b = -1, 0, 1, 2, 3$. Having obtained

³When $b = 1$, the momenta p_1 and p_2 are separately conserved and the problem immediately reduces to quadratures in $q = q_1 - q_2$ and $Q = q_1 + q_2$.

$q(t)$ from the quadrature, the momentum difference $p(t)$ is found from (74) via the algebraic expression

$$p^2 = P^2 - \frac{4H}{(1 - g(q))^{b-1}}, \quad (77)$$

in terms of q and the constants of motion P and H . Finally, the sum $Q(t)$ is found by a further quadrature. The remainder of the solution for arbitrary b and g closely follows Fringer and Holm [22] for the case $b = 2$.

Upon writing the quantities H , P and G as

$$H = c_1 c_2, \quad P = c_1 + c_2, \quad G = \frac{1}{2}c_1^2 + \frac{1}{2}c_2^2 = \frac{1}{2}P^2 - H, \quad (78)$$

in terms of the asymptotic speeds of the pulsons, c_1 and c_2 , we find the relative momentum relation,

$$p^2 = (c_1 + c_2)^2 - \frac{4c_1 c_2}{(1 - g(q))^{b-1}}. \quad (79)$$

This equation has several implications for the qualitative properties of the 2-pulson collisions.

Definition 5.2 *Overtaking, or rear-end, pulson collisions satisfy $c_1 c_2 > 0$, while head-on pulson collisions satisfy $c_1 c_2 < 0$.*

The pulson order $q_1 < q_2$ is preserved in an overtaking, or rear-end, collision when $b > 1$. This follows, as

Proposition 5.3 (Preservation of pulson order) *For overtaking, or rear-end, collisions when $b > 1$, the 2-pulson dynamics preserves the sign condition $q = q_1 - q_2 < 0$.*

Proof. Suppose the peaks were to overlap in a collision for $b > 1$, thereby producing $q = 0$ during a collision. The condition $g(0) = 1$ implies that the second term in (79) diverges for $b > 1$ when the overlap occurs. However, this divergence would contradict $p^2 \geq 0$. \square

Consequently, seen as a collision between two initially well-separated “particles” with initial speeds c_1 and c_2 , the separation $q(t)$ reaches a nonzero distance of closest approach q_{min} in an overtaking, or rear-end, collision that may be expressed in terms of the pulse shape as,

Corollary 5.4 (Minimum separation distance) *The minimum separation distance reachable in two-pulson collisions with $c_1 c_2 > 0$ is given by*

$$(1 - g(q_{\min}))^{b-1} = \frac{4c_1 c_2}{(c_1 + c_2)^2}. \quad (80)$$

Proof. Set $p^2 = 0$ in equation (79). \square

Remark 5.5 *We shall use result (80) later in checking the accuracy of our numerical simulations of these two-pulson interactions.*

Proposition 5.6 (Head-on collisions admit $q \rightarrow 0$) *The 2-pulson dynamics allows the overlap $q \rightarrow 0$ when $b > 1$ in head-on collisions.*

Proof. Because $p^2 \geq 0$, the overlap $q \rightarrow 0$ implying $g \rightarrow 1$ is only possible in equation (79) with $b > 1$ for $c_1 c_2 < 0$. That is, for the case of head-on collisions. \square

Remarks about head-on collisions. For $b > 1$, equation (79) implies that $p^2 \rightarrow \infty$ diverges when $q \rightarrow 0$ in head-on collisions. The case $b = 1$ is regular and equation (79) reduces to the constant relation $p^2 = (c_1 - c_2)^2$. For $0 < b < 1$, the quantity p^2 no longer diverges when $q \rightarrow 0$ and the solution for the relative momentum in head-on collisions is again regular.

5.4 Pulson-antiPulson interactions for $b > 1$ and symmetric g

Head-on Pulson-antiPulson collision. We consider the special case of *completely antisymmetric* pulson-antipulson collisions, for which $p_1 = -p_2 = p/2$ and $q_1 = -q_2 = q/2$ (so that $P = 0$ and $Q = 0$). In this case, the quadrature formula (76) reduces to⁴

$$\pm(t - t_0) = \frac{1}{\sqrt{-4H}} \int_{q(t_0)}^{q(t)} \frac{dq'}{(1 - g(q'))^{(3-b)/2}}, \quad (81)$$

⁴For $b = 3$, the quadrature formula (81) for the separation distance in the pulson-antipulson collision reduces to straight line motion, $q(t) - q(t_0) = \pm 2c(t - t_0)$.

and the second constant of motion in (74) satisfies

$$-4H = p^2(1 - g(q))^{b-1}. \quad (82)$$

After the collision, the pulson and antipulson separate and travel oppositely apart; so that asymptotically in time $g(q) \rightarrow 0$, $p \rightarrow 2c$, and $H \rightarrow -c^2$, where c (or $-c$) is the asymptotic speed (and amplitude) of the pulson (or antipulson). Setting $H = -c^2$ in equation (82) gives a relation for the pulson-antipulson (p, q) phase trajectories for any kernel,

$$p = \pm \frac{2c}{(1 - g(q))^{(b-1)/2}}. \quad (83)$$

Notice that p diverges for $b > 1$ (and switches branches of the square root) when $q \rightarrow 0^+$, because $g(0) = 1$. In contrast, p remains constant for $b = 1$ and vanishes for $b < 1$ (and again switches branches of the square root) when $q \rightarrow 0^+$. Note that our convention for switching branches of the square root allows us to keep $q > 0$ throughout, so the particles retain their order.

Remark about preservation of particle identity in collisions. The relative separation distance $q(t)$ in pulson-antipulson collisions is determined by following a phase point along a level surface of the second constant of motion H in the phase space with coordinates (q, p) . Because H is quadratic, the relative momentum p has two branches on such a level surface, as indicated by the \pm sign in equation (83). At the pulson-antipulson collision point, both $q \rightarrow 0^+$ and either $1/p \rightarrow 0^+$ or $p \rightarrow 0^+$, so following a phase point through a collision requires that one must choose a convention for which branch of the level surface is taken after the collision. Taking the convention that p changes sign (corresponding to a “bounce”), but q does not change sign (so the “particles” keep their identity) is convenient, because it allows the phase points to be followed more easily through multiple collisions. This choice is also consistent with the pulson-pulson and antipulson-antipulson collisions. In these other “rear end” collisions, as implied by equation (79), the separation distance always remains positive and again the particles retain their identity.

Theorem 5.7 (Pulson-antiPulson exact solution) *The exact analytical solution for the pulson-antipulson collision for any b and any symmetric g*

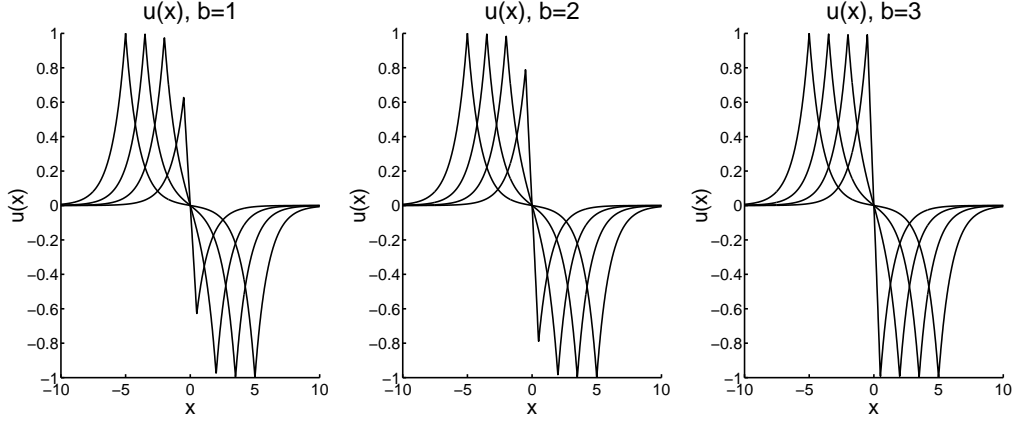


Figure 12: **Peakon-antipeakon collisions for $b = 1, 2, 3$.** Inviscid b -family, $b = 1, 2, 3$, $\alpha = 1$, initial width $w = 1$.

may be written as a function of position x and the separation between the pulses q for any pulse shape or kernel $g(x)$ as

$$u(x, q) = \frac{c}{(1 - g(q))^{(b-1)/2}} \left[g(x + q/2) - g(x - q/2) \right], \quad (84)$$

where c is the pulson speed at sufficiently large separation and the dynamics of the separation $q(t)$ is given by the quadrature (81) with $\sqrt{-4H} = 2c$.

Proof. The solution (63) for the velocity $u(x, t)$ in the head-on pulson-antipulson collision may be expressed in this notation as

$$u(x, t) = \frac{p}{2}g(x + q/2) - \frac{p}{2}g(x - q/2). \quad (85)$$

In using equation (83) to eliminate p this solution becomes equation (84). \square

Figure 12 shows the exact solutions for the Peakon-antiPeakon collision in the cases $b = 1$, $b = 2$, and $b = 3$. The positive and negative peaks approach each other until the solution develops a negative vertical slope in finite time. As the separation $q \rightarrow 0$, the positive and negative peaks “bounce,” thereby reversing polarity, after which they separate in opposite directions.

5.5 Specializing Pulsons to Peakons for $b = 2$ and $b = 3$

We now restrict to $g(x) = e^{-|x|}$, the Green's function for the 1D Helmholtz operator satisfying

$$\left(1 - \frac{d^2}{dx^2}\right)e^{-|x|} = 2\delta(x). \quad (86)$$

In this case, $m = u - \alpha^2 u_{xx}$, the pulson traveling wave solution is given by $u(x, t) = cg(x - ct) = ce^{-|x-ct|}$, has a discontinuity in derivative at its peak, and is called the peakon. For $b = 2$ and $b = 3$ in the peakon case, the main results are:

- For $b = 2$ and $g(x) = e^{-|x|}$, equation (1) becomes the zero-dispersion limit of the integrable Camassa-Holm equation for shallow water waves discovered in Camassa and Holm [7]. Upon restoring its linear dispersion, this equation was recently proved to be a higher-order accurate asymptotic description of shallow water waves in Dullin et al. [17].
- For $b = 3$ and $g(x) = e^{-|x|}$, equation (1) becomes the integrable partial differential equation studied in Degasperis, Holm and Hone [15].
- When $g(x) = e^{-|x|}$ the N -peakon dynamics for both $b = 2$ and $b = 3$ turns out to be integrable – as is the dynamics of the original PDE (1). The solutions of the initial value problem for (1) for both $b = 2$ and $b = 3$ may be found analytically by using the Isospectral Scattering Transform (IST) method.
- The two cases $b = 2$ and $b = 3$ have quite different isospectral eigenvalue problems. These are discussed in Camassa and Holm [7] and in Dullin et al. [17] for the case $b = 2$, and in Degasperis, Holm and Hone [15] for the case $b = 3$. See also Beals, Sattinger and Smigajski [6] for a discussion of solving the inverse isospectral problem using classical methods for the case $b = 2$ for initial momentum distributions $m(x, 0)$ of a single sign.

6 Peakons of width α for arbitrary b

When $g = e^{-|x|/\alpha}$, we may invert the velocity-momentum relation $u = g * m$ by using the Green's function expression (86) with the Helmholtz operator

to find $m = u - \alpha^2 u_{xx}$. Hence, equation (1) may be rearranged into the local **momentum conservation law**,

$$m_t = -\frac{\partial}{\partial x} \left(mu + \frac{b-1}{2} u^2 - \frac{b-1}{2} \alpha^2 u_x^2 \right). \quad (87)$$

This conservation law for peakons may also be rewritten in **convection form**,

$$u_t + uu_x = -\tau_x \quad \text{with} \quad (1 - \alpha^2 \partial_x^2) \tau = \frac{b}{2} u^2 + \frac{3-b}{2} \alpha^2 u_x^2. \quad (88)$$

The two forms (87) and (88) of the b-family of equations (1) suggest that values $b = 0, 1, 3$ are special. These values of b are natural candidates for boundaries, or bifurcation points for changes in solution behavior.

Equation (88) describes peakons of shape $g(x) = e^{-|x|/\alpha}$. This peakon equation will form the basis of the rest of our study.

6.1 Slope dynamics for Peakons: inflection points and the steepening lemma when $1 < b \leq 3$

We shall consider solution dynamics of equation (88) in the peakon case satisfying (51), or equivalently, equation (1) with $g(x) = e^{-|x|/\alpha}$, which satisfies

$$(1 - \alpha^2 \partial_x^2) e^{-|x|/\alpha} = 2\alpha \delta(x). \quad (89)$$

For this case, and with vanishing boundary conditions at spatial infinity, equations (88) and (89) imply the peakon equation on the real line,

$$u_t + uu_x = -\frac{1}{2\alpha} \int_{-\infty}^{\infty} e^{-|x-y|/\alpha} \left(buu_y + (3-b)\alpha^2 u_y u_{yy} \right) dy. \quad (90)$$

Taking the x -derivative gives the equation for the slope $u_x(x, t)$

$$\begin{aligned} u_{xt} + uu_{xx} + u_x^2 &= -\frac{1}{2\alpha} \frac{\partial}{\partial x} \int_{-\infty}^{\infty} e^{-|x-y|/\alpha} \left(buu_y + (3-b)\alpha^2 u_y u_{yy} \right) dy \\ &= \frac{1}{2\alpha^2} \int_{-\infty}^{\infty} e^{-|x-y|/\alpha} \operatorname{sgn}(x-y) \left(buu_y + (3-b)\alpha^2 u_y u_{yy} \right) dy. \end{aligned} \quad (91)$$

We shall use these expressions to prove the following.

Proposition 6.1 (Peakon Steepening Lemma) *For b in the range $1 < b \leq 3$ a sufficiently negative slope at an inflection point of u will become vertical in finite time under the dynamics of the peakon equation (90).*

Proof. Following Camassa and Holm [7], we shall consider the evolution of the slope u_x at an inflection point $x = \bar{x}(t)$. Define the slope at the inflection point as $s(t) = u_x(\bar{x}(t), t)$ and note that $u_{xx}(\bar{x}(t), t) = 0$. Then equation (91) yields the following evolution equation for $s(t)$

$$\frac{ds}{dt} + s^2 = \frac{1}{2\alpha^2} \int_{-\infty}^{\infty} e^{-|\bar{x}(t)-y|/\alpha} \operatorname{sgn}(\bar{x}(t) - y) \frac{1}{2} \frac{\partial}{\partial y} \left(bu^2 + (3-b)\alpha^2 u_y^2 \right) dy \quad (92)$$

Integrating by parts using the definition $|y| = y \operatorname{sgn}(y)$, so that $d|y|/dy = \operatorname{sgn}(y) + 2y\delta(y)$, and recalling that $y\delta(y) = 0$, gives

$$\frac{ds}{dt} = - \left(\frac{b-1}{2} \right) s^2 + \frac{b}{2\alpha^2} u^2 - \frac{1}{2\alpha^2} \int_{-\infty}^{\infty} e^{-|\bar{x}(t)-y|/\alpha} \frac{1}{2\alpha} \left(bu^2 + (3-b)\alpha^2 u_y^2 \right) dy$$

Hence, in the range $0 \leq b \leq 3$ the last term is negative and we have the slope inequality,

$$\frac{ds}{dt} \leq - \left(\frac{b-1}{2} \right) s^2 + \frac{b}{2\alpha^2} u^2 \quad \text{for } 0 \leq b \leq 3. \quad (93)$$

We suppose the solution satisfies $(bu^2/\alpha^2) < M$ for some constant M .⁵ Then,

$$\frac{ds}{dt} \leq - \left(\frac{b-1}{2} \right) s^2 + \frac{M}{2} \quad \text{for } 0 \leq b \leq 3. \quad (94)$$

Consequently, if $b > 1$,

$$\frac{dX}{1-X^2} = d \coth^{-1}(X) \leq \sqrt{M} \quad \text{for } X = \sqrt{\frac{b-1}{M}} s. \quad (95)$$

This implies, for $s \leq -\sqrt{M}$ initially negative, that

$$s \leq \sqrt{M} \coth \left(\sigma + \sqrt{\frac{b-1}{M}} \frac{M}{2} t \right) \quad \text{for } 1 < b \leq 3, \quad (96)$$

where the dimensionless integration constant $\sigma < 0$ determines the initial slope, which is negative. Under these circumstances, the slope at the inflection point must become vertical by time $t = -2\sigma/\sqrt{M(b-1)}$. \square

⁵If this inequality is violated, we have another type of singularity. However, for $b = 2$, the constant M can be estimated by using a Sobolev inequality. In fact, $M = 4H_1(u)/\alpha^2$ because for this case we have

$$\max_{x \in \mathbf{R}} [u^2(x, t)] \leq \frac{1}{\alpha} \int_{-\infty}^{\infty} (u^2 + \alpha^2 u_x^2) dx = 2H_1 = \text{const} \quad \text{for } b = 2.$$

Remarks for $1 < b \leq 3$.

- If the initial condition is antisymmetric, for $1 < b \leq 3$, then the inflection point at $u = 0$ is fixed and $d\bar{x}/dt = 0$, due to the mirror reflection symmetry $(u, x) \rightarrow (-u, -x)$ admitted by equation (90). In this case, $M = 0$ and equation (94) implies

$$\frac{ds}{dt} \leq -\left(\frac{b-1}{2}\right)s^2 \quad \Rightarrow \quad s(t) \leq \frac{-2}{b-1}\left(\frac{1}{t_0-t}\right). \quad (97)$$

Hence, verticality $s = -\infty$ will develop in finite time, regardless of how small the initial slope $|s(0)|$, provided it is negative, $s(0) < 0$, as in figure 12. If the initial slope is positive, then under this evolution it will relax to zero from above.

- Consequently, traveling wave solutions of (90) cannot have the usual sech-like shape for solitons because inflection points with sufficiently negative slope can produce unsteady changes in the shape of the solution profile.
- In this context, for $b = 2$, a result in the paper [11] shows that the slope of the solution $u(x, t)$ is always bounded if the initial distribution of momentum $m(x, 0)$ does not change sign.

Caveat Strictly speaking, the formal proof of the Peakon Steepening Lemma in Proposition 6.1 requires additional regularity assumptions on the initial data, since the slope function $s(t)$ is generally not differentiable. However, provided that the initial data is regular enough, e.g., initial velocity in the Sobolev space $u(x, 0) \in H^2(R)$, this formal argument can be made rigorous. See Theorem 2.1 in [12] for an example. Under this additional regularity assumption, one finds that equations (93) and (94) in the proof hold almost everywhere in time, but the result of the Proposition (96) holds everywhere.

6.2 Cases $0 \leq b \leq 1$

In the range $0 \leq b \leq 1$, we have from (25) that

$$\int_{-\infty}^{\infty} |m|^{1/b} dx = \int_{-\infty}^{\infty} |m_0|^{1/b} dx, \quad \text{where} \quad m_0(x) = m(x, 0). \quad (98)$$

This conservation law implies an elliptic regularity estimate showing that the slope $s = u_x$ is always bounded under the dynamics of the peakon equation (90). See [30] for a proof of this result and more discussion of its implications.

7 Adding viscosity to peakon dynamics

In the remainder of this paper, we shall restrict our one-dimensional considerations to the peakon case $g(x) = e^{-|x|/\alpha}$ with length scale α , and investigate the fate of the peakon solutions when viscosity is introduced for given values of b and α . For purposes of comparison with previous results in the literature, we shall also extend equation (1) to a new family of equations that includes the Burgers equation by introducing two additional real parameters. These are the viscosity ν and a multiplier β for the stress, or pressure gradient.

First, we shall introduce constant viscosity $\nu > 0$ into (1) to form the viscous b-family of equations for the peakon case $g(x) = e^{-|x|/\alpha}$, as follows,

$$m_t + \underbrace{um_x}_{\text{convection}} + \underbrace{bu_xm}_{\text{stretching}} = \underbrace{\nu m_{xx}}_{\text{viscosity}}, \quad \text{with } m = u - \alpha^2 u_{xx}. \quad (99)$$

As in equation (55), this equation with viscosity may be expressed solely in terms of the velocity $u(x, t)$ as

$$\begin{aligned} u_t + (b+1)uu_x - \nu u_{xx} &= \alpha^2(u_{xxt} + uu_{xxx} + bu_xu_{xx} - \nu u_{xxxx}) \quad (100) \\ &= \alpha^2 \partial_x \left(u_{xt} + uu_{xx} - \nu u_{xxx} + \frac{b-1}{2} u_x^2 \right) \\ &= \alpha^2 \partial_x^2 \left(u_t + uu_x - \nu u_{xx} + \frac{b-3}{2} u_x^2 \right). \end{aligned}$$

Thus, the nonlinear steepening term increases with b as $(b+1)uu_x$. When $\alpha \rightarrow 0$ the previous equation reduces to

$$u_t + (b+1)uu_x - \nu u_{xx} = 0, \quad (101)$$

and one then recovers the usual **Burgers equation** either by rescaling dimensions, or by setting $b = 0$. For $b = 2$, equation (99) is the one-dimensional version of the three-dimensional Navier-Stokes-alpha model for turbulence [9]. For $b = -1$, the evolution in (100) occurs only by higher order terms.

The viscous b-family of peakon equations (99) may be rearranged into two other equivalent forms that are convenient for introducing a stress multiplier. These are either its equivalent **conservative form**,

$$m_t = -\frac{\partial}{\partial x} \left(mu + \frac{b-1}{2} u^2 - \frac{b-1}{2} \alpha^2 u_x^2 \right) + \nu m_{xx}, \quad (102)$$

or its equivalent **convective form**,

$$(1 - \alpha^2 \partial_x^2) (u_t + uu_x - \nu u_{xx}) = -\partial_x \left(\frac{b}{2} u^2 + \frac{3-b}{2} \alpha^2 u_x^2 \right). \quad (103)$$

Stress multiplier β . Next, we shall introduce a stress multiplier β as a second parameter that for $\beta \neq 1$ deforms the convective form of the viscous b-family of equations (103) into the following family of Burgers-like equations with four parameters b , α , ν and β ,

$$u_t + uu_x - \nu u_{xx} = -\beta \tau_x \quad \text{with} \quad (1 - \alpha^2 \partial_x^2) \tau = \frac{b}{2} u^2 + \frac{3-b}{2} \alpha^2 u_x^2. \quad (104)$$

When $\beta = 0$, the Burgers- $\alpha\beta$ equation (104) recovers the usual Burgers equation. When $\beta = 1$, equation (104) recovers the viscous b-family of peakon equations (99).

We shall seek solutions of the Burgers- $\alpha\beta$ equation (104), either on the real line and vanishing at spatial infinity, or in a periodic domain, for various values of its four parameters b , α , ν and β . Under these boundary conditions, when $\beta \rightarrow 1$, equation (104) recovers the convective form (103) of the viscous b-family for peakons with $g(x) = e^{-|x|/\alpha}$. Thus, the viscous b-family of equations (99-103) deforms into the Burgers- $\alpha\beta$ equation (104) when $\beta \neq 1$ and the Burgers- $\alpha\beta$ equation (104) reduces to the usual Burgers equation when $\beta = 0$. We shall be interested in the effects of the four parameters b , α , ν and β on the solutions of the Burgers- $\alpha\beta$ equation (104). We shall be interested especially in the fate of the peakon solutions upon introducing the parameters ν and β so as to retain H_α^1 control of the velocity. As we shall see, such control requires a special relation between the parameters b and β , namely, $(3-b)\beta = 1$.

7.1 Burgers– $\alpha\beta$ equation: analytical estimates

Proposition 7.1 (H_α^1 control of the velocity) *The Burgers– $\alpha\beta$ equation (104) controls the α –weighted H^1 norm of the velocity,*

$$\|u\|_{H_\alpha^1}^2 = \int_{-\infty}^{\infty} (u^2 + \alpha^2 u_x^2) dx$$

for $\alpha^2 \neq 0$, provided $(3 - b)\beta = 1$.

Proof. The spatial derivative of the Burgers– $\alpha\beta$ equation (104) yields the dynamics for the slope $s = u_x$ as

$$\begin{aligned} u_t + uu_x - \nu u_{xx} &= -\beta \tau_x, \\ s_t + us_x + s^2 - \nu s_{xx} &= -\beta \tau_{xx}, \quad \text{with } s = u_x, \\ -\alpha^2 \tau_{xx} &= \frac{b}{2} u^2 + \frac{3-b}{2} \alpha^2 u_x^2 - \tau. \end{aligned}$$

In turn, these slope dynamics equations imply the following evolution of the α –weighted H^1 density, cf. equation (92),

$$\begin{aligned} \frac{\partial}{\partial t} \left(\frac{1}{2} u^2 + \frac{\alpha^2}{2} s^2 \right) &= \frac{\partial}{\partial x} \left(\frac{1}{3} \left(1 - \frac{b\beta}{2} \right) u^3 + \beta u \tau + \frac{\alpha^2}{2} u s^2 + \nu u u_x + \nu \alpha^2 s s_x \right) \\ &\quad - \nu u_x^2 - \nu \alpha^2 s_x^2 + \frac{\alpha^2}{2} \left((3 - b)\beta - 1 \right) s^3. \end{aligned}$$

Thus, provided

$$(3 - b)\beta = 1,$$

the last term will vanish. Under this condition, for periodic or vanishing boundary conditions the α –weighted H^1 norm

$$\|u\|_{H_\alpha^1}^2 = \int_{-\infty}^{\infty} (u^2 + \alpha^2 u_x^2) dx$$

will decay monotonically under the Burgers– $\alpha\beta$ dynamics for $\alpha^2 \neq 0$. \square

Remarks.

- When $\nu \rightarrow 0$ in the Burgers- $\alpha\beta$ equation, the α -weighted H^1 norm is conserved for $(3-b)\beta = 1$. This relation cannot be satisfied for $b = 3$. Thus, the proof of decay of the α -weighted H^1 norm under the Burgers- $\alpha\beta$ dynamics is inconclusive for $\nu \neq 0$ when $b = 3$. However, one can expect on physical grounds that this norm will also decay for $b = 3$ if ν is sufficiently large.
- We shall restrict our remaining considerations to those values of b and β for which the α -weighted H^1 norm is bounded, or decays monotonically. In one dimension, this control of the α -weighted H^1 norm implies the solution for the velocity will be *continuous*.
- Namely, we shall consider the following cases with $(3-b)\beta = 1$
($b=0, \beta = 1/3$), ($b=1, \beta = 1/2$) and ($b=2, \beta = 1$).

Proposition 7.2 (Burgers- $\alpha\beta$ Steepening Lemma) *For b and β in the range $(3-b)\beta \leq 2$ a sufficiently negative slope at an inflection point of velocity u will become vertical in finite time under the dynamics of the inviscid Burgers- $\alpha\beta$ equation, (104) with $\nu = 0$.*

Proof. The proof follows that for the Peakon Steepening Lemma 6.1 and uses the slope equation following from the Burgers- $\alpha\beta$ equation (104) with $\nu = 0$ that corresponds to (91) for the Peakons, modified to include β ,

$$\begin{aligned} u_{xt} + uu_{xx} + u_x^2 &= -\frac{\beta}{2\alpha} \frac{\partial}{\partial x} \int_{-\infty}^{\infty} e^{-|x-y|/\alpha} \left(buu_y + (3-b)\alpha^2 u_y u_{yy} \right) dy \\ &= \frac{\beta}{2\alpha^2} \int_{-\infty}^{\infty} e^{-|x-y|/\alpha} \operatorname{sgn}(x-y) \left(buu_y + (3-b)\alpha^2 u_y u_{yy} \right) dy. \end{aligned} \quad (105)$$

Equation (105) yields the inviscid Burgers- $\alpha\beta$ evolution of the slope $s(t) = u_x(\bar{x}(t), t)$ at an inflection point $x = \bar{x}(t)$ as

$$\frac{ds}{dt} \leq -\left(2 - (3-b)\beta\right) \frac{s^2}{2} + \frac{\beta M}{2} \quad \text{for } 0 \leq b \leq 3. \quad (106)$$

This holds provided we assume the solution satisfies $(bu^2/\alpha^2) < M$ for some constant M . Consequently, if $2 - (3-b)\beta > 0$, we have

$$\frac{dX}{1-X^2} = d \coth^{-1}(X) \leq \sqrt{M} \quad \text{for } X = \sqrt{\frac{2 - (3-b)\beta}{M\beta}} s. \quad (107)$$

For $s \leq -\sqrt{M}$ initially negative and $\beta > 0$, this implies

$$s \leq \sqrt{M} \coth\left(\sigma + \sqrt{\frac{2 - (3 - b)\beta}{M\beta}} \frac{M}{2} t\right) \quad \text{for } 0 \leq 3 - \frac{2}{\beta} < b \leq 3, \quad (108)$$

where the dimensionless integration constant $\sigma < 0$ determines the initial slope, which is negative. Under these circumstances, provided the inflection point continues to exist, its negative slope must become vertical by time $t = \frac{-2\sigma}{M} \sqrt{\frac{M\beta}{2 - (3 - b)\beta}}$. □

Caveat As for the Peakon Steepening Lemma in Proposition 6.1, this formal proof for Proposition 7.2 via the slope dynamics for $s(t)$ requires an additional assumption of regularity on the initial data to make it rigorous. Under the additional regularity assumption $u(x, 0) \in H^2(R)$, one may show as in [12] that (106) holds almost everywhere in time, while the result (108) holds everywhere.

Corollary 7.3 (Inviscid Burgers– $\alpha\beta$ shocks) *Solutions of the inviscid Burgers– $\alpha\beta$ equation (104) with $\nu = 0$ that remain continuous in velocity must develop negative vertical slope in finite time.*

Proof. According to Proposition 7.1, continuity of the velocity and, hence, control of the H^1 norm $\|u\|_{H_\alpha^1}$ requires that $(3 - b)\beta = 1$. This is in the parameter range where Proposition 7.2 applies. Consequently, verticality will form at an inflection point of negative slope under the dynamics of the inviscid Burgers– $\alpha\beta$ equation (104) with $\nu = 0$ for $(3 - b)\beta \leq 2$. □

Remark 7.4 *Hence, to remain continuous without viscosity, the solution of the inviscid Burgers– $\alpha\beta$ equation must either develop verticality at an inflection point of negative slope, or it must evolve to eliminate such points entirely.*

7.2 Burgers– $\alpha\beta$ traveling waves for $\beta(3 - b) = 1$ & $\nu = 0$

For $\nu = 0$, the Burgers– $\alpha\beta$ equation (104) has traveling waves given by

$$(u - c)u' + \beta\tau' = 0 \quad \text{and} \quad \tau - \alpha^2\tau'' = \frac{b}{2}u^2 + \frac{3 - b}{2}\alpha^2(u')^2, \quad (109)$$

which yields after one integration

$$\frac{u^2}{2} - cu + \beta\tau = K, \quad (110)$$

where K is the first integral. Consequently, we find

$$\tau - \alpha^2 \tau'' = \frac{1}{\beta} \left(K + cu - \frac{u^2}{2} + \alpha^2 ((u - c)u'' + (u')^2) \right). \quad (111)$$

The second equation in (109) integrates for the special case of $\beta(3 - b) = 1$,

$$2Ku + cu^2 - \beta u^3 + \alpha^2(u - c)(u')^2 = 2H. \quad (112)$$

For the special case $K = 0 = H$ this becomes

$$\alpha^2(u - c)(u')^2 = (\beta u - c)u^2 \quad \text{for } \beta(3 - b) = 1, \quad (113)$$

and we recover the peakon solution $u(z) = ce^{-|z|/\alpha}$ for $\beta = 1$. In the general case that $K \neq 0$ and $H \neq 0$, we rearrange equation (112) into the following quadrature for inviscid Burgers- $\alpha\beta$ traveling waves,

$$\pm \frac{dz}{\alpha} = \frac{(u - c)^{1/2} du}{\left[2H - 2Ku - cu^2 + \beta u^3 \right]^{1/2}} \quad \text{for } \beta(3 - b) = 1 \text{ \& } \nu = 0. \quad (114)$$

In what follows, we shall consider the cases $(b = 0, \beta = 1/3)$, $(b = 1, \beta = 1/2)$ and $(b = 2, \beta = 1)$ when $\nu \neq 0$.

8 The fate of peakons under (1) adding viscosity and (2) Burgers- $\alpha\beta$ evolution

8.1 The fate of peakons under adding viscosity

The following set of four figures shows the effects on the initial value problem for the viscous b-equation (99) of varying α and b at fixed viscosity for an initial velocity distribution given by a peakon of width $w = 5$ and initial height $U \simeq 0.1$. The parameter b takes the values $b = 0, 1, 2, 3$. In these four figures, the resolution is 2^{13} points on a domain size of 200 with viscosity $\nu = 0.005$. This corresponds to a grid-scale Reynolds number of $Re_{\Delta x} = U\Delta x/\nu = O(1)$ for velocity $U \simeq 0.1$. The pair of figures after these four then shows the effects on the same problem of increasing viscosity ν at fixed α for $b = 2$ and $b = 3$.

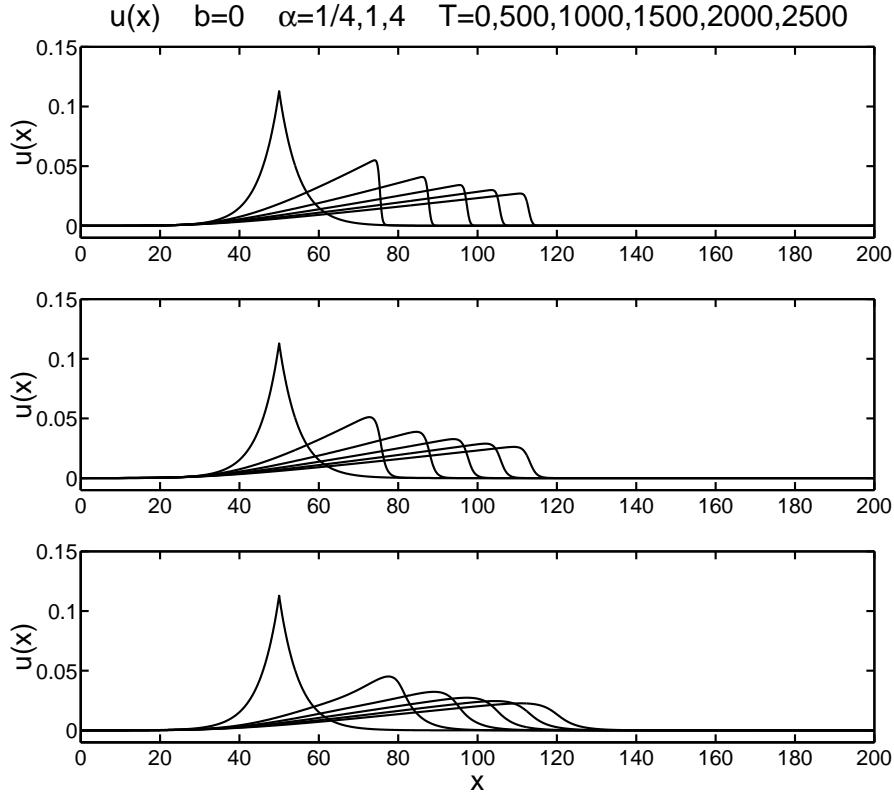


Figure 13: **Effect of increasing α for $b = 0$.** Viscous b -family, $b = 0$, $\alpha = 1/4, 1, 4$, $\nu = 0.005$, initial width $w = 5$.

Figure 13 shows three plots of the evolution of the velocity profile under the viscous b -equation (99) of an initial peakon of width five, as a function of increasing $\alpha = 1/4, 1, 4$ at fixed viscosity $\nu = 0.005$ for $b = 0$. The peakon leans to the right and develops a Burgers-like triangular shock, or ramp and cliff, whose width increases and peak height decreases as α increases. These three plots show no discernable differences for $b = 0$ as the viscosity is decreased to $\nu = 10^{-6}$. Hence the width of the cliff in the ramp and cliff structure for $b = 0$ is set by the value of α in this range of parameters.

Figure 14 shows three plots of the same type of evolution from a peakon initial condition of width $w = 5$, as α is varied for $b = 1$. The front

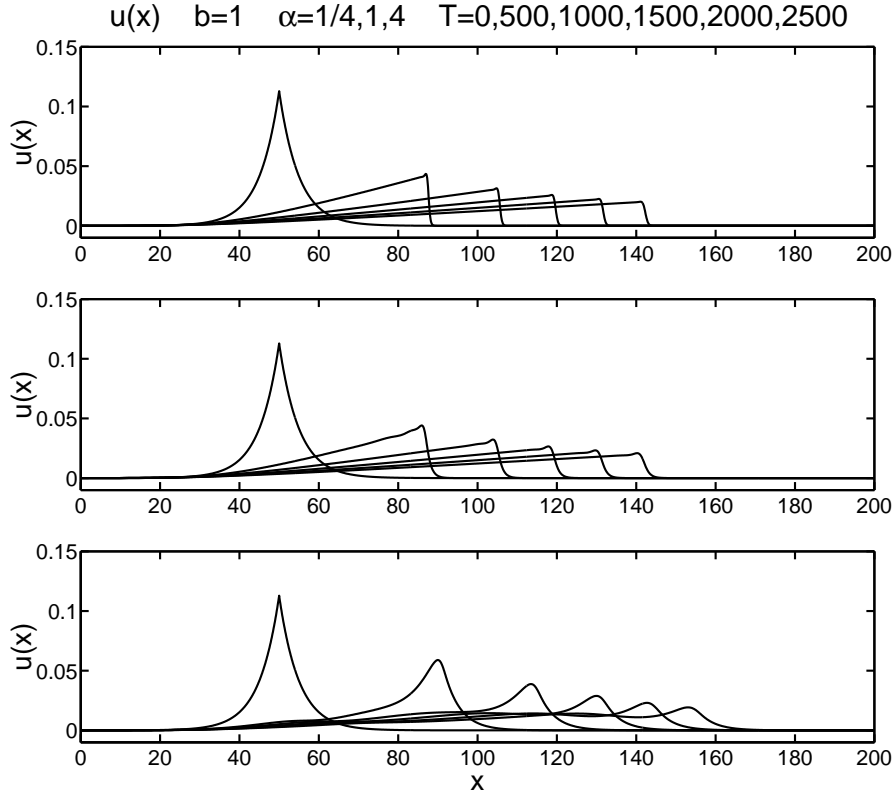


Figure 14: **Effect of increasing α for $b = 1$.** Viscous b -family, $b = 1$, $\alpha = 1/4, 1, 4$, $\nu = 0.005$, initial width $w = 5$.

of the ramp and cliff structure propagates faster and is sharper for $b = 1$ than for $b = 0$ when $\alpha = 1/4$ and $\alpha = 1$. This increase in speed appears to occur because the coefficient increases in the steepening term $(b + 1)uu_x$ in equation (100). A nascent peakon begins to form close behind the front at the top of the ramp, then eventually gets absorbed into the ramp and cliff. For $\alpha = 4$, however, this nascent peakon forms more completely and nearly escapes.

Figure 15 again shows three plots of the evolution from a peakon initial condition of width $w = 5$, as α is varied, this time for $b = 2$. The ramp and cliff structure is faster for $b = 2$ than for $b = 1$ when $\alpha = 1/4$. When $\alpha = 1$ a series of three nascent peakons forms close behind the

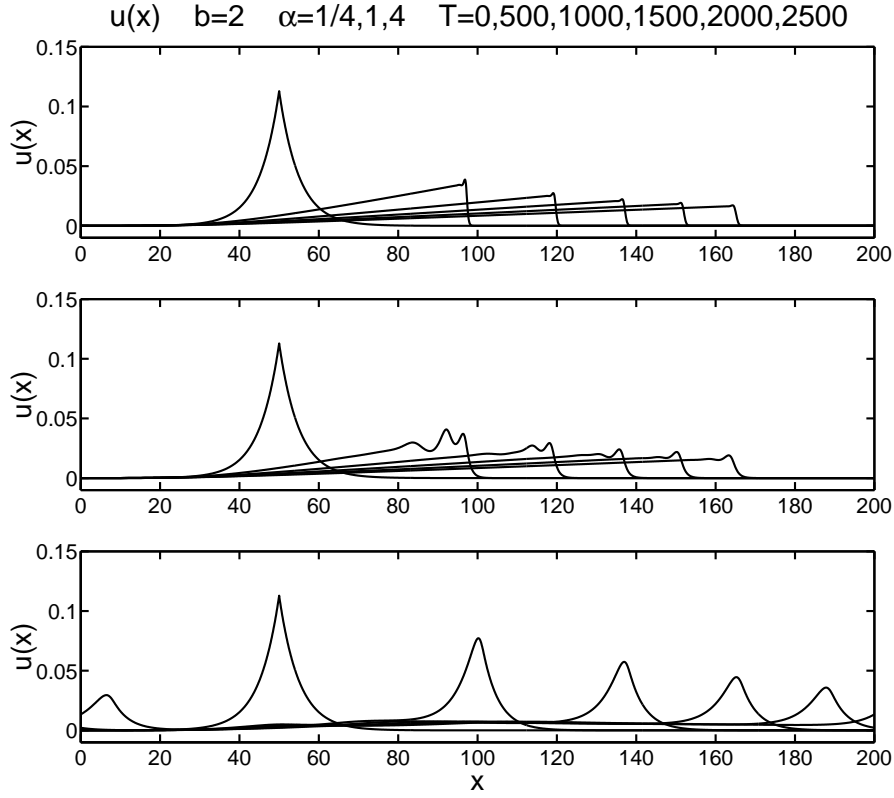


Figure 15: **Effect of increasing α for $b = 2$.** Viscous b -family, $b = 2$, $\alpha = 1/4, 1, 4$, $\nu = 0.005$, initial width $w = 5$.

front, then overtakes the ramp and cliff structure and slightly affects its propagation before eventually being absorbed. For $\alpha = 4$, however, the initial peakon simply propagates and decays under viscosity, although it is slightly rounded at the top.

Figure 16 also shows three plots of the evolution from a peakon initial condition of width $w = 5$, as α is varied, this time for $b = 3$. The ramp and cliff structure moves faster yet, and a single nascent peakon appears just behind the front already for $\alpha = 1/4$. When $\alpha = 1$, a series of three nascent peakons forms initially close behind the front and they nearly escape before being slowed by viscosity. The leading peakon decays and slows due to viscosity. Then the following ones overtake

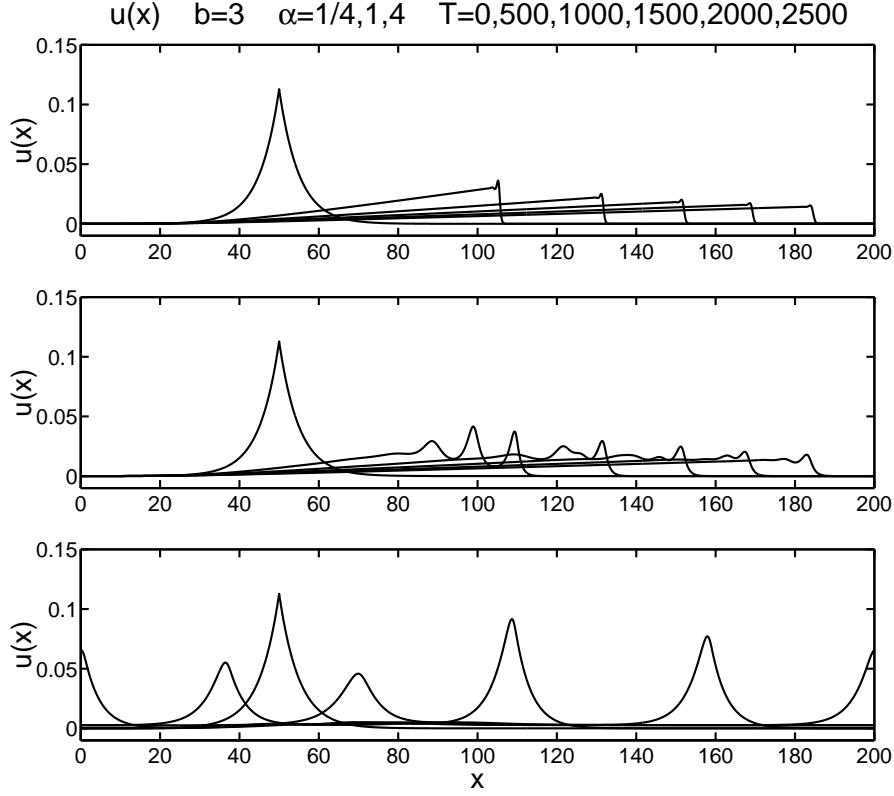


Figure 16: **Effect of increasing α for $b = 3$.** Viscous b -family, $b = 3$, $\alpha = 1/4, 1, 4$, $\nu = 0.005$, initial width $w = 5$.

and collide with the ones ahead as the ramp and cliff structure forms. These collisions occur at higher relative velocity for $b = 3$ than for $b = 2$ and they significantly affect the propagation and eventual formation of the ramp and cliff. In contrast, for $\alpha = 4$, the initial peakon keeps its integrity and simply propagates rightward and decays under viscosity. The propagating peakon for $\alpha = 4$ at this viscosity decays more slowly and is sharper at the top for $b = 3$ than for $b = 2$.

Remark 8.1 (Exchange of stability) *To see the exchange of stability between the ramp/cliff structure and the peakon as b changes, we perform the following numerical experiment. First, we run the viscous b -equation (99) with $b = 0$, $\alpha = 1$, $\nu = 10^{-5}$, and an initial peakon of width $w = 5$. As*

we see in Figures 17 and 18, this evolves into the ramp and cliff formation even for nearly zero viscosity. Once the final ramp/cliff state is formed, we then use it as the new initial condition for equation (99) with either $b = 2$ or $b = 3$. The new evolution breaks the ramp/cliff structure into peakons and the new final state is a rightward moving train of peakons ordered by height.

For Figures 19 and 20, we ran the same numerical experiment, this time with a value $\alpha = 5$ equal to the width of the initial peakon. The initial peakon “borrows from the negative” to form a ramp, which is not quite antisymmetric because the total area of the initial peakon must be preserved. At time $T = 150$ we switch to $b = 2$ (top plot) or $b = 3$ (bottom plot), and again observe a train of stable peakons emerging from the now-unstable ramp.

Finally, for Figures 21 and 22, we again run the numerical experiment with $\alpha = 1$ and an initial peakon width $w = 5$, but this time changing to $b = -2$ or $b = -3$ after the ramp has formed. The new evolution breaks the ramp/cliff structure into leftons like those in Figures 6 and 7.

Remark 8.2 (Increasing viscosity) *The effect of increasing viscosity on the evolution of the peakon initial condition can be estimated from the α -scale Reynolds number defined by,*

$$Re_\alpha = U\alpha/\nu = (\alpha/\Delta x)Re_{\Delta x}.$$

For $(\alpha/\Delta x) = 40$, $U = 0.1$ and increasing viscosity ν , the Reynolds numbers $Re_{\Delta x}$ and Re_α decrease as

$$Re_{\Delta x} \simeq 2, 0.2, 0.02 \quad \text{and} \quad Re_\alpha \simeq 80, 8, 0.8 \quad \text{for} \quad \nu = 0.01, 0.1, 1.0.$$

Perhaps not surprisingly, when $Re_\alpha = O(1)$ the viscosity will diffuse through the initial peakon before it can fully form. Figures 23 and 24 show that this effect increases as Re_α decreases.

8.2 The fate of peakons under Burgers- $\alpha\beta$ evolution

Figures 25 and 26 show the effects on the peakon initial value problem for the Burgers- $\alpha\beta$ evolution of varying α and b with $(3-b)\beta = 1$ at constant viscosity. We shall consider the following cases with $(3-b)\beta = 1$:

$$b = 0, \beta = 1/3, \nu = 0.005, \alpha = 1/4, 1, 4, \text{ and}$$

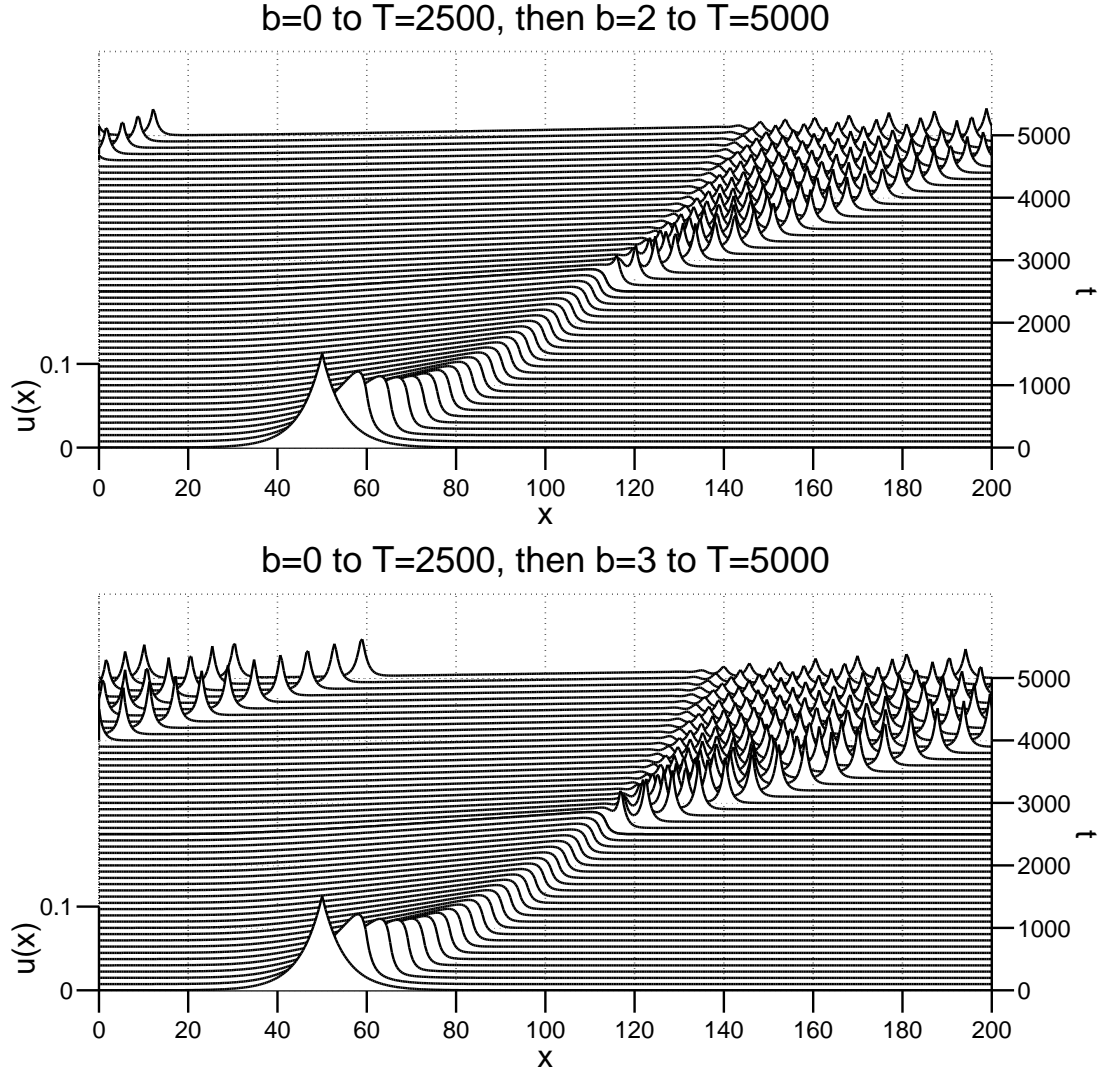


Figure 17: **Exchange of stability between ramps and peakons for $b = 0, 2, 3$, when $\text{width} > \alpha$.** Viscous b -family, $b = 0 \rightarrow 2, 3$, $\alpha = 1$, $\nu = 10^{-5}$, initial width $w = 5$.

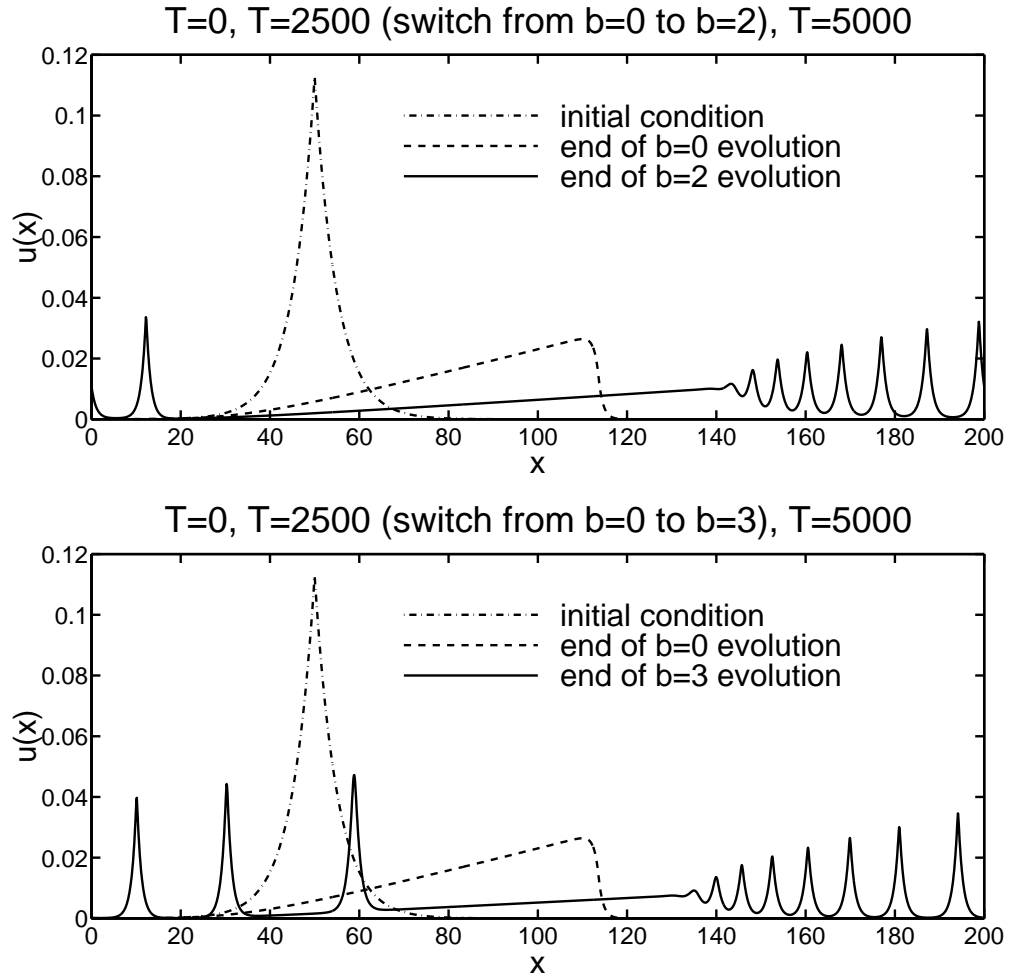


Figure 18: **Exchange of stability between ramps and peakons for $b = 0, 2, 3$, when $\text{width} > \alpha$: profiles.** Viscous b -family, $b = 0 \rightarrow 2, 3$, $\alpha = 1$, $\nu = 10^{-5}$, initial width $w = 5$.

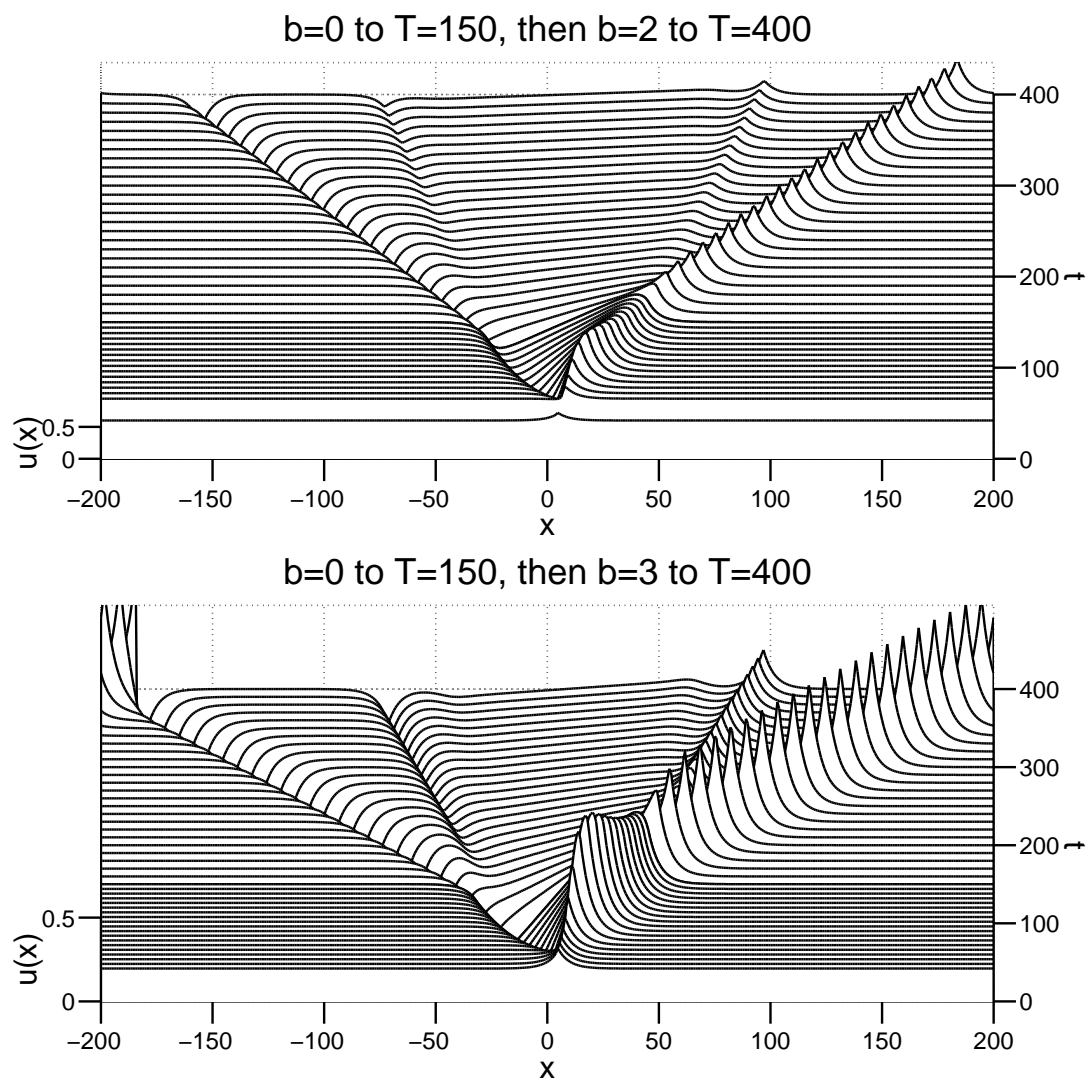


Figure 19: **Exchange of stability between ramps and peakons for $b = 0, 2, 3$, when width $= \alpha$.** Viscous b -family, $b = 0 \rightarrow 2, 3$, $\alpha = 5$, $\nu = 10^{-5}$, initial width $w = 5$.

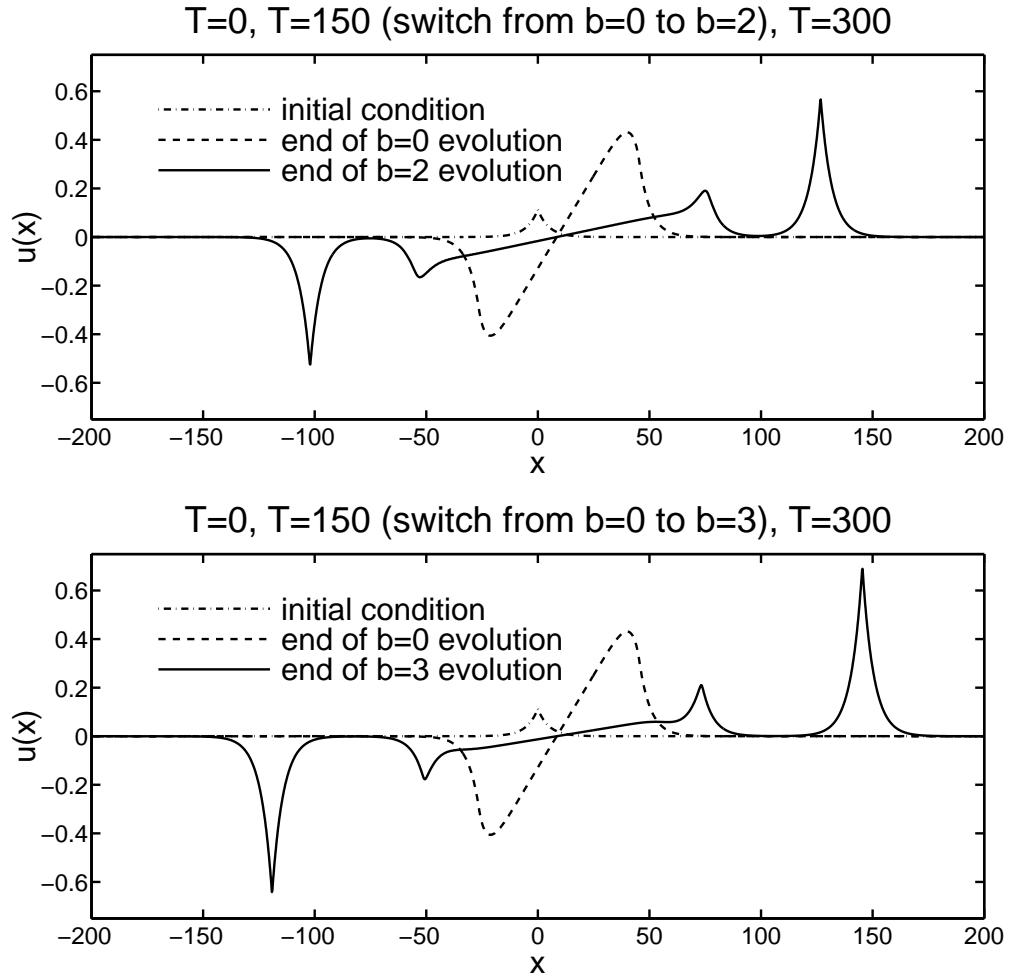


Figure 20: **Exchange of stability between ramps and peakons for $b = 0, 2, 3$, when width $= \alpha$: profiles.** Viscous b -family, $b = 0 \rightarrow 2, 3$, $\alpha = 5$, $\nu = 10^{-5}$, initial width $w = 5$.

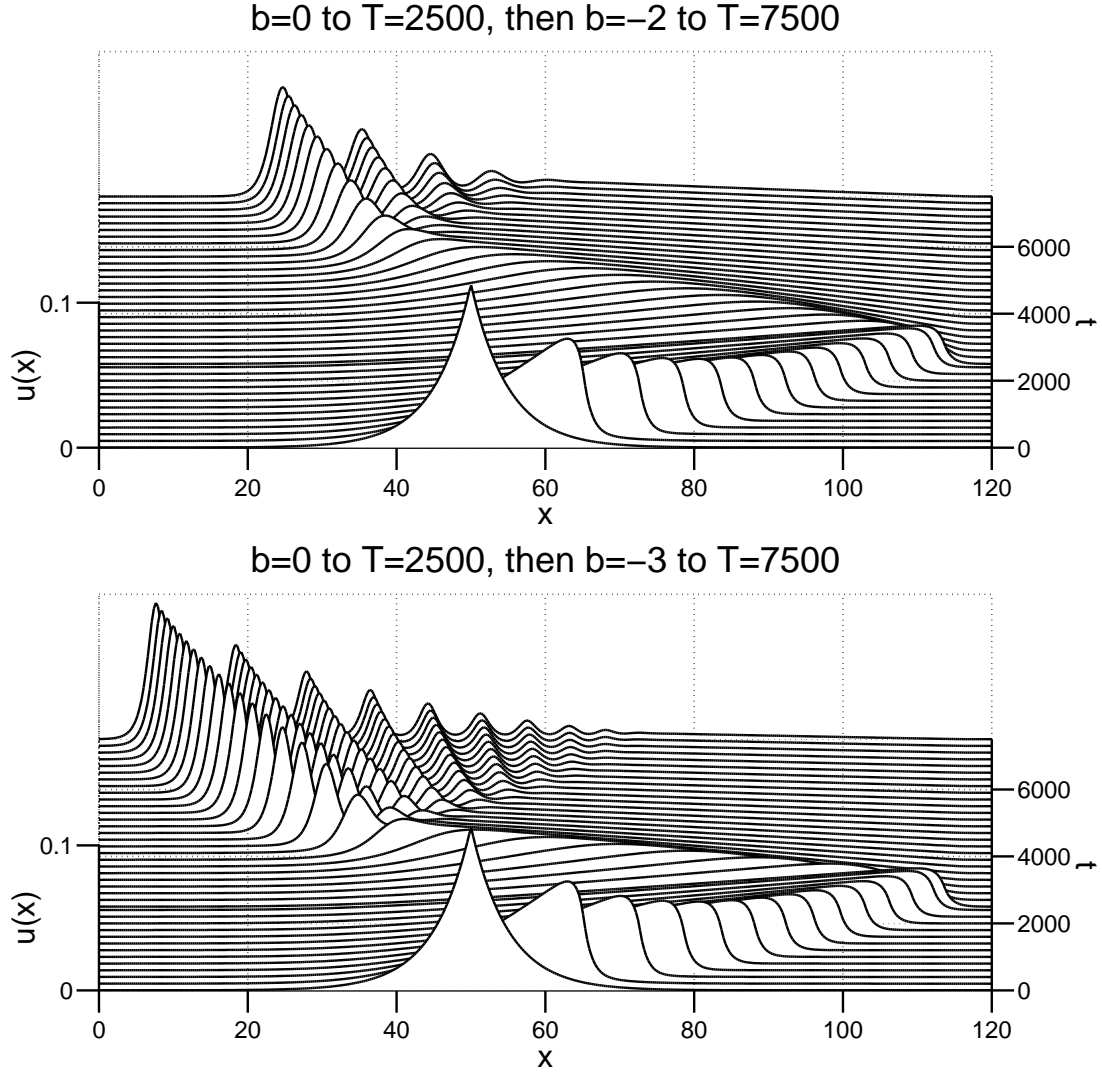


Figure 21: **Exchange of stability between ramps and leftons for $b = 0, -2, -3$, when $\text{width} > \alpha$.** Viscous b -family, $b = 0 \rightarrow -2, -3$, $\alpha = 1$, $\nu = 10^{-5}$, initial width $w = 5$.

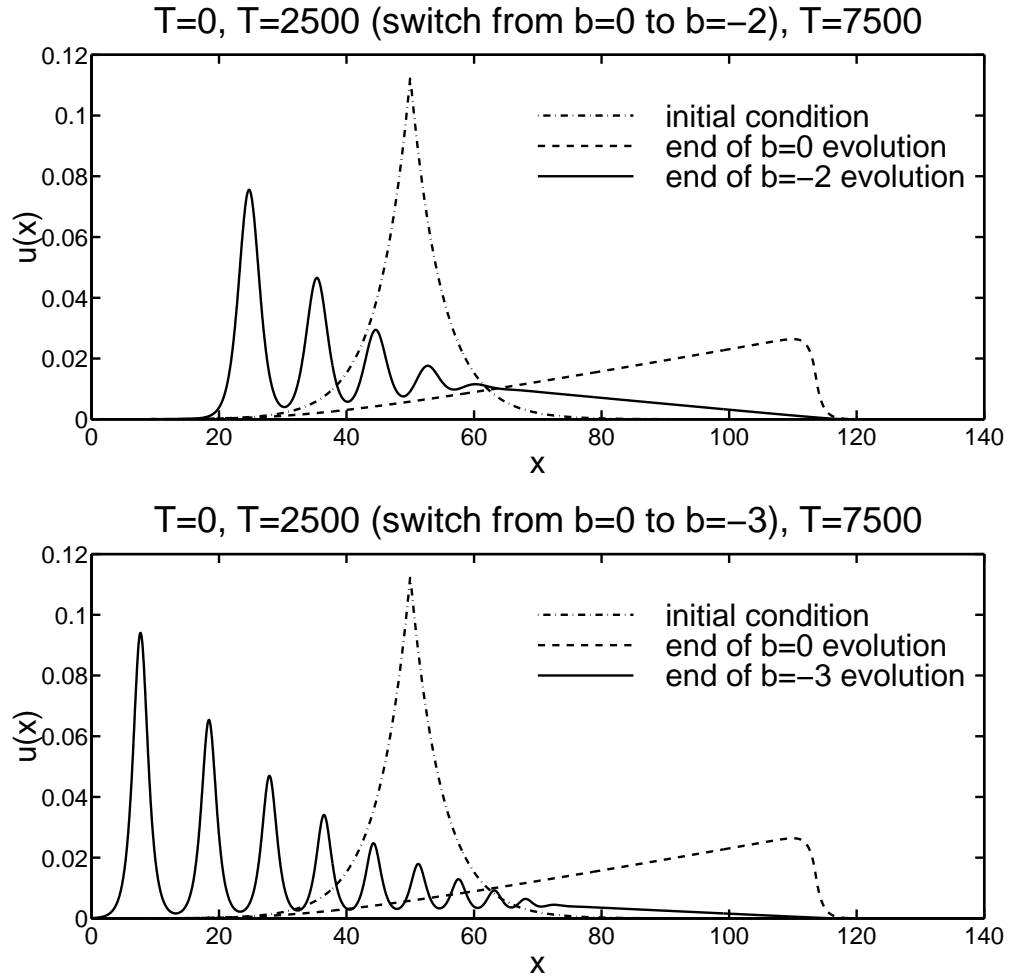


Figure 22: **Exchange of stability between ramps and leftons for $b = 0, -2, -3$, when width $> \alpha$: profiles.** Viscous b -family, $b = 0 \rightarrow -2, -3$, $\alpha = 1$, $\nu = 10^{-5}$, initial width $w = 5$.

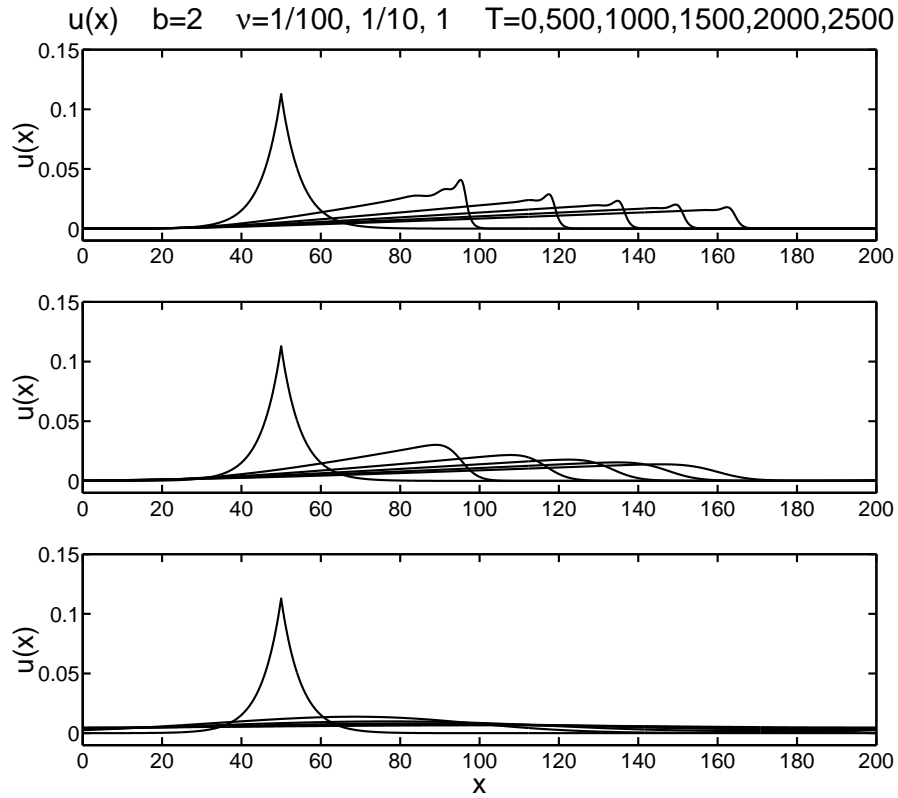


Figure 23: **Effect of increasing viscosity for $b = 2$.** Viscous b -family, $b = 2$, $\alpha = 1$, $\nu = 1/100, 1/10, 1$, initial width $w = 5$.

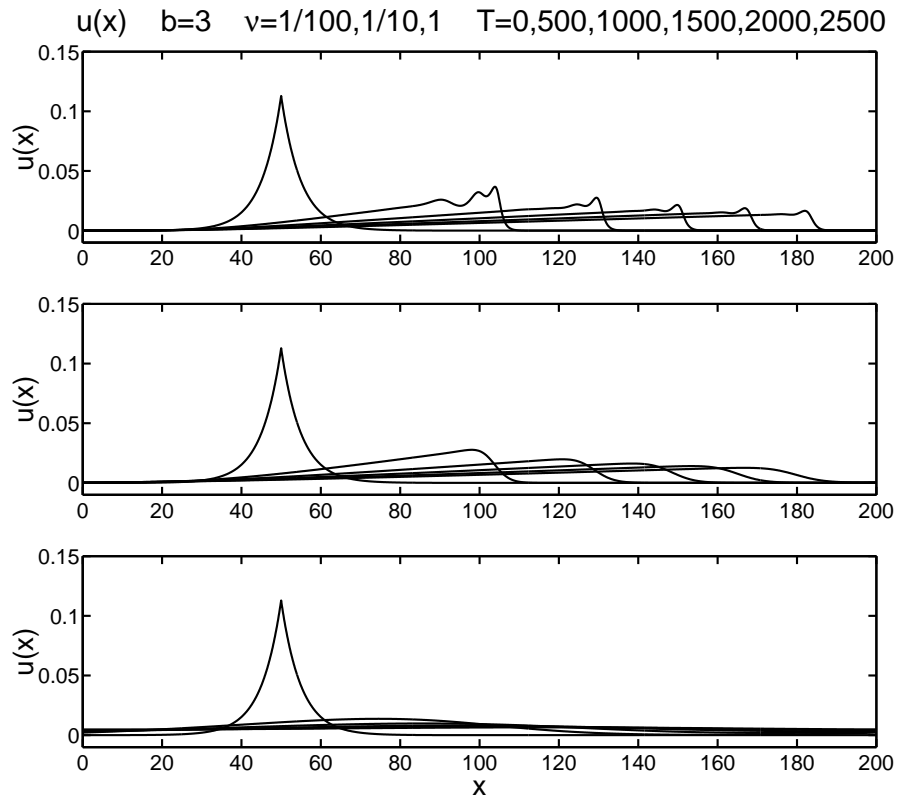


Figure 24: **Effect of increasing viscosity for $b = 3$.** Viscous b -family, $b = 3$, $\alpha = 1$, $\nu = 1/100, 1/10, 1$, initial width $w = 5$.

$b = 1, \beta = 1/2, \nu = 0.005, \alpha = 1/4, 1, 4.$

Remark 8.3 (Lowering β has little effect on the ramp/cliff) *Lowering β to follow $(3 - b)\beta = 1$ instead of keeping $\beta = 1$ has little effect on the development of the ramp/cliff solution for $b = 0$ and $b = 1$. Lowering β for these cases only makes the activity slightly less lively at the front for $(b = 0, \beta = 1/3)$ and $(b = 1, \beta = 1/2)$ than for the corresponding cases of $b = 0$ and $b = 1$ with $\beta = 1$ in Figures 13 and 14. This lessened activity at lower β can only be discerned in the solution for the largest value $\alpha = 4$. The remaining case $(b = 2, \beta = 1)$ recovers the viscous b -equation (99) for $b = 2$ in Figure 15, in which the larger b produces much livelier steepening and, hence, more activity at the front of the rightward moving pulses.*

9 Numerical results for peakon scattering and initial value problems

We shall begin by summarizing the results in the figures given earlier, and then we shall describe the numerical methods used in producing them and discuss some of the ways we verified and validated the results.

9.1 Peakon initial value problems

9.1.1 Inviscid b -family of equations

Ramps and cliffs for $b = 0$. Figure 1 shows the formation of a ramp and cliff pattern for $b = 0, \alpha = 1$, and a set of Gaussian initial conditions of increasing width $w = 2.5, 5, 10$.

Peakons for $b = 2, 3$. Figures 2 and 3 show the formation of peakons for $b = 2$ and $b = 3$, for $\alpha = 1$ and a set of Gaussian initial conditions of increasing width $w = 2.5, 5, 10$.

Ramps and cliffs for $b = -1/2$. Figure 4 shows the formation of a ramp and cliff pattern for $b = -1/2, \alpha = 1$, and a set of Gaussian initial conditions of increasing width $w = 10, 15, 20$.

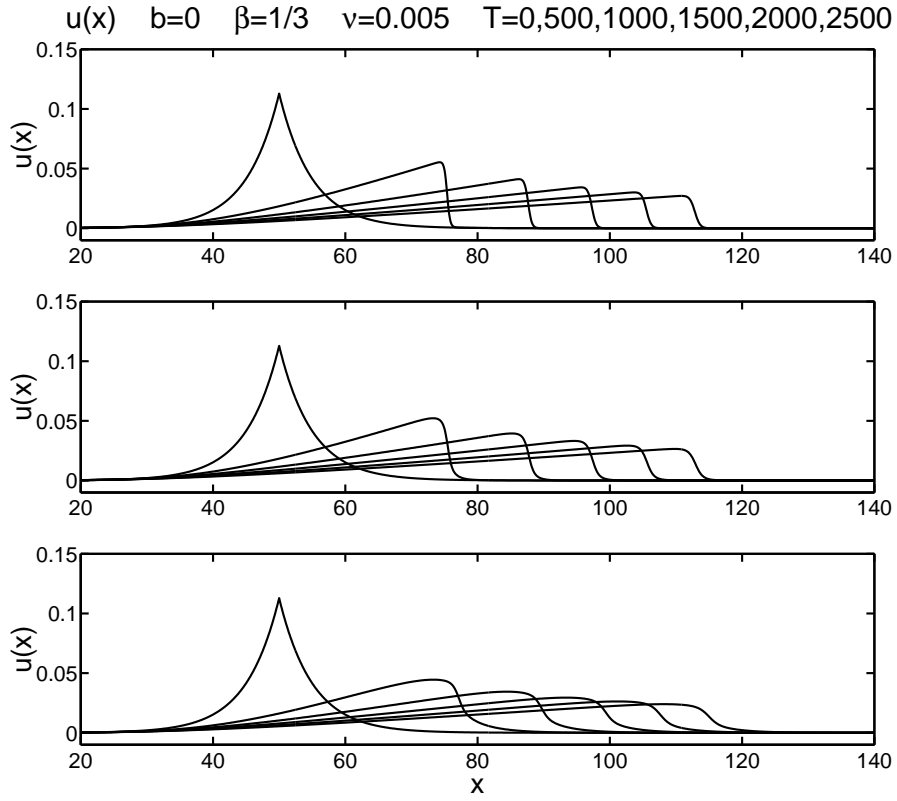


Figure 25: **Effect of increasing α when $(3 - b)\beta = 1$, for $b = 0$ and $\beta = 1/3$.** Burgers- $\alpha\beta$, $b = 0$, $\alpha = 1/4, 1, 4$, $\beta = 1/3$, $\nu = 0.005$, initial width $w = 5$.

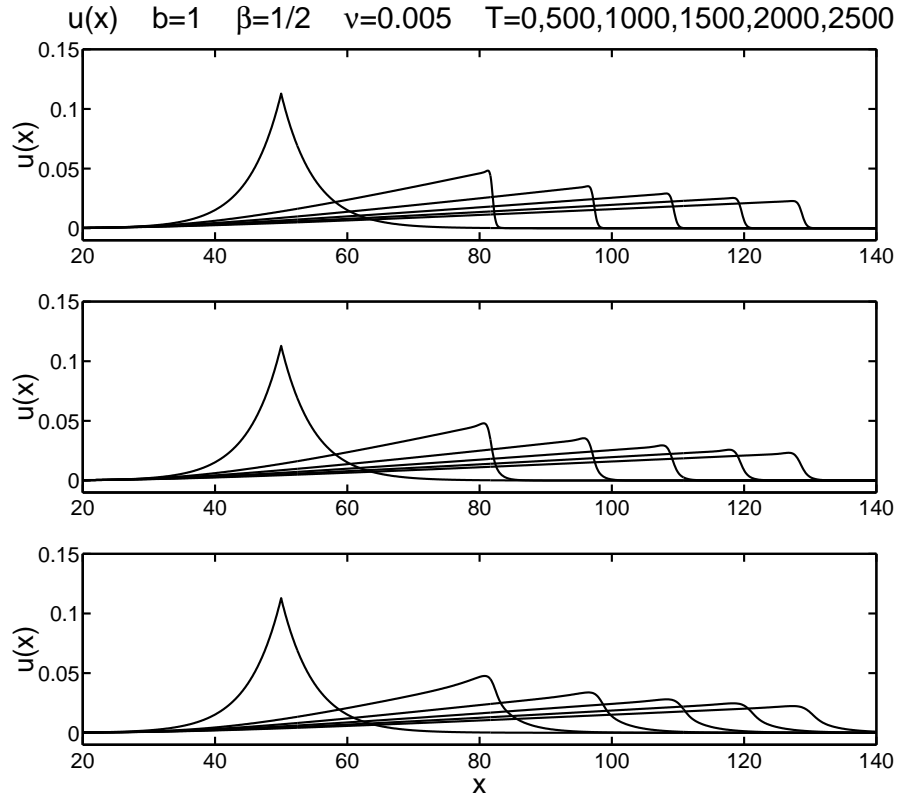


Figure 26: **Effect of increasing α when $(3 - b)\beta = 1$, for $b = 1$ and $\beta = 1/2$.** Burgers- $\alpha\beta$, $b = 1$, $\alpha = 1/4, 1, 4$, $\beta = 1/2$, $\nu = 0.005$, initial width $w = 5$.

Stationary solutions for $b \leq -1$. Figure 5 shows an essentially stationary solution with a slight rightward drift and leaning slightly to the right due to nonlinear curvature terms with higher order derivatives in equation (55), for $\alpha = 1$ and a set of Gaussian initial conditions of increasing width $w = 10, 15, 20$. For the same α and same set of initial conditions, Figures 6 and 7 show the emergence of leftons.

Figure 8 shows the leftons at time $T = 2500$ for the $b = -2$ case, versus the analytical $u(x) \simeq \text{sech}^2(x/(2\alpha))$ from equation (58), and for the $b = -3$ case, versus the analytical $u(x) \simeq \text{sech}(x/\alpha)$.

Peakons of width α for $b = 2, 3$. Figures 9 and 10 show 2-peakon and 3-peakon interactions for $b = 2$ and for $b = 3$, beginning with initial peakons of width $w = \alpha = 5$.

Peakons of width $> \alpha$ for $b = 2, 3$. Figure 11 shows the emergence of peakons of width $\alpha = 1$ when we begin with peakons of width $w = 5$ greater than α , for $b = 2$ and $b = 3$.

Peakon-antipeakon collisions for $b = 1, 2, 3$. Figure 12 shows the dynamics of a peakon-antipeakon collision for $b = 1$, $b = 2$, and $b = 3$, for $\alpha = 1$, at four successive times.

9.1.2 Viscous b-family of equations

Effect of α for $b = 0, 1, 2, 3$. Figures 13 – 16 show the evolution of an initial peakon of width $w = 5$ as a function of increasing $\alpha = 1/4, 1, 4$ at fixed viscosity $\nu = 0.005$, for $b = 0$, $b = 1$, $b = 2$, and $b = 3$.

Exchange of stability between ramps and peakons. Figures 17 and 18 show the exchange of stability between ramps and peakons suggested in the previous four figures, with $\alpha = 1$ and an initial peakon of width $w = 5$, but this time with a very small viscosity $\nu = 10^{-5}$ so that the peakons, when stable, do not noticeably decay. The exchange of stability occurs when we switch from $b = 0$ to $b = 2$ or $b = 3$. Figures 19 and 20 again show the exchange of stability, this time using $\alpha = 5$ so that the initial peakon has width α .

Exchange of stability between ramps and leftons. Figures 21 and 22 show the exchange of stability as in Figures 17 and 18, but we switch

to $b = -2$ or $b = -3$ instead, and see the emergence of stable leftons from the ramp.

Effect of viscosity for $b = 2, 3$. Figures 23 and 24 show the effect of increasing viscosity $\nu = 0.01, 0.1, 1$ on the evolution of an initial peakon of width $w = 5$, with $\alpha = 1$ and $b = 2$ or $b = 3$.

9.1.3 Burgers- $\alpha\beta$ equation

Effect of α when $(3 - b)\beta = 1$. Figures 25 and 26 show the effect of increasing $\alpha = 1/4, 1, 4$ on the evolution of an initial peakon of width $w = 5$, for fixed $\nu = 0.005$ and two sets of values for b and β for which $(3 - b)\beta = 1$: $b = 0, \beta = 1/3$ for the first figure, and $b = 1, \beta = 1/2$ for the second figure.

9.2 Description of our numerical methods

For our numerical runs we advanced equations (88), (103), and (104) with an explicit, variable timestep fourth/fifth order Runge-Kutta-Fehlberg (RKF45) predictor/corrector. We selected the timestep for numerical stability by trial and error, while our code selected the timestep for numerical accuracy (not to exceed the timestep for numerical stability) according to the well-known formula from numerical analysis,

$$h_i = \gamma h_{i-1} \left(\frac{\epsilon |h_{i-1}|}{\|\bar{u}_i - \hat{u}_i\|} \right)^{1/p}. \quad (115)$$

This is used in the following way. At step i of the calculation, we know the predicted solution \bar{u}_i , the corrected solution \hat{u}_i , and the previous timestep h_{i-1} . The predictor's order of accuracy is $p = 4$, while the corrector's order of accuracy is $p + 1$. A new timestep h_i is chosen from (115) based on the old timestep h_{i-1} and the norm of the difference between the current predicted and corrected solutions. We used a very strict relative error tolerance per timestep, $\epsilon = 10^{-8}$, a safety factor $\gamma = 0.9$, and an L_2 norm $\|\cdot\|_2$.

We computed spatial derivatives using 4th order finite differences, generally at resolutions of $2^{13} = 8192$ or $2^{14} = 16384$ zones. To invert the Helmholtz operator in transforming between $m(x, t)$ and $u(x, t)$, we convolved $m(x, t)$ with the Green's function in Fourier space. When the numerical approximation of the nonlinear terms had aliasing errors in the high

wavenumbers, we applied the following high pass filtered artificial viscosity,

$$\nu(k) = \begin{cases} 0 & \text{if } 0 \leq k \leq \frac{N}{3}, \\ \frac{3\delta}{N} \left(k - \frac{N}{3}\right) & \text{if } \frac{N}{3} < k < \frac{2N}{3}, \\ \delta & \text{if } \frac{2N}{3} \leq k \leq N, \end{cases} \quad (116)$$

where $\delta = 0.01$ for the present simulations. N is one-half the number of zones, because for each zone we have both a Fourier sine coefficient and a Fourier cosine coefficient.

The quality of the numerical convergence may be checked analytically in the case of rear-end two-pulson collisions, for which equation (80) in Corollary 5.4 yields

$$g(q_{min}) = g(q) \Big|_{p=0} = 1 - \left(\frac{4c_1c_2}{(c_1 + c_2)^2} \right)^{1/(b-1)}. \quad (117)$$

For peakons with $b = 2$ and $g(x) = e^{-|x|/\alpha}$, this formula gives the minimum separation,

$$q_{min} = -2\alpha \ln \left(\frac{c_1 - c_2}{c_1 + c_2} \right) > 0. \quad (118)$$

When $c_1 = 1$, $c_2 = 1/2$, and $\alpha = 5$, as in figure 9, this formula implies $q_{min} = 10 \ln 3 = 10.9861$. Our numerical results with the resolution of 2^{14} zones yield $q_{min} = 11.0049$. The very small discrepancy, less than 0.2%, occurs largely because our numerical measurement of q_{min} is obtained by examining the peakon positions at each internal timestep in the code, while the code's time discretization effectively means we're unlikely to land exactly on the time at which the minimum separation occurs. The code's true accuracy is thus better than the above measure indicates, because the intermediate steps involved in advancing the solution from one discrete time to the next with an RKF45 method cancel the higher-order discretization errors.

Likewise, for peakons with $b = 3$ and $g(x) = e^{-|x|/\alpha}$, formula (117) gives the minimum separation,

$$q_{min} = -\alpha \ln \left(1 - \frac{\sqrt{c_1c_2}}{(c_1 + c_2)/2} \right) > 0. \quad (119)$$

When $c_1 = 1$, $c_2 = 1/2$, and $\alpha = 5$, as in figure 10, this formula implies $q_{min} = 5 \ln (3/(3 - \sqrt{8})) = 14.3068$. This time our numerical results yield $q_{min} = 14.2924$, a discrepancy of only 0.1%.

Of course, the two-body collision is rather simple compared to the plethora of other multi-wave dynamics that occurs in this problem. For this reason, we also checked the convergence of our numerical algorithms by verifying that the relative phases of the peakons in the various figures remained invariant under grid refinement. Moreover, the integrity of the waveforms in our figures attests to the convergence of the numerical algorithm – after scores of collisions, the waveforms given by the Green’s function for each case are still extremely well preserved. The preservation of these soliton waveforms after so many collisions would not have occurred unless the numerics had converged well.

10 Conclusions

Equation (1) introduced a new family of reversible, parity invariant, evolutionary 1+1 PDEs describing motion by convection and stretching,

$$m_t + \underbrace{um_x}_{\text{convection}} + \underbrace{bu_xm}_{\text{stretching}} = 0, \quad \text{with} \quad u = g * m. \quad (120)$$

We analyzed the transformation properties and conservation laws of this family of equations, which led us to choose g to be an even function. Then we classified its traveling waves and numerically identified the bifurcations of its traveling wave solutions as a function of the balance parameter b . For some choices of the convolution kernel $g(x)$ we studied its particle-like solutions and their interactions when $b > 1$. These were obtained by superposing N traveling wave solutions $u(x, t) = cg(x - ct)$ as

$$u(x, t) = \sum_{i=1}^N p_i(t)g(x - q_i(t)) \quad \text{and} \quad m(x, t) = \sum_{i=1}^N p_i(t)\delta(x - q_i(t)), \quad (121)$$

for any real constant b and $u = g * m$, in which the function g is even $g(-x) = g(x)$, so that $g'(0) = 0$, and is bounded, so we may set $g(0) = 1$.

Following [22], we call these solutions “pulsons.” We have shown that for any $b > 1$, once they are initialized on their invariant manifold (which may be finite dimensional), the pulsons undergo particle-like dynamics in terms of the moduli variables $p_i(t)$ and $q_i(t)$, with $i = 1, \dots, N$. The pulson dynamics we studied for $b > 1$ in this framework on a finite-dimensional invariant manifold displayed all of the classical soliton interaction behavior

for pulsons found in [22] for the case $b = 2$. This behavior included pairwise elastic scattering of pulsons, dominance of the initial value problem by confined pulses and asymptotic sorting according to height – all without requiring complete integrability. Thus, the “emergent pattern” for $b > 1$ in the nonlinear evolution governed by the convection equation (1) was the rightward moving pulson train, ordered by height. The moduli variables $p_i(t)$ and $q_i(t)$ are collective coordinates on an invariant manifold for the PDE motion governed by equation (1). Once initialized for $b > 1$, these collective degrees of freedom persist and emerge as a train of stable pulses, arranged in order of their heights, that then undergo particle-like collisions.

In contrast, the emergent pattern in the Burgers parameter region $0 \leq b < 1$ is the classic ramp/cliff structure as in Figure 13. That the behavior should depend on the value of b is clear from the velocity form of equation (1) written in (100),

$$\begin{aligned} u_t + (b+1)uu_x - \nu u_{xx} &= \alpha^2(u_{xxt} + uu_{xxx} + bu_xu_{xx} - \nu u_{xxx}) \quad (122) \\ &= \alpha^2 \partial_x \left(u_{xt} + uu_{xx} - \nu u_{xxx} + \frac{b-1}{2} u_x^2 \right) \\ &= \alpha^2 \partial_x^2 \left(u_t + uu_x - \nu u_{xx} + \frac{b-3}{2} u_x^2 \right). \end{aligned}$$

Thus, nonlinear terms in this equation change sign at four integer values of the parameter b . Nonlinear α^2 -terms change sign when $b = 0, 1, 3$. Also, the nonlinear steepening term increases with b as $(b+1)uu_x$. So this term changes sign when $b = -1$. In the parameter regime $b > -1$ (resp. $b < -1$) the solutions of equation (1) move rightward (resp. leftward), provided the terms on the right hand side of equation (122) are sufficiently small.

Three regions of b . We found that the solution behavior for equation (1) changes its character near the boundaries of the following three regions in the balance parameter b .

- (B1) In the stable pulson region $b > 1$, the Steepening Lemma for peakons proven for $1 < b \leq 3$ in Proposition 6.1 allows inflection points with negative slopes to escape verticality by producing a jump in spatial derivative at the peak of a traveling wave that eliminates the inflection points altogether. Pulson behavior dominates this region, although ramps of positive slope are also seen to coexist with the pulsons. When

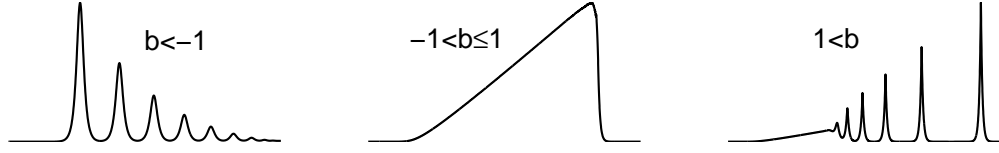


Figure 27: **Leftons** ($b < -1$), **ramps and cliffs** ($-1 < b \leq 1$), and **peakons** ($b > 1$) are solutions of the b -family of equations, $m_t + um_x + bu_xm = 0$, with $m = u - \alpha^2 u_{xx}$.

$b \leq 1$ we found the solution behavior of the convection equation (1) changed its character and excluded the pulsons entirely.

- (B2) In the Burgers region $0 \leq b \leq 1$, the $L^{1/b}$ norm of the variable m is controlled⁶ and the solution behavior is dominated by ramps and cliffs, as for the usual Burgers equation. Similar ramp/cliff solution properties hold for the region $-1 \leq b \leq 0$, for which the $L^{1/b}$ norm of the variable $1/|m|$ is controlled. At the boundary of the latter region, for $b = -1$, the convection equation (1) admits stationary plane waves as exact nonlinear solutions.
- (B3) In the steady pulse region $b < -1$, pulse trains form that move leftward from a positive velocity initial condition (instead of moving rightward, as for $b > -1$). These pulse trains seem to approach a steady state.

Figure 27 illustrates this solution behavior in the region B3 at left, B2 in the center, and B1 at right. For illustrative purposes, the curves are drawn at different scales; recall that the evolution of equation (1) preserves the area under the curve.

Effects of viscosity. Almost any numerical investigation will introduce some viscosity, or other dissipation. Consequently, we studied the fate of the peakons when viscosity was added to the b -family in equation (99). Viscous solutions of equation (99) for the peakon case $g(x) = e^{-|x|/\alpha}$ with $\alpha = 1$ were studied in each of the three solution regions (B1)-(B3). In the Burgers region (B2) near $b = 0$ we focused on the shock-capturing properties of the

⁶For $b = 0$, this is a maximum principle for $|m|$.

solutions of equation (1) and this family of equations was extended for $\beta \neq 1$ to the Burgers– $\alpha\beta$ equation (104),

$$u_t + uu_x - \nu u_{xx} = -\beta \tau_x \quad \text{with} \quad (1 - \alpha^2 \partial_x^2) \tau = \frac{b}{2} u^2 + \frac{3-b}{2} \alpha^2 u_x^2. \quad (123)$$

According to Proposition 7.1, the Burgers– $\alpha\beta$ equation (123) controls the α –weighted H^1 norm of the velocity for $\alpha^2 \neq 0$, provided $(3-b)\beta = 1$. This analytical property guided our study of this new equation by identifying a class of equations for which a priori estimates guarantee continuity of the solution $u(x, t)$. The shock-capturing properties of the Burgers– $\alpha\beta$ equation (123) and its $\alpha \rightarrow \infty$ limit will be reported in a later paper [28].

11 Outlook: the vector b –equation for compressible motion of momentum filaments and surfaces in n –dimensions

We shall generalize to n –dimensions the one-dimensional pulson solutions of equation (1) with defining relation (2) studied earlier in section 5.

11.1 n –dimensional vector b –equation

In n –dimensional vector notation, the b –equation (1) may be written explicitly in Euclidean coordinates as a partial differential equation for a co-vector function $\mathbf{m}(\mathbf{x}, t) : R^n \times R^1 \rightarrow R^n$. Namely,

$$\frac{\partial}{\partial t} \mathbf{m} + \underbrace{\mathbf{u} \cdot \nabla \mathbf{m}}_{\text{convection}} + \underbrace{\nabla \mathbf{u}^T \cdot \mathbf{m} + (b-1) \mathbf{m}(\text{div } \mathbf{u})}_{\text{stretching}} = 0, \quad (124)$$

for a defining relation,

$$\mathbf{u} = G * \mathbf{m} \equiv \int G(|\mathbf{x} - \mathbf{y}|) \mathbf{m}(\mathbf{y}) d^n y, \quad (125)$$

in which we assume the function (filter) $G(|\mathbf{x}|)$ is isotropic. To interpret the stretching terms in the vector b –equation (124), we shall recall the interpretation of the scalar b –equation (1) as preservation at constant Lagrangian coordinate X of the differential form (28),

$$m(x, t) dx^{\otimes b} = m(X, 0) dX^{\otimes b}. \quad (126)$$

Taking the partial time derivative of this equation at constant Lagrangian coordinate X and using $dx/dt|_X = u$ yields equation (1), as shown earlier in equation (29).

To lift this interpretation of the vector b -equation to n dimensions, we regard the momentum $\mathbf{m}(\mathbf{x}, t)$ as the vector coefficient in an invariant one-form density expressed as,

$$\mathbf{m}(\mathbf{x}, t) \cdot d\mathbf{x} \otimes (dV)^{\otimes (b-1)} = \mathbf{m}(\mathbf{X}, 0) \cdot d\mathbf{X} \otimes (dV_0)^{\otimes (b-1)}, \quad (127)$$

where $dV = d^n x$ and $dV_0 = d^n X$ are, respectively, the Eulerian and Lagrangian volume elements. The symbol \otimes denotes tensor product. Taking the partial time derivative of this equation at constant Lagrangian coordinate \mathbf{X} and using $\left. \frac{d}{dt} \right|_{\mathbf{x}} \mathbf{x} = \mathbf{u}$ yields,

$$\begin{aligned} \left. \frac{d}{dt} \right|_{\mathbf{x}} (\mathbf{m} \cdot d\mathbf{x} \otimes (dV)^{\otimes (b-1)}) &= \left. \frac{d\mathbf{m}}{dt} \right|_{\mathbf{x}} \cdot d\mathbf{x} \otimes (dV)^{\otimes (b-1)} \\ &+ \mathbf{m} \cdot d\mathbf{u} \otimes (dV)^{\otimes (b-1)} \\ &+ (b-1) \mathbf{m} \cdot d\mathbf{x} \otimes (\nabla \cdot \mathbf{u})(dV)^{\otimes (b-1)} = 0. \end{aligned} \quad (128)$$

We have used the identities, $\left. \frac{d}{dt} \right|_{\mathbf{x}} d\mathbf{x} = d\mathbf{u} = \mathbf{u}_{,j} dx^j$ and $\left. \frac{d}{dt} \right|_{\mathbf{x}} dV = (\operatorname{div} \mathbf{u})dV$ for the Lagrangian time derivatives of the line element $d\mathbf{x}$ and the volume element dV . Collecting coefficients in equation (127) yields the vector b -equation (124) and explains the sources of its convection and stretching terms.

Equivalently, in terms of the operators div , grad and curl , in $2D$ and $3D$, the Euclidean-coordinate vector b -equation (124) becomes,

$$\frac{\partial}{\partial t} \mathbf{m} - \mathbf{u} \times \operatorname{curl} \mathbf{m} + \nabla(\mathbf{u} \cdot \mathbf{m}) + (b-1) \mathbf{m}(\operatorname{div} \mathbf{u}) = 0. \quad (129)$$

Euler-Poincaré (EP) equation Setting $b = 2$ in the vector b -equation in either of its equivalent forms, (124) or (129), yields the pressureless Euler-Poincaré (EP) equation, whose abstract form is [26, 27],

$$\frac{\partial}{\partial t} \mathbf{m} + \operatorname{ad}_{\mathbf{u}}^* \mathbf{m} = 0, \quad \mathbf{m} = \frac{\delta \ell[\mathbf{u}]}{\delta \mathbf{u}}, \quad (130)$$

and $\text{ad}_{\mathbf{u}}^* \mathbf{m}$ is defined as in equation (124) for $b = 2$. Thus, we have the EP equation for pressureless compressible motion in vector notation,

$$\frac{\partial}{\partial t} \mathbf{m} + \underbrace{\mathbf{u} \cdot \nabla \mathbf{m}}_{\text{convection}} + \underbrace{\nabla \mathbf{u}^T \cdot \mathbf{m} + \mathbf{m}(\text{div } \mathbf{u})}_{\text{EP stretching}} = 0, \quad \mathbf{m} = \frac{\delta \ell[\mathbf{u}]}{\delta \mathbf{u}}. \quad (131)$$

When the Lagrangian $\ell[\mathbf{u}]$ is taken as the kinetic energy, which is also a norm, $\ell[\mathbf{u}] = \frac{1}{2} \|\mathbf{u}\|^2$, then the EP equation (131) describes geodesic motion on the diffeomorphism group, with respect to this kinetic energy norm.

For $b = 2$, the scalar product of the EP equation in div-grad-curl form (129) with the velocity \mathbf{u} shows that evolution under this equation preserves the kinetic energy,

$$\int \mathbf{u} \cdot \mathbf{m} d^n x \equiv \langle \mathbf{u}, \mathbf{m} \rangle, \quad (132)$$

as a constant of the motion, only for this value of b . For the case that velocity is defined in terms of momentum as $\mathbf{u} = G * \mathbf{m}$ in equation (125), we shall assume that the convolution kernel G may be taken as the Green's function for a symmetric positive definite operator Q_{op} . We may then write

$$Q_{op} \mathbf{u} = \mathbf{m}, \quad (133)$$

where \mathbf{u} satisfies appropriate boundary conditions for the relation $\mathbf{u} = G * \mathbf{m}$ to be satisfied. When Q_{op} is assumed to be a symmetric positive definite operator, the kinetic energy in equation (132) will define a kinetic energy norm $\|\mathbf{u}\|^2$ that may be written as,

$$\|\mathbf{u}\|^2 = \int \mathbf{u} \cdot \mathbf{m} d^n x = \int \mathbf{u} \cdot Q_{op} \mathbf{u} d^n x = \langle \mathbf{u}, Q_{op} \mathbf{u} \rangle, \quad (134)$$

for appropriate boundary conditions at spatial infinity. Hence, we have

Proposition 11.1 ($b = 2$ vector b -equation for geodesic motion)

When the defining relation (125) between momentum \mathbf{m} and velocity \mathbf{u} may be written equivalently in operator form as (133) with a symmetric, positive definite operator Q_{op} for which (134) defines a norm, then for $b = 2$ the vector b -equation (124), or (129), describes geodesic motion on the diffeomorphism group, with respect to this kinetic energy norm.

EP equation for computational anatomy Thus, the EP equation (131) describes geodesic motion when the Lagrangian $\ell[\mathbf{u}]$ is the kinetic energy, which is also a norm. This EP equation has the *same form* as the template matching equation [38], which is used in computational anatomy [37].

11.2 n -dimensional analogs of pulsons for the vector b -equation

The momentum for the one-dimensional pulson solution (63) on the real line is supported at points via the Dirac delta measures in its solution ansatz,

$$m(x, t) = \sum_{i=1}^N p_i(t) \delta(x - q_i(t)), \quad m \in R^1. \quad (135)$$

For the vector b -equation (124), or (129), we shall develop n -dimensional analogs of these one-dimensional pulson solutions by generalizing the solution ansatz to allow measure-valued n -dimensional vector solutions. In these solutions, the momentum $\mathbf{m} \in R^n$ is supported on co-dimension- k subspaces R^{n-k} moving with the flow, where $k \in [1, n]$ is an integer. In an example in section 11.2.3, we shall consider a two-dimensional vector momentum $\mathbf{m} \in R^2$ in the plane that is supported on one-dimensional curves (momentum fronts). Likewise, in three dimensions, one could consider two-dimensional momentum surfaces (sheets) and one-dimensional momentum filaments, each moving with the local flow velocity. The corresponding vector momentum ansatz that we shall use is a vector version of the pulson solutions (135), namely,

$$\mathbf{m}(\mathbf{x}, t) = \sum_{i=1}^N \int \mathbf{P}_i(s, t) \delta(\mathbf{x} - \mathbf{Q}_i(s, t)) ds, \quad \mathbf{m} \in R^n. \quad (136)$$

Here, $\mathbf{P}_i, \mathbf{Q}_i \in R^n$ for $i = 1, 2, \dots, N$. For example, when $n - k = 1$, so that the Lagrangian coordinate $s \in R^1$ is one-dimensional, the delta function in solution (136) supports an evolving family of vector-valued curves, which we shall call **momentum filaments**. (For simplicity of notation, we suppress the implied subscript i in the arclength s for each \mathbf{P}_i and \mathbf{Q}_i .) The defining relation $\mathbf{u} = G * \mathbf{m}$ in (125) implies that the velocity corresponding to the

momentum filament ansatz (136) is,

$$\mathbf{u}(\mathbf{x}, t) = G * \mathbf{m} = \sum_{j=1}^N \int \mathbf{P}_j(s', t) G(\mathbf{x} - \mathbf{Q}_j(s', t)) ds'. \quad (137)$$

The function (filter) $G(|\mathbf{x}|)$ defined in (125) is isotropic, so $G'(0) = 0$. We shall choose $G(0) = 1$, so $\mathbf{P}_j(s', t)$ is the velocity of the j -th filament at $\mathbf{x} = \mathbf{Q}_j(s', t)$ and $s' \in R^1$ is a Lagrangian coordinate along the filament. Just as for the 1D case of the pulsions in equations (64) and (65), we shall show that substitution of the n -D solution ansatz (136) and (137) into the vector b -equation (124) produces a closed system of equations for the n -dimensional vector parameters $\mathbf{Q}_i(s, t)$ and $\mathbf{P}_i(s, t)$, $i = 1, 2, \dots, N$. When $b = 2$, these equations will become geodesic Hamiltonian equations for canonically conjugate variables, $\mathbf{Q}_i(s, t)$ and $\mathbf{P}_i(s, t)$.

11.2.1 Momentum filaments in R^n

For definiteness, we shall consider the example of momentum filaments, for which the parameter s is one dimensional. Such filaments have vector-valued momenta $\mathbf{m} \in R^n$ supported on one-dimensional space curves in R^n , so $s \in R^1$ in equation (136) is the arclength parameter of one of these curves. This solution ansatz is reminiscent of the Biot-Savart Law for vortex filaments, although the flow is not incompressible. The dynamics of momentum surfaces, for $s \in R^k$ with $k < n$, follow essentially the same analysis as that given below for $k = 1$.

Substituting the momentum filament ansatz (136) for $s \in R^1$ and its corresponding velocity (137) into the vector b -equation (124), then integrating against a smooth test function $\phi(\mathbf{x})$, implies the following equations, in which summation is explicit on $j \in 1, 2, \dots, N$ and there is no sum on i ,

$$\begin{aligned} \frac{\partial}{\partial t} \mathbf{Q}_i(s, t) &= \sum_{j=1}^N \int \mathbf{P}_j(s', t) G(\mathbf{Q}_i(s, t) - \mathbf{Q}_j(s', t)) ds', \\ \frac{\partial}{\partial t} \mathbf{P}_i(s, t) &= - \sum_{j=1}^N \int (\mathbf{P}_i(s, t) \cdot \mathbf{P}_j(s', t)) \frac{\partial}{\partial \mathbf{Q}_i(s, t)} G(\mathbf{Q}_i(s, t) - \mathbf{Q}_j(s', t)) ds' \\ &\quad - (b-2) \mathbf{P}_i(s, t) \sum_{j=1}^N \int \mathbf{P}_j(s', t) \cdot \frac{\partial}{\partial \mathbf{Q}_i(s, t)} G(\mathbf{Q}_i(s, t) - \mathbf{Q}_j(s', t)) ds'. \end{aligned} \quad (138)$$

The dot product $\mathbf{P}_i \cdot \mathbf{P}_j$ denotes the inner, or scalar, product of the two vectors \mathbf{P}_i and \mathbf{P}_j in R^n . Thus, the solution ansatz (136) yields a closed set of integro-partial-differential equations (IPDEs) given by (138) for the vector parameters $\mathbf{Q}_i(s, t)$ and $\mathbf{P}_i(s, t)$ with $i = 1, 2 \dots N$. Equations (138) for the n -dimensional dynamics of the momentum filaments should be compared with the 1D pulson equations (64) and (65). Note that $b = 2$ is a simplifying special case.

11.2.2 Canonical Hamiltonian dynamics of momentum filaments in R^n for $b = 2$

For $b = 2$, the momentum filament equations (138) simplify to canonical Hamiltonian equations,

$$\frac{\partial}{\partial t} \mathbf{Q}_i(s, t) = \frac{\delta H_N}{\delta \mathbf{P}_i}, \quad \frac{\partial}{\partial t} \mathbf{P}_i(s, t) = - \frac{\delta H_N}{\delta \mathbf{Q}_i}. \quad (139)$$

The corresponding Hamiltonian function $H_N : (R^n \times R^n)^{\otimes N} \rightarrow R$ is,

$$H_N = \frac{1}{2} \iint \sum_{i, j=1}^N (\mathbf{P}_i(s, t) \cdot \mathbf{P}_j(s', t)) G(\mathbf{Q}_i(s, t) - \mathbf{Q}_j(s', t)) ds ds'. \quad (140)$$

This Hamiltonian arises by substituting the momentum ansatz (136) into the kinetic energy norm (134). Thus, for $b = 2$, the evolutionary IPDE system (138) represents canonically Hamiltonian motion on the space of curves in R^n . Moreover, this Hamiltonian motion for $b = 2$ is geodesic with respect to the co-metric given on these curves in (140) by the Green's function G . The Hamiltonian $H_N = \frac{1}{2} \|\mathbf{P}\|^2$ in (140) for this motion defines the norm $\|\mathbf{P}\|$ in terms of this co-metric.

Summary The momentum filament ansatz (137) reduces, or **collects** the solution of the evolutionary vector b -equation (124) for $b = 2$ in n spatial dimensions into the system (138) of $2N$ evolutionary IPDEs in one spatial dimension (arclength along each filament). For $b = 2$, the collective equations describe geodesic flow on the space of vector-valued curves in R^n with respect to the co-metric given on these curves in (140).

The momentum filament equations (138) are not typical As far as we know, the IPDEs for momentum filaments in (138) have never been considered before in the literature, even for the Hamiltonian case $b = 2$. Even the Hamiltonian evolution of a single momentum filament interacting with itself has not appeared in the literature, to our knowledge. There is a faint similarity of this system to vortex dynamics for the incompressible Euler equations. However, there are also fundamental differences. The main difference from the Hamiltonian motion of vortex filaments is that the momentum filaments possess *inertia*, while vortex filaments do not. Thus, N vortex filaments in an incompressible flow are described by N first-order equations, while N momentum filaments in a pressureless compressible flow are described by the $2N$ first-order equations in (138). The main question one would like to answer is, “When do the momentum filament solutions represent the *dominant* emergent pattern in the initial value problem for the vector b -equation (124)?” The next subsection reports an example in which this occurs, for momentum filaments in the plane, in a certain approximation for 2D shallow water waves.

11.2.3 Zero-dispersion shallow water waves in 2D: Two interesting choices for the operator Q_{op} when $b = 2$

The operator Q_{op} in the momentum relation $\mathbf{m} = Q_{op}\mathbf{u}$ in (133) corresponding to $m = u - \alpha^2 u_{xx}$ in the 1D CH equation (11) for zero-dispersion shallow water waves may be defined in two dimensions as *either* of two natural choices,

$$\mathbf{m} = \mathbf{u} - \alpha^2 \Delta \mathbf{u}, \quad \text{or} \quad \mathbf{m} = \mathbf{u} - \alpha^2 \nabla \operatorname{div} \mathbf{u}. \quad (141)$$

For the first choice of momentum definition in (141), the vector EP equation (131) corresponds to the (pressureless) Euler-alpha model, whose Lagrangian $\ell[\mathbf{u}] = \frac{1}{2} \|\mathbf{u}\|^2$ is the conserved H^1 norm,⁷

$$\|\mathbf{u}\|_{H^1}^2 = \int \mathbf{u} \cdot (1 - \alpha^2 \Delta) \mathbf{u} \, dx \, dy = \int |\mathbf{u}|^2 + \alpha^2 (\operatorname{div} \mathbf{u})^2 + \alpha^2 |\operatorname{curl} \mathbf{u}|^2 \, dx \, dy.$$

⁷When incompressibility ($\operatorname{div} \mathbf{u} = 0$) is imposed as an additional constraint in this Lagrangian via a Lagrange multiplier (the pressure), then the corresponding vector EP equation (131) becomes the 2D Lagrangian averaged Euler equation derived in [26] as a generalization of the 1D CH equation for incompressible flow. The Hamilton’s principles defined by the kinetic energy norms $\|\mathbf{u}\|_{H^1}^2$ and $\|\mathbf{u}\|_{KS}^2$ have no pressure constraint, so their corresponding EP equations (131) allow compressible motion.

The last equality assumes either homogeneous, or periodic boundary conditions, so that boundary terms may be neglected upon integrating by parts.

For the second natural choice of momentum in (141), the conserved kinetic energy norm becomes, instead,

$$\|\mathbf{u}\|_{KS}^2 = \int \mathbf{u} \cdot (1 - \alpha^2 \nabla \operatorname{div}) \mathbf{u} \, dx \, dy = \int |\mathbf{u}|^2 + \alpha^2 (\operatorname{div} \mathbf{u})^2 \, dx \, dy,$$

and kinetic energy conservation no longer controls $\operatorname{curl} \mathbf{u}$. This is the norm associated with vertically-averaged kinetic energy that arises when one approximates the Green-Naghdi equations for shallow water motion by neglecting variations in surface elevation in the potential energy and in the Lagrange-to-Euler Jacobian.⁸ The second term proportional to α^2 approximates (twice) the vertically-averaged kinetic energy due to vertical motion. For more details of the latter approximation for the 2D CH shallow water equation, see Kruse and Schreule [34].

The EP equation (131) was numerically integrated in [29], in the form

$$\frac{\partial}{\partial t} \mathbf{m} - \mathbf{u} \times \operatorname{curl} \mathbf{m} + \nabla(\mathbf{u} \cdot \mathbf{m}) + \mathbf{m}(\operatorname{div} \mathbf{u}) = 0, \quad (142)$$

for both choices of the momentum-velocity relation in equation (141). This numerical integration was performed by using a difference scheme that preserved the properties of the operators div , grad and curl ($\operatorname{div} \operatorname{curl} = 0$ and $\operatorname{curl} \operatorname{grad} = 0$). The main discovery in the numerical results of [29] was that the evolution of the geodesic PDE (142) was found to be dominated by the emergent dynamics of momentum filaments, arising from confined initial conditions for *either* choice of momentum-velocity relation in equation (141). Thus, the momentum filament solutions in both of these cases were stable, and *no other types of solution* were observed in the numerical evolution of

⁸In this approximation for 2D shallow water waves, $\operatorname{curl} \mathbf{m} = \operatorname{curl} \mathbf{u}$ and $\operatorname{div} \mathbf{m} = (1 - \alpha^2 \Delta) \operatorname{div} \mathbf{u}$. Thus, setting $\mathbf{u} = \hat{\mathbf{z}} \times \nabla \psi - \nabla \phi$ allows one to solve for the stream function ψ and velocity potential ϕ from the momentum \mathbf{m} via,

$$\hat{\mathbf{z}} \cdot \operatorname{curl} \mathbf{m} = -\Delta \psi \quad \text{and} \quad \operatorname{div} \mathbf{m} = -\Delta(1 - \alpha^2 \Delta) \phi.$$

These two relations allow one to update the potentials ψ and ϕ for the velocity \mathbf{u} , given the momentum \mathbf{m} at each time step, provided these potentials satisfy boundary conditions that allow inversion of the Laplacian operator for ψ and the Helmholtz-Laplace operator for ϕ . Whether these boundary conditions are consistent with the diffeomorphism group is an open question.

equation (142) in the periodic plane. The dynamics of the momentum filaments that emerged was quasi-one-dimensional, with greater variation of the solution in the direction transverse to the filaments than along the tangential direction. Thus, the interaction dynamics for the momentum filaments was found to be dominantly in the direction transverse to the filaments. This meant the filament interaction was governed primarily by elastic-scattering dynamics reminiscent of the one-dimensional solutions, as seen in soliton dynamics. In fact, the one-dimensional soliton collision rules were found to provide a good interpretation of the interactions among the momentum filaments. These interactions were found to allow reconnection of the quasi-one-dimensional momentum filaments. For more information and discussion of numerical results, see [29].

References

- [1] M.J. Ablowitz and P.A. Clarkson, *Solitons, Nonlinear Evolution Equations and Inverse Scattering*, Cambridge University Press (1991).
- [2] M. Alber, R. Camassa, D. D. Holm and J. E. Marsden, The geometry of peaked solitons and billiard solutions of a class of integrable PDE's. *Lett. Math. Phys.* **32**, 137 (1994).
- [3] M. Alber, R. Camassa, D. D. Holm and J. E. Marsden, On the link between umbilic geodesics and soliton solutions of nonlinear PDE's. *Proc. Roy. Soc.* **450**, 677-692 (1995).
- [4] M. Alber, R. Camassa, V. N. Fedorov, D. D. Holm and J. E. Marsden, On billiard solutions of nonlinear PDE's. *Phys. Lett. A* **264**, 171-178 (1999).
- [5] M. Alber, R. Camassa, V. N. Fedorov, D. D. Holm and J. E. Marsden, The complex geometry of piecewise solutions of integrable nonlinear PDE's of shallow water and Dym type. *Commun. Math. Phys.* **221**, 197-227 (2001).
- [6] R. Beals, D. H. Sattinger and J. Szmigielski, Multipeakons and the classical moment problem *Adv. in Math.* **154**, 229-257 (2000).
- [7] R. Camassa and D. D. Holm, An integrable shallow water equation with peaked solitons, *Phys. Rev. Lett.* **71**, 1661-1664 (1993). <http://xxx.lanl.gov/abs/patt-sol/9305002>.

- [8] R. Camassa, D. D. Holm and J. M. Hyman, A new integrable shallow water equation. *Adv. Appl. Mech.*, Academic Press: Boston, 1994, vol **31**, pp 1–33.
- [9] S. Chen, C. Foias, D. D. Holm, E. J. Olson, E. S. Titi and S. Wynne, The Camassa-Holm equations as a closure model for turbulent channel and pipe flows. *Phys. Rev. Lett.*, **81**, 5338-5341 (1998). <http://xxx.lanl.gov/abs/chao-dyn/9804026>.
- [10] A. Constantin, On the scattering problem for the Camassa-Holm equation. *Proc. Roy. Soc. London* **457**, 953-970 (2001).
- [11] A. Constantin and J. Escher, Global existence and blow-up for a shallow water equation. *Ann. Scuola Norm. Sup. Pisa* **26**, 303-328 (1998).
- [12] A. Constantin and J. Escher, Wave breaking for nonlinear nonlocal shallow water equations. *Acta Mathematica* **181**, 229-243 (1998).
- [13] A. Constantin and W. A. Strauss, Stability of peakons. *Comm. Pure Appl. Math.* **53**, 603-610 (2000).
- [14] H.-H. Dai and Y. Huo, Solitary shock waves and other travelling waves in general compressible hyperelastic rods. *Proc. Roy. Soc. London* **456**, 331-363 (2000).
- [15] A. Degasperis, D. D. Holm and A. N. W. Hone, A new integrable equation with peakon solutions. *Theoret. and Math. Phys.* **133**, 1463-1474 (2002). <http://xxx.lanl.gov/abs/nlin.SI/0205023>.
- [16] A. Degasperis and M. Procesi, Asymptotic integrability, in *Symmetry and Perturbation Theory*, edited by A. Degasperis and G. Gaeta, World Scientific (1999) pp.23-37.
- [17] H. Dullin, G. Gottwald and D. D. Holm, An integrable shallow water equation with linear and nonlinear dispersion. *Phys. Rev. Lett.* **87**, 194501-04 (2001).
- [18] H. R. Dullin, D.D. Holm and G. Gottwald, Camassa-Holm, Korteweg-de Vries-5 and other asymptotically equivalent equations for shallow water waves. *Fluid Dyn. Res.* To appear, (2003).

- [19] A. S. Fokas, On a class of physically important integrable equations. *Physica D* **87**, 145-150 (1995).
- [20] A. S. Fokas and B. Fuchssteiner, Backlund-transformations for hereditary symmetries. *Nonlinear Anal. TMA* **5**, 423-432 (1981).
- [21] A. S. Fokas and Q. M. Liu, Asymptotic integrability of water waves. *Phys. Rev. Lett.* **77**, 2347-2351 (1996).
- [22] O. Fringer and D. D. Holm, Integrable vs. nonintegrable geodesic soliton behavior. *Physica D* **150**, 237-263 (2001). <http://xxx.lanl.gov/abs/solv-int/9903007>.
- [23] B. Fuchssteiner and A. S. Fokas, Symplectic structures, their Bäcklund transformations and hereditary symmetries. *Physica D* **4**, 47-66 (1981/82).
- [24] B. Fuchssteiner, The Lie algebra structure of nonlinear evolution equations admitting infinite-dimensional abelian symmetry groups. *Progr. Theoret. Phys.* **65**, 861-876 (1981).
- [25] B. Fuchssteiner, Some tricks from the symmetry-toolbox for nonlinear equations: generalizations of the Camassa-Holm equation. *Physica D* **95**, 229-243 (1996).
- [26] D. D. Holm, J. E. Marsden and T. S. Ratiu, The Euler–Poincaré equations and semidirect products with applications to continuum theories. *Adv. in Math.* **137**, 1-81 (1998).
- [27] D. D. Holm, J. E. Marsden and T. S. Ratiu, Euler–Poincaré models of ideal fluids with nonlinear dispersion. *Phys. Rev. Lett.* **80**, 4173-4177 (1998).
- [28] D. D. Holm, R. B. Lowrie and M. F. Staley, Shock-capturing properties of the Burgers– $\alpha\beta$ equation. In preparation.
- [29] D.D. Holm and M.F. Staley, Momentum filament dynamics in a family of 2+1 evolutionary PDEs. In preparation (2003).
- [30] D. D. Holm and E. S. Titi, PDE results for peakon dynamics. In preparation (2003).

- [31] J. K. Hunter and R. H. Saxton, Dynamics of director fields. *SIAM J. Appl. Math.* **51**, 1498-1521 (1991).
- [32] R. S. Johnson, Camassa-Holm, Korteweg-de Vries and related models for water waves. *J. Fluid. Mech.* **455**, 63-82 (2002).
- [33] Y. Kodama, On integrable systems with higher order corrections. *Phys. Lett. A* **107**, 245-249 (1985); Normal forms for weakly dispersive wave equations. *Ibid* **112**, 193-196 (1985); On solitary-wave interaction. *Ibid* **123**, 276-282 (1987).
- [34] H. P. Kruse, J. Schreule and W. Du, A two-dimensional version of the CH equation. In *Symmetry and Perturbation Theory: SPT 2001* Edited by D. Bambusi, G. Gaeta and M. Cadoni. World Scientific: New York, pp 120-127 (2001).
- [35] Z. Li and N.R. Sibgatullin, An improved theory of long waves on the water surface. *J. Appl. Maths. Mech.* **61**, 177-182 (1997).
- [36] A.S. Mikhailov and V. Novikov, (private communication).
- [37] M. I. Miller, A. Trouné and L. Younes, On the metrics and Euler-Lagrange equations of computational anatomy. *Annu. Rev. Biomed. Eng.* **4**, 375-405 (2002).
- [38] D. Mumford, Pattern theory and vision. In *Questions Mathématiques En Traitement Du Signal et de L'Image*, Chapter 3, pp. 7-13. Paris: Institut Henri Poincaré (1998).